DIGITALCOMMONS
@WAYNESTATE

Wayne State University

Wayne State University Dissertations

1-1-2015

Rheology Of Cross-Linked Polymers And Polymer Foams: Theory And Experimental Results

John Herman
Wayne State University,

Follow this and additional works at: http://digitalcommons.wayne.edu/oa_dissertations

Recommended Citation
Herman, John, "Rheology Of Cross-Linked Polymers And Polymer Foams: Theory And Experimental Results" (2015). *Wayne State University Dissertations.* Paper 1138.

This Open Access Dissertation is brought to you for free and open access by DigitalCommons@WayneState. It has been accepted for inclusion in Wayne State University Dissertations by an authorized administrator of DigitalCommons@WayneState.

المنارة للاستشارات

www.manaraa.com

RHEOLOGY OF CROSS-LINKED POLYMERS AND POLYMER FOAMS: THEORY AND EXPERIMENTAL RESULTS

by

JOHN N. HERMAN

DISSERTATION

Submitted to the Graduate School

of Wayne State University,

Detroit, Michigan

in partial fulfillment of the requirements

for the degree of

DOCTOR OF PHILOSOPHY

2015

MAJOR: MECHANICAL ENGINEERING

_____

Advisor: Date

_____

_____

_____

www.manaraa.com

© COPYRIGHT BY

JOHN N. HERMAN

2015

All Rights Reserved

www.manaraa.com

ACKNOWLEDGMENT

I can no other answer make but thanks,

And thanks, and ever thanks.

- William Shakespeare, *Twelfth Night*, Act 3, Scene 3

My deepest appreciation and heartfelt thanks goes to Mr Karel Bos (1928), who saw in me something I did not see in myself. Without his encouragement, I would have never started down this path of higher education. His support allowed me to discover many truths about myself, and opened my eyes to a broad spectrum of opportunities and possibilities. The journey has been challenging, frustrating, educational, and vastly rewarding. However, it ends not with this dissertation, but instead, this work has laid the foundation to other unexplored personal discoveries. Let the journey continue...

www.manaraa.com

TABLE OF CONTENTS

www.manaraa.com

www.manaraa.com

www.manaraa.com

LIST OF FIGURES

www.manaraa.com

www.manaraa.com

www.manaraa.com

www.manaraa.com

www.manaraa.com

www.manaraa.com

LIST OF SYMBOLS

$A,\ \hat{A}$	constant, dimensionless amplitude
$a,\ b,\ c$	Lagrangian indices
$a,\ b,\ c,\ d$	dynamic material parameters
C	constant
$const$	constant
D	diffusion coefficient
F	force, free energy per unit volume
$\mathcal{F}$	free energy
$\mathbb{F}$	free energy
f	external force on chain
$G,\ \hat{G}$	Volterra stress kernel, Laplace transformed kernel
$G,\ \tilde{G}$	constants
G	shear modulus
$\mathring{g}_{\cdot\cdot}$	metric tensor
H	potential, periodic potential
h	period of potential field
$h_{\cdot\cdot}$	symmetric matrix
$i,\ j,\ k$	Eularian indices
k	spring constant
$J,\ \hat{J}$	Volterra strain kernel, Laplace transformed kernel
K	bulk modulus
l	length of Kuhn segment
N	number of chains
n	constant, number of monomers, number of Kuhn segments
$O_{\cdot\cdot}$	orthogonal matrix
$p,\ p_{\cdot\cdot}$	constant, second stress tensor
q	constant
$R,\ R_{\cdot},\ R_{\cdot\cdot}$	distance between chain ends
$r,\ r_{\cdot\cdot}$	distance to chain sticking point
$\mathbb{S},\ \mathring{\mathbb{S}}$	entropy, initial entropy
S	entropy per monomer
s	Laplace transform variable
T	temperature
$t,\ t_o$	time, initial time
$\mathcal{U}$	internal energy
u	energy per monomer
$\|V\|$	volume of specimen
$v,\ \hat{v}$	average velocity, dimensionless velocity
$\dot{w}$	white noise
$x,\ x_{\cdot\cdot}$	coordinate/distance, distortion matrix

www.manaraa.com

α	constant
β	magnitude of random excitation, constant
Γ	Gamma function
γ	simplification variable
$\delta_{\cdot}^{\cdot}$	Kronecker's delta
$\varepsilon,\ \varepsilon_o,\ \varepsilon_{\cdot}^{\cdot}$	strain, initial strain, strain tensor
$\dot{\varepsilon}$	strain rate
$\zeta,\ \bar{\zeta}$	excitation force, generic material property
η	viscosity, distance between chains
$\Lambda,\ \hat{\Lambda}$	simplification variable, external force, dimensionless external force
λ	Lamé first parameter
μ	friction coefficient, shear modulus
$\xi_{\cdot\cdot}$	material internal parameter
$\rho,\ \bar{\rho}$	ratio chain end-to-end distance to overall length, relative density
$\sigma,\ \sigma_o,\ \sigma_{\cdot}^{\cdot}$	stress, initial stress, stress tensor
$\dot{\sigma}$	stress rate
τ	time parameter
υ	Poisson's ratio
$\Phi,\ \hat{\Phi}$	notation variable, dimensionless periodic force
Ψ	velocity function
$\langle\cdot\rangle$	average
$\mathring{\cdot}$	initial condition
$\cdot'$	deviator
$\breve{\cdot}$	equilibrium value

www.manaraa.com

CHAPTER 1

Introduction

Polymers enjoy wide-spread usage in today's society. Under loading, typical polymers exhibit a time-dependent behavior which manifests itself in stress relaxation or creep. These effects can degrade the capability of a polymer structure to perform its function properly. The time-dependent behavior of solid polymers is so diverse that, at the moment, no better recipe exists to describe the material behavior other than fitting experimental results by either Volterra non-local stress-strain relations or their finite-dimensional truncations. The latter can be interpreted as a combination of springs and dashpots. In such approaches a potentially useful piece of information, the micromechanic behavior of the polymer, is lost. This research proposes a theory to microscopic polymer chain movement, and develops a model based on this theory to predict the macroscopic creep and stress relaxation response of a polymer foam. Based on the slip/stick of polymer chains as they move past each other, this model successfully predicts the response of a polymethacrylimide (PMI) polymer foam under tensile loads.

The PMI foam selected for this research is Rohacell IG, widely used in the aviation and marine industries, and manufactured by Evonik Industries. When possible, industry standard test methods are employed to obtain tensile creep and stress relaxation results. To minimize variability in the analysis, only those specimens which share nearly the same elastic modulus are used for the final parameter fitting comparisons. A common set of parameters is fitted to the data, resulting in good correlation between model predictions and experimental responses. Success of this fitting helps to validate the proposed polymer micromechanic theory of chain movement. This model lends insight into polymer microscopic behavior, which may be helpful for the development of future polymer materials.

To set a groundwork of understanding, some highlights of the vast field of polymers and polymer micromechanics are briefly reviewed in Chapter 2. Basic categories of polymers and definitions are reviewed. Classic models based on springs and dashpots, or the Volterra integral for materials with memory have historically been used to predict viscoelastic behavior.

www.manaraa.com

An evaluation of these models and their inadequacies in predicting the performance of the test material are presented. In the literature review [Courtney, 2005, Findley et al., 1989], it is observed that the focus is on the simple creep test, while either ignoring or only giving a cursory mention of the stress relaxation test. This chapter provides a comprehensive summary of both.

Chapter 3 describes the development of a micromechanics-based model for predicting polymer creep and stress relaxation. The model is loosely based on polymer micromechanics in which a theorized interaction between chains under loading is proposed. A complete thermodynamic justification of the model is provided.

Chapter 4 addresses the specifics of the test materials and methods. Various grades (i.e. densities) of PMI exist between 31 kg/m^3 and 110 kg/m^3. While this work focuses on 31 IG, some work with 51 IG and 71 IG is also included. In order to determine the model material parameters, tensile creep and tensile stress relaxation tests are performed at two different load levels. This allows a linear fitting of the model parameters and provides good correlation between the model predictions and experimental data. Variability makes the performance of any model suspect, and in practice, of little use to predicting material behavior. An important aspect of the testing regime is to identify potential sources of variability. One variability study performed is an investigation of the elastic modulus and material density relationship using nominal foam densities of 31 kg/m^3, 51 kg/m^3, 71 kg/m^3.

An interesting feature of the PMI foam is its behavior once unloaded. Many models focus on predicting the material performance during the hold phase after the initial loading. A more complex loading involves the addition of an unloading, then recovery phase. Additional model fittings/evaluations are performed for this complex loading, as well as load/partial-unload/hold, and load/instantaneous-unload cycles, in Chapter 5. During the loading and subsequent unloading, a residual strain builds up in the test specimen. This residual strain in not permanent, and in fact, when no load is applied to the specimen, the strain eventually returns to zero. Therefore, for the model's micromechanic reasoning to be valid, the model must be able to "close the loop" in the stress-strain plot in a similar fashion. It should also predict the material behavior nuances observed in other loading cycles.

Chapter 6 summarizes the key points contained herein and offers potential areas of further

www.manaraa.com

exploration. These areas may provide additional insight into polymer chain motion with the use of the developed model. The completion of this research adds to the database of engineering knowledge with the development of a micromechanics-based model for polymer foam behavior. This model predicts the behavior of a grade of PMI foam quite closely. Future research will hopefully extend the model to cover other loading conditions, along with the application to other polymer materials.

www.manaraa.com

CHAPTER 2

Polymers and Rheology

A myriad of information has been written on the subject of polymers. Indeed, there are many individuals who have spent their life's work advancing the field of polymer science. One aim of this chapter is to simply introduce the reader to this vast field, and briefly review some key points of polymer mechanics to aid in the understanding of the work herein. For additional insights, the reader is encouraged to review works by Courtney, Flory, and Gibson [Courtney, 2005, Flory, 1990, Gibson and Ashby, 1997]. Section 2.1 summarizes basic definitions. Section 2.2 summarizes polymers and polymer micromechanics. A brief overview of the manufacturing and construction of PMI foam is given in Section 2.3. Sections 2.4 and 2.5 review the basic rheology of polymers and the classic models which have been used to describe this behavior. The models are based on linear springs and dashpots. Shortcomings of the use of these models are discussed. Section 2.6 reviews the use of the Volterra integral to describe the viscoelastic behavior.

2.1 Polymer Structure

The term polymer denotes a molecule made by the repetition of a simpler unit, the mer or monomer. Polymerization is the process of joining together monomers into larger chain-like macromolecules. The monomers are generally held together as macromolecules by covalent bonds, the sharing of electrons between atoms. The attractive force between the individual chains can be comprised of covalent bonds or weaker van der Waals forces, that are usually due to polarization. Van der Waals forces are relatively weak compared to covalent bonds. In general, covalent bonds govern the thermal and photochemical stability of polymers. Van der Waals forces determine most of the physical properties associated with specific compounds. Melting, dissolving, vaporizing, absorption, diffusion, deformation, and flow involve the making and breaking of intermolecular bonds so that the polymer chains can move past one another or away from each other.

The addition of cross-links, i.e. covalent bonds between polymer chains, provides "mem-

www.manaraa.com

ory" of the initial state to the polymer structure. Without cross-links, the individual chains would slide freely past each other. Cross-links generate strong interchain bonds and thus restrict this motion.

The macroscopic rheological model developed in this research is motivated by an idea on modeling the breaking and reforming of the weak interchain bonds that occur when materials deform.

2.2 Categories of Polymers

Polymers can be broadly classified on the basis of their mechanical characteristics, which in turn, are determined by the polymer's molecular architecture. In general, three broad categories of polymers exist: thermosets, thermoplastics, and elastomers.

Thermosets are polymers in which the primary bonding lies not only along a chain, but assumes a skeletal or three-dimensional character between chains. While thermosets are capable of elastic and viscoelastic deformation, their structure does not allow for permanent deformation at ordinary temperatures; thermosets decompose at a temperature above which permanent deformation could be accomplished in them. Thermosets are permanently cured into a given shape, generally through the application of heat. Curing results in an irreversible chemical reaction in which permanent connections (cross-links) are made between the material's molecular chains.

Thermoplastics consist of long molecular chains with covalent bonding along the chains. The individual chains are held together by much weaker van der Waals bonds or, in certain thermoplastics, hydrogen bonds. No cross-links are formed in a thermoplastic. The thermoplastic process is reversible in that the material may be remelted and reformed into new shapes without degradation of the base material.

Elastomers are highly kinked long-chain polymers periodically cross-linked in such a way that permanent displacement of the chains (i.e. plastic deformation) does not take place in them. Elastomers differ significantly from thermosets and thermoplastics in that the glass transition temperature is significantly below room temperature. Therefore, elastomers can undergo deformation on the order of 500%, while still returning to their original shape after

www.manaraa.com

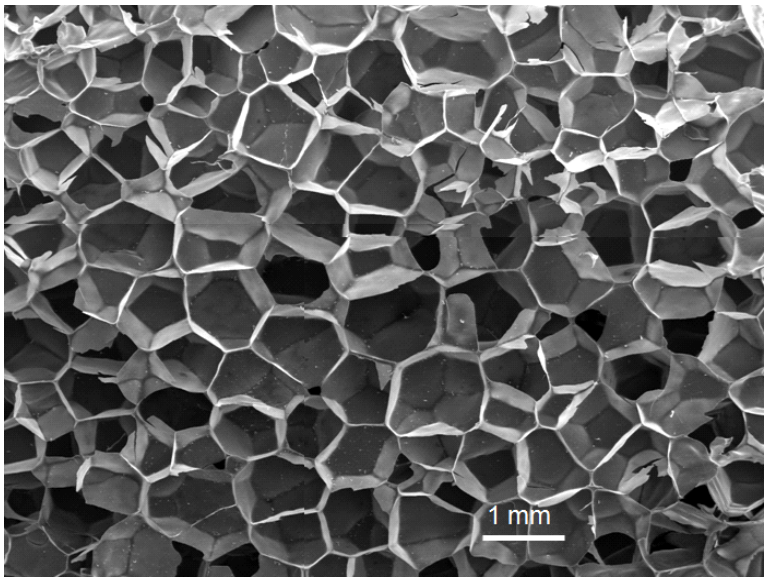

Figure 2.1: Tensile-loading fracture surface of Rohacell 31 IG PMI foam. Vertices, edges, and faces which comprise the closed-cell foam's macrostructure are apparent.

unloading. The structural basis for this is the elastic uncoiling and recoiling of the polymer molecules.

2.3 PMI Foams

2.3.1 Microgeometry

The rheology of Evonik's Rohacell IG, a thermoset foam manufactured from polymethacrylimide, is studied herein. This material is widely used as a core material in sandwich plate construction in the aviation, marine, and sports industries [Black, 2014, Evonik Industries, 2014]. The microgeometry of the foam is shown in Figs. 2.1-2.3. Fig. 2.1 is an image of a foam fracture surface of Rohacell 31 IG. The average cell size diameter is about 0.8 mm. The cell walls are quite thin, about 14 μm on average, while the average edge thickness is 2-3 time higher. High definition cross-section images which more clearly identify the cell faces and edges, Figs. 2.2, 2.3, were provided by Dr. Jie Shen from University of Michigan-Dearborn.

www.manaraa.com

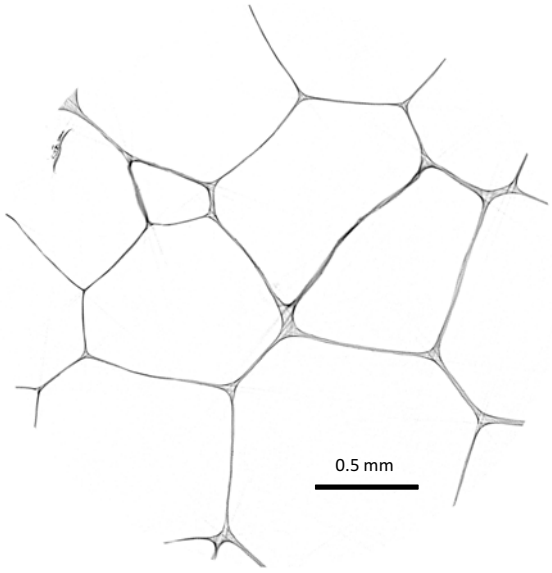

Figure 2.2: High definition cross section (0.7 μm / pixel) CT scan of Rohacell 51 IG foam. This is a true cross section, and not a surface image as in Fig. 2.1. Here the cell faces and edges are more clearly defined. The face thickness averages 14 μm, while the edge thickness averages 34 μm. Average cell size is approximately 0.8 mm in diameter.

2.3.2 Manufacturing

Rohacell IG is manufactured as follows (R. Averill, email communication, July 2011) [United States Patent 5928459, 1999]. Methacrylic acid and methacrylonitrile are injected into glass castings. The castings are placed into a water bath at elevated temperature to start the polymerization process. As the reaction begins, the water bath temperature is closely monitored to control the exothermic reaction. Depending on thickness, in 2-4 weeks the newly polymerized product becomes a polymethacrylimide (PMI) sheet. It is amber in color and similar to Plexiglas at this point. The sheets are formatted and hung vertically in a convection oven. With the addition of heat, the sheets are free foamed into bun format. Finally, the buns are formatted and cut into sheets. The foam density is controlled by the size of the cells.

www.manaraa.com

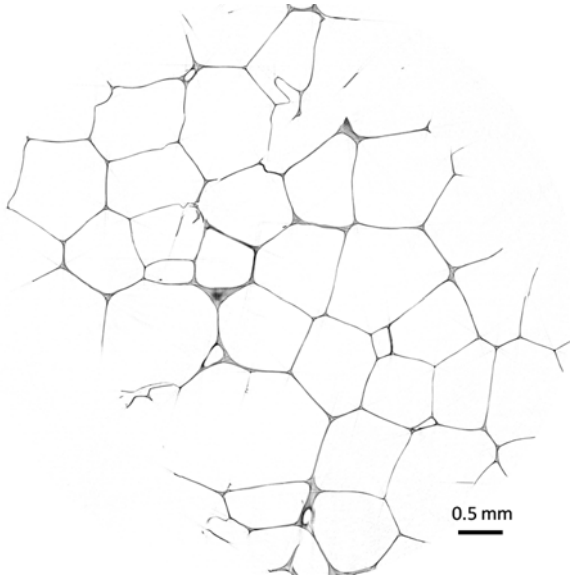

Figure 2.3: Low definition cross section (1.7 μm / pixel) CT scan of Rohacell 51 IG foam. A larger piece of the specimen is captured because of the reduced resolution. The variation in cell shape and size is more apparent.

2.4 Rheology

Viscoelasticity is a material response wherein a material's behavior, when subjected to forces, is viscous as well as elastic in nature. These forces may be surface forces (e.g. a tensile load), or body forces (e.g. the specimen's weight). Upon application of a force, the elastic response occurs immediately and the material responds in a linear manner. An elastic material stores 100% of its energy during deformation, and returns that energy once unloaded. The viscous response is "delayed", and thus the material's response is time dependent. During deformation, a viscoelastic material stores part of the energy in an elastic manner, and dissipates some of its energy in a viscous manner, causing hysteresis. For thermosets, the long polymer chains along with cross-linking at the molecular scale result in viscoelastic behavior at the macroscale. Three tests can be used to quantify a materials' rheologic behavior in simple tension: creep, stress relaxation, and periodic loading. In this study we focus on creep and stress relaxation.

www.manaraa.com

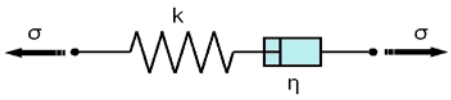

Figure 2.4: Maxwell model, a spring and dashpot in series.

2.5 Classic Constitutive Models

Simple models have been developed to predict the elastic and viscous response of materials. The mechanical equivalent to an elastic response is the Hookean spring. An ideal spring exhibits instantaneous response/recovery to a change in the applied strain or stress. The linear dashpot response is proportional to the rate at which the strain is applied. The spring displacement is linearly proportional to applied force, $F = kx$, k being the spring constant. For materials, the equivalent linear relationship is Hooke's Law, $\sigma = E\varepsilon$. An elastic material stores 100% of its energy during deformation. The viscous response is characterized by material flow over a period of time. As such, the material's response is a function of time. The mechanical equivalent is the Newtonian dashpot. The dashpot velocity is proportional to the applied force, $F = \eta\dot{x}$, η being the viscosity. For materials, the equivalent relationship is $\sigma = \eta\dot{\varepsilon}$. A viscous material does not store energy during deformation. Rather, it dissipates some of this energy as heat.

To represent elastic and viscous behavior, springs and dashpots are arranged in various combinations. These combinations can be tuned to react differently to the constant strain test (i.e. stress relaxation), and constant stress test (i.e. creep). Additional insight can be gained by looking at a more complex loading/unloading/recovery cycle for each of the models. Following is a brief review of the classic models which are relevant to the polymer foam being tested. References made to the material behavior are from the results of numerous test loops, some of which are reviewed in Chapter 4.

2.5.1 Maxwell Model

The Maxwell model is composed of a spring and dashpot connected in series, Fig. 2.4. For such a model, the stress on each element is the same, and equal to the imposed stress. The strain is divided between the spring and dashpot elements. The stress-strain function

www.manaraa.com

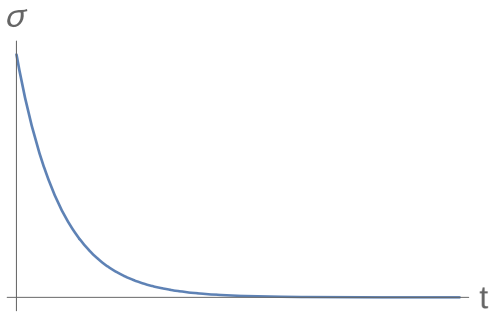

Figure 2.5: Stress response of Maxwell model in a stress relaxation test.

for this model can be described by the constitutive equation:

$$\frac{\eta}{k}\dot{\sigma} + \sigma = \eta\dot{\varepsilon}. \tag{2.1}$$

When subjected to a constant strain as in a stress relaxation test, $\varepsilon(t) = \varepsilon_o = const$, the solution to (2.1) with boundary condition $\sigma(0) = k\varepsilon_o$ demonstrates the stress decays exponentially:

$$\sigma\left(t\right) = k\varepsilon_o \exp\left(-\frac{t - t_o}{\eta/k}\right). \tag{2.2}$$

The qualitative plot of (2.2) is shown in Fig. 2.5. For (2.2), the limit value of stresses as $t \longrightarrow \infty$ is zero, i.e. the material relaxes completely no matter how large the initial strain.

When subjected to a constant stress as in a creep test, $\sigma(t) = \sigma_o = const$, the solution to (2.1) with boundary condition $\varepsilon(0) = \sigma_o/k$, demonstrates the strain responds linearly:

$$\varepsilon\left(t\right) = \frac{\sigma_o}{\eta k}(kt + \eta). \tag{2.3}$$

The plot of (2.3) is shown in Fig. 2.6. The creep test in the Maxwell model exhibits an unbounded increase in strains. Linear creep, while not exactly consistent with the polymer foam material being studied, can in some cases be used as a good approximation for long-term performance, but is lacking in it's ability to predict short-term behavior.

Additional issues arise with the Maxwell model if a prescribed stress loading cycle is evaluated. For such a situation, upon loading/unloading a residual amount of strain remains in

www.manaraa.com

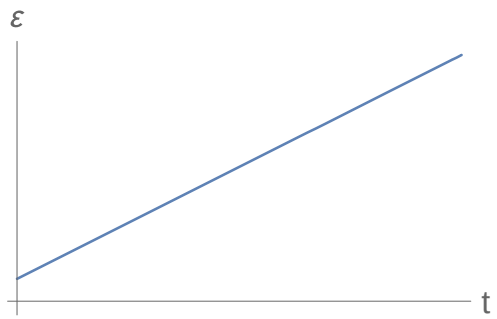

Figure 2.6: Strain response of Maxwell model in a creep test.

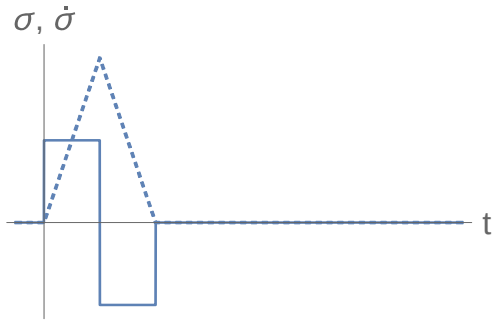

Figure 2.7: Qualitative depiction of a complex stress-controlled loading cycle. Stress rate (solid line) is a linear loading/unloading up to time t_1, then zero for $t > t_1$. This produces the stress time history profile (dashed line) shown.

the material, Fig. 2.8. It is with this test that the Maxwell model breaks down for predicting the material response. This response is not consistent with the material being studied, and thus the Maxwell model is not sufficient to describe the polymer material behavior. During testing, it was observed that the polymer foam material eventually "closes the loop" on the stress-strain plot, whereas the Maxwell model does not. This can be shown with the following analysis. Starting with (2.1), we assume a complex load/unload/recovery similar to Fig. 2.7 where the loading/unloading takes place up to t_1.

At the exact ending moment of the unloading period t_1, $\varepsilon(t_1) \neq 0$ and for $t > t_1$, $\dot{\varepsilon} = 0$, thus (2.1) becomes:

$$\frac{\eta}{k}\int_0^{t_1} \dot{\sigma}dt + \int_0^{t_1} \sigma dt = \eta \int_0^{t_1} \dot{\varepsilon}dt \tag{2.4}$$

www.manaraa.com

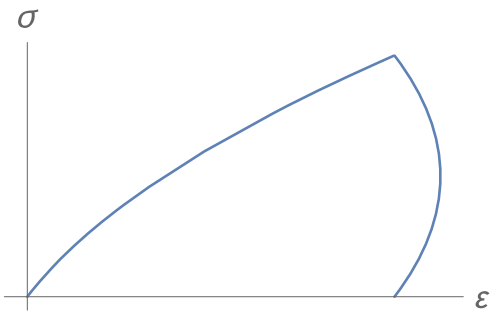

Figure 2.8: Maxwell model does not "close the loop" for the complex load/unload/recovery test. A residual strain is observed and remains indefinately when the stress is returned to zero after unloading.

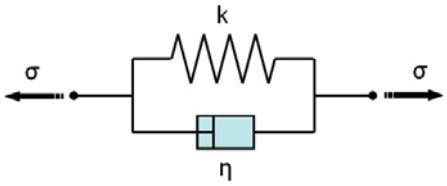

Figure 2.9: Voigt model, a spring and dashpot in parallel.

$$\frac{\eta}{k}[\sigma(t_1) - \sigma(0)] + \int_0^{t_1} \sigma dt = \eta[\varepsilon(t_1) - \varepsilon(0)]. \tag{2.5}$$

Since $\sigma(0) = 0$ and $\sigma(t \geq t_1) = 0$, the first term of (2.5) vanishes. The integral term, which is the area under the $\sigma - t$ curve, is not equal to zero for all $t \geq t_1$, thus $\varepsilon(t \geq t_1)$ is a constant and non-zero. This is in direct conflict of the material behavior where $\varepsilon(t \to \infty) = 0$.

2.5.2 Voigt-Kelvin Model

The Voigt model (aka Kelvin model) is composed of a spring and dashpot connected in parallel, Fig. 2.9. For such a model, the strain on each element is the same, and equal to the imposed strain. The stress is divided between the spring and dashpot elements. The constitutive equation for this model is:

$$\sigma = k\varepsilon + \eta\dot{\varepsilon}. \tag{2.6}$$

When subjected to a constant strain, $\varepsilon(t) = \varepsilon_o = const$, the total stress in the Voigt

www.manaraa.com

Figure 2.10: Stress response of Voigt model in a stress relaxation test.

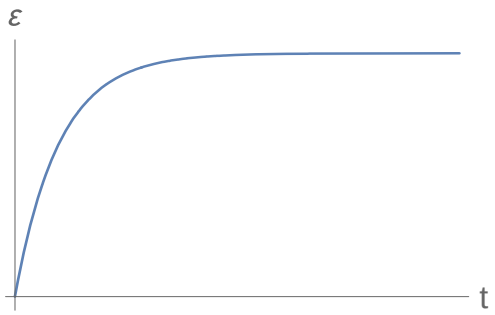

Figure 2.11: Strain response of Voigt model in a creep test.

model is constant, i.e. no stress relaxation takes place regardless of the level of strain loading as shown in Fig. 2.10. This is in direct conflict with the material response which does relax.

When subjected to a constant stress, $\sigma(t) = \sigma_o = const$, the solution to (2.6) with boundary condition $\varepsilon(0) = 0$ is:

$$\varepsilon(t) = \frac{\sigma_o}{k}\left(1 - \exp\left(-\frac{t - t_o}{\eta/k}\right)\right). \tag{2.7}$$

It is seen that the strain goes to the limit value, $\varepsilon(t_\infty) = \sigma_o/k$, dependent on the initial stress level, Fig. 2.11.

If a prescribed complex strain-controlled load/unload/recovery cycle is evaluated, an additional issue arises with the Voigt model. Starting with (2.6), we assume a load/unload/recovery similar to Fig. 2.12 where the loading/unloading takes place up to t_1. At the exact ending moment of the unloading period t_1, $\varepsilon(t_1) = 0$ and for $t > t_1$, $\dot{\varepsilon} = 0$, thus (2.6) becomes:

www.manaraa.com

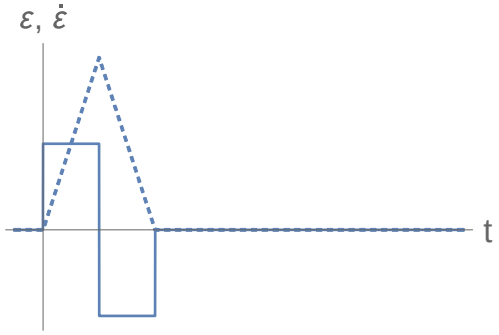

Figure 2.12: Qualitative depiction of a complex strain-controlled loading cycle. Strain rate (solid line) is a linear loading/unloading up to time t_1, then zero for $t > t_1$. This produces the strain time history profile (dashed line) shown.

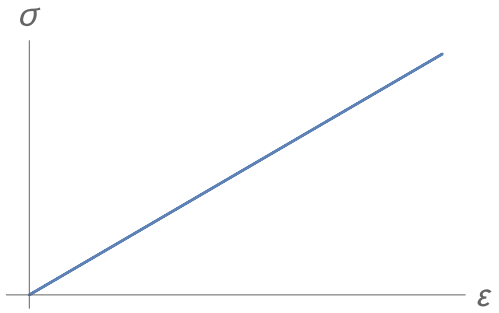

Figure 2.13: When subjected to a strain-controlled load/unload/recovery cycle, the stress-strain plot for the Voight model shows a linear response and is not consistent with the test material.

$$\int_0^{t_1} \sigma dt = k \int_0^{t_1} \varepsilon dt + \eta \int_0^{t_1} \dot{\varepsilon} dt \tag{2.8}$$

$$\int_0^{t_1} \sigma dt = k \int_0^{t_1} \varepsilon dt + \eta[\varepsilon(t_1) - \varepsilon(0)]. \tag{2.9}$$

Since $\varepsilon(0) = 0$, $\varepsilon(t \geq t_1) = 0$, only the integral terms remain. Here we observe the area under the $\sigma - t$ curve is linearly proportional to the area under the $\varepsilon - t$ curve. For such a condition, the model reacts in a purely linear fashion and results in no hysteresis on the stress-strain plot, Fig. 2.13. This is not consistent with the material being studied, and thus the Voigt model is discounted.

www.manaraa.com

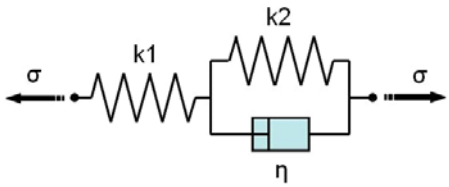

Figure 2.14: Voigt form of the SLS model includes an additional spring in series with a Voigt unit.

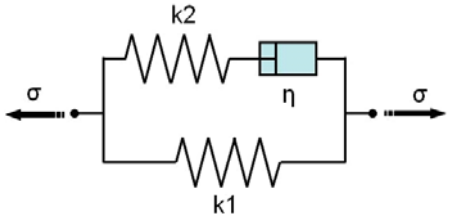

Figure 2.15: Maxwell form of the SLS model includes an additional spring in parallel with a Maxwell unit.

2.5.3 Standard Linear Solid (SLS) Model

Most polymers do not exhibit the unrestricted creep permitted by the Maxwell model, nor the purely elastic response in the Voigt model. To correct for this, several forms of the Standard Linear Solid model have been suggested.

Voigt-SLS

The Voigt-SLS model includes the addition of a spring element in series with a Voigt unit, Fig. 2.14.

The stress-strain relation for the Voigt-SLS model is:

$$\frac{1}{k_1}\dot{\sigma} + \left(\frac{k_1 + k_2}{\eta k_1}\right)\sigma = \dot{\varepsilon} + \frac{k_2}{\eta}\varepsilon. \tag{2.10}$$

Maxwell-SLS

The Maxwell-SLS model includes the addition of a spring element in parallel with the Maxwell unit, Fig. 2.15.

www.manaraa.com

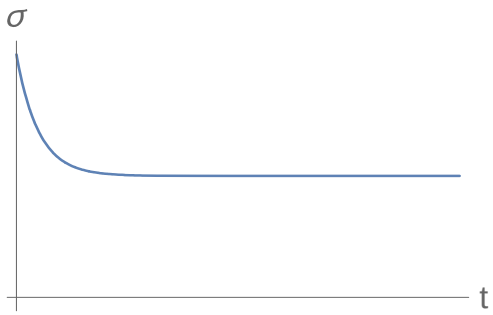

Figure 2.16: Normalized stress response of the SLS model to a stress relaxation test. With the appropriate choice of variables, the Maxwell form and the Voigt form of the SLS models are interchangeable.

The stress-strain relation for the Maxwell-SLS model is:

$$\dot{\sigma} + \frac{k_2}{\eta}\sigma = (k_1 + k_2)\,\dot{\varepsilon} + \frac{k_1 k_2}{\eta}\varepsilon. \tag{2.11}$$

It can be shown that with the proper choice of k_1, k_2, η that (2.10) and (2.11) are equivalent. Thus conclusions drawn for appropriateness of the SLS models are the same for both the Maxwell and the Voigt forms. Evaluating (2.11), when subjected to a constant strain, $\varepsilon(t) = \varepsilon_o = const$, the solution to (2.11) with boundary condition $\sigma(0) = (k_1 + k_2)\varepsilon_o$ is:

$$\sigma(t) = \left[k_1 + k_2 \exp\left(-\frac{k_2}{\eta}(t - t_o)\right)\right]\varepsilon_o. \tag{2.12}$$

For (2.12), $\lim_{t\longrightarrow\infty}\sigma\,(t) = k_1\varepsilon_o = C$, which demonstrates stress relaxation continues until a constant value, dependent on the material properties and the initial strain level, is reached, Fig. 2.16.

When subjected to a constant stress, $\sigma(t) = \sigma_o = const$, the solution to (2.11) with boundary condition $\varepsilon(0) = \sigma_o/(k_1 + k_2)$, is:

$$\varepsilon(t) = \left[\frac{1}{k_1} - \frac{k_2}{k_1(k_1 + k_2)}\exp\left(-\frac{k_1 k_2}{\eta(k_1 + k_2)}(t - t_o)\right)\right]\sigma_o. \tag{2.13}$$

For (2.13), $\lim_{t\longrightarrow\infty}\varepsilon\,(t) = \sigma_o/k_1 = C$, which demonstrates creep continues until a constant value, dependent on the material properties and initial stress level, is reached, Fig.

www.manaraa.com

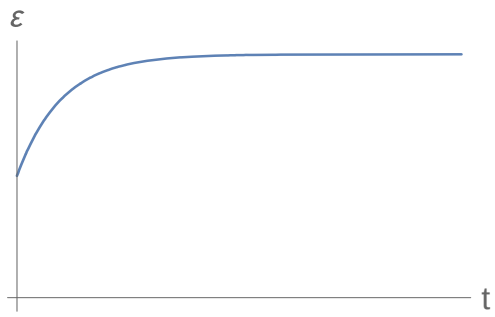

Figure 2.17: Normalized strain response of the SLS model to a creep test. With the appropriate choice of variables, the Maxwell form and the Voigt form of the SLS models are interchangeable.

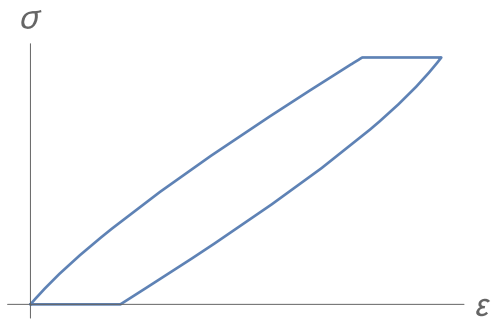

Figure 2.18: Stress-strain plot of the SLS model when subjected to a stress controlled, complex loading cycle. During the recovery phase, the SLS model closes the stress-strain loop and returns to its starting point.

2.17.

If a stress load/unload/recovery cycle is evaluated, the SLS models do "close the loop" on the stress-strain plot, Fig. 2.18, which is consistent with the overall material behavior.

2.5.4 Wiechert Model

More complex behaviors can be modeled with increasing complexity of the spring and dashpot models. One popular modification is the Wiechert model which is an extension of the Maxwell-SLS model. A n-component Wiechert model is shown in Fig. 2.19.

The constitutive equation for the Wiechert model is the ordinary differential equation of n^{th} order linking σ and ε. It can also be written as n first order differential equations, where the subscripts on σ represent the individual branches of the model:

www.manaraa.com

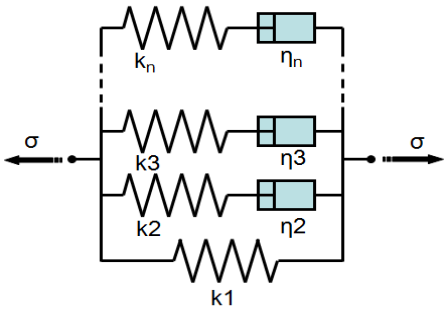

Figure 2.19: Wiechert model is a generalized version of the Maxwell-SLS model. To improve modeling flexibility, an increasing number of Maxwell units are added to the Maxwell-SLS model.

$$\begin{aligned} \sigma(t) &= k_1\varepsilon(t) + \sigma_2 + \sigma_3 + ... + \sigma_n \\ k_2\sigma_2 + \eta_2\dot{\sigma}_2 &= \eta_2 k_2\dot{\varepsilon} \\ k_3\sigma_3 + \eta_3\dot{\sigma}_3 &= \eta_3 k_3\dot{\varepsilon} \\ &.... \\ k_n\sigma_n + \eta_n\dot{\sigma}_n &= \eta_n k_n\dot{\varepsilon}. \end{aligned} \tag{2.14}$$

The advantage of the Wiechert model is it can be tailored to the decay rate more precisely than the SLS models. As many Maxwell units as needed can be added to the arrangement to approximate the material response. For a stress relaxation test, when the strain is constant:

$$\sigma(t) = \left[k_1 + \sum_{i=2,n}\left\{k_i \exp\left(-\frac{k_i}{\eta_i}(t-t_o)\right)\right\}\right]\varepsilon_o. \tag{2.15}$$

For (2.15), $\lim_{t\longrightarrow\infty}\sigma\,(t) = k_1\varepsilon_o = C$, which demonstrates stress relaxation continues until a constant value, dependent on material properties and initial strain level, is reached.

An operational shortcoming with this model is the absence of clear physical meaning of the material parameters involved, $k_1,\ k_2, ..., k_n$ and $\eta_2,\ \eta_3, ..., \eta_n$.

www.manaraa.com

2.6 Nonlocal Constitutive Equations

Instead of a model based on linear and viscous elements, the polymer material's stress-strain behavior can be represented using the Volterra integral. For material stress, the following relationship is used:

$$\sigma(t) = \int_0^t G(t-\tau)\dot{\varepsilon}(\tau)d\tau. \tag{2.16}$$

Equation (2.16) can be inversed to obtain material strain:

$$\varepsilon(t) = \int_0^t J(t-\tau)\dot{\sigma}(\tau)d\tau. \tag{2.17}$$

The functions $J(t)$ and $G(t)$ are referred to as kernels. The kernel determines the model response to the loading. Since creep and stress relaxation are two aspects of the same viscoelastic material behavior, it is expected that they are related. Indeed, it can be shown using Laplace transforms [Zenkert et al., 2006],

$$\hat{J}(s)\hat{G}(s) = \frac{1}{s^2}, \tag{2.18}$$

where $\hat{J}(s)$ and $\hat{G}(s)$ are the Laplace transforms of the kernels $J(t)$ and $G(t)$, respectively. To experimentally measure the kernel $G(t)$, one can apply the strain and release it in a step-function manner. This appears to create an ambiguity in equations (2.16) and (2.17) at $t = 0$. In practice, due to equipment limitations, the load (or elongation) application is actually over a short, finite time interval.

Because of the material's memory to prior loadings, the stress rate (or strain rate as appropriate) must be prescribed for the entire loading cycle beginning from its initial loading, which is assumed to be at $t = 0$. In order to be appropriate for predicting the performance of the polymer material, the Volterra integral (2.16) and (2.17) must be able to "close the loop" in the stress-strain plot for the complex load/hold/unload/recovery test. Let us take

www.manaraa.com

the following loading profile:

$$\dot{\sigma} = \left\{ \begin{array}{cc} 0 & t \leq 0 \\ C & 0 \leq t \leq t_1 \\ 0 & t_1 \leq t \leq t_2 \\ -C & t_2 \leq t \leq t_3 \\ 0 & t_3 \leq t \end{array} \right\}. \tag{2.19}$$

To determine the final strain at a time $t > t_3$, we have from (2.17):

$$\varepsilon(t) = \int_0^t J(t-\tau)\dot{\sigma}(\tau)d\tau \tag{2.20}$$
$$= \int_0^{t_1} J(t-\tau)\dot{\sigma}(\tau)d\tau + \int_{t_1}^{t_2} J(t-\tau)\dot{\sigma}(\tau)d\tau + \int_{t_2}^{t_3} J(t-\tau)\dot{\sigma}(\tau)d\tau + \int_{t_3}^{t} J(t-\tau)\dot{\sigma}(\tau)d\tau.$$

Substituting the loading conditions of (2.19) into (2.20) results in the simplified form

$$\varepsilon(t) = \int_0^{t_1} J(t-\tau)Cd\tau - \int_{t_2}^{t_3} J(t-\tau)Cd\tau. \tag{2.21}$$

Let us take the kernel used by [Findley et al., 1989] as an example:

$$J(t) = At^n. \tag{2.22}$$

Thus;

$$G(t) = \frac{1}{A\Gamma(1+n)\Gamma(1-n)}t^{-n}. \tag{2.23}$$

Evaluating (2.21) with kernel (2.22) results in:

$$\varepsilon(t) = \frac{CA}{n+1}[-(t-t_1)^{n+1} + t^{n+1} + (t-t_3)^{n+1} - (t-t_2)^{n+1}]. \tag{2.24}$$

Unfortunately, for such a kernel, only under the conditions of

$$n = 0, \qquad t_1 + t_2 = t_3, \tag{2.25}$$

can it be guaranteed that the Volterra integral with kernel (2.22) will close the loop for the prescribed loading cycle, limiting its usefulness. When n is not a whole number, as is typically

www.manaraa.com

the case in fitting, it is not a trivial task to explicitly verify whether or not the material will return to zero strain on the stress-strain curve. Indeed, for the case $n = 2$, (2.24) can be shown to diverge from zero in the positive direction as $t \to \infty$.

Though potentially limited in scope, the careful choice of parameters A and n in (2.22) allows the Volterra integral to predict simple creep and stress relaxation performance of the material. However, as more complex loading cycles are introduced, the kernel must be chosen wisely to insure appropriate model responses. Unfortunately from a physical perspective, the choice of the Volterra integral kernel is not apparently related to any of the microscopic structural qualities of the polymer (e.g. chain length, amount of cross-linking). Thus no insight can be gained into the microscopic behavior of the polymer chains.

2.7 Summary

Creep, and stress relaxation tests on several grades (i.e. densities) of PMI foam indicate the material does not respond in a purely elastic, nor plastic manner. Rather, the response is viscoelastic. Attempting to fit the material's response using classic viscoelastic models can only be satisfactorily done with the Wiechert model. The other classic models suffer deficiencies in predicting some portion of the creep, stress relaxation, or complex load/unload/recovery cycle response. With an appropriate kernel choice, use of the Volterra integral can result in satisfactory predictive performance, but leaves unanswered the question as to the microscopic behavior of the polymer chains. Because of the desire to gather further insight, a micromechanics-based model is developed based on the diffusion phenomena described by the Fokker-Planck equation. Details of this development are reviewed in Chapter 3.

www.manaraa.com

CHAPTER 3

Theory

The time-dependent behavior of solid polymers is so diverse that, at the moment, no better recipe exists to describing the material behavior other than fitting experimental results by either Volterra non-local stress-strain relations or their finite-dimensional truncations. The latter can be interpreted as a combination of springs and dashpots. Needless to say, the physics of the deformation process is completely lost in such an approach. In the case of non-linear material responses, the situation becomes much worse. The variety of nonlinear versions of Volterra relations is boundless. Therefore, it seems important to restrict the class of feasible models suggesting possible micromechanisms of the time dependence, and deriving the macroscopic relations from statistical reasoning. This is the aim of our work.

We employ a highly simplified picture of the deformation of a cross-linked polymer chain schematically shown in Fig. 3.1. Two ends of the chain, A and B, are pinned at cross-links. The chain is moving inside the polymer, which is composed of an ensemble of polymer chains. Some parts of the chain come close to other chains and form weak links that, in contrast to cross-links, are easily broken by deformation. The horizontal line cc' represents another chain; point C is a weak link. During elongation in the x-direction, the cross-links A and B follow macroscopic deformation. If the distance between A and B changes, point C is no longer in equilibrium; there is a non-zero force acting on C. To compensate, point C starts moving along cc' changing the overall distribution of internal forces. This is the assumed microscopic origin of the time-dependent behavior to be discussed further.

To model the behavior of point C, we assume that it is similar to the motion of a point in a periodic potential $H(x)$ under the action of a random force, Fig. 3.2. The origin of the random force is the conformation motion of the polymer chain. The assumption of periodicity is made only to make this problem treatable analytically. One obtains qualitatively similar results for the random potential as well.

We end up with a model which is schematically presented by Fig. 3.3. The most essential feature of the model is the highly nonlinear dashpot behavior. Statistical reasonings employed

www.manaraa.com

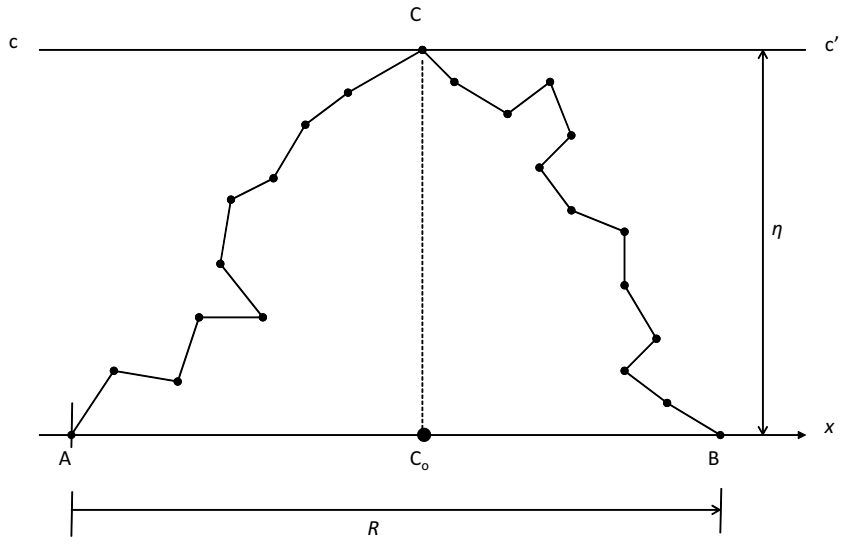

Figure 3.1: Sketch of the interaction of a polymer chain with neighboring chains.

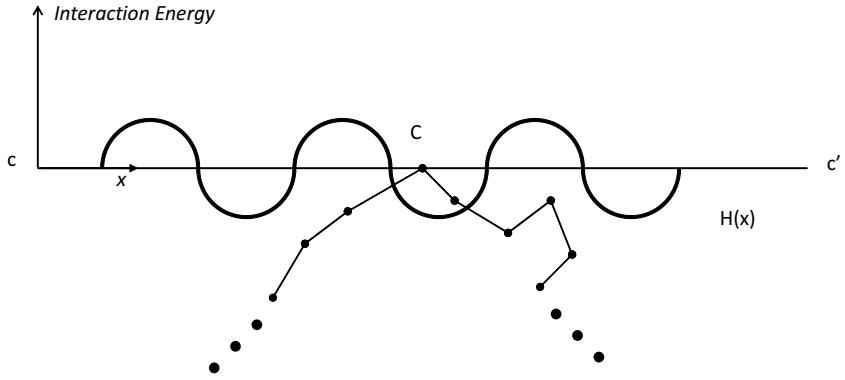

Figure 3.2: Motion of a weak link is modeled as a point in a periodic potential.

www.manaraa.com

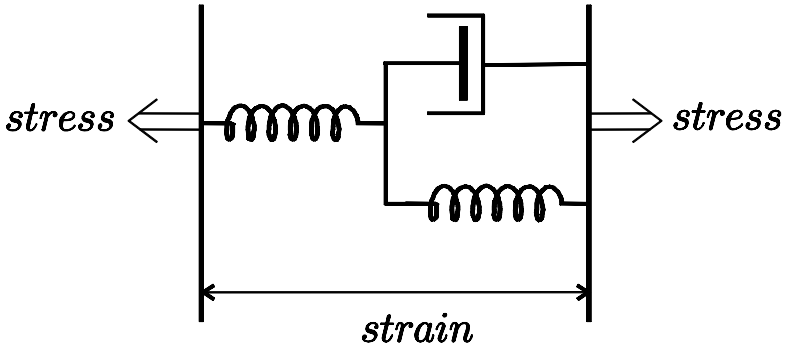

Figure 3.3: Spring and dashpot scheme of the model.

determine the dependence of the model parameters on temperature.

As will be shown, our model captures correctly the most salient feature of macroscopic response: in a stress relaxation test, the fast decay of stresses at the beginning of the process followed by a long slow evolution, and in a creep test, the fast occurring strain at the beginning of the process followed by a long slow evolution.

In Section 3.1, we start with a reminder of some basic facts from thermodynamics of polymer chains, which are the building blocks of our model. In Section 3.2, we derive the dynamic equation for polymer chains with one fixed end and one end loaded by an external force. Section 3.3 and Appendix B discuss in detail the problem of particle motion in a periodic potential. Section 3.4 derives the dynamic equation for a polymer chain, a piece of which is weakly connected to another chain. In Section 3.5, thermodynamic functions of a cross-linked polymer are constructed. The closed system of macroscopic equations is formulated in Section 3.6. Its linearized version is considered in Appendix A. In Section 3.7, we construct a modification of nonlinear theory that yields Treloar theory for equilibrium states. Finally, we extend the results to polymer foams in Section 3.8.

It can be shown that our model, up to physical interpretation of the terms involved, is mathematically equivalent in the linearized case to the model proposed by [Bergstrom, 1999]. In the nonlinear regime, which is of major interest at least due to nonlinearity of the dashpot, the models are different.

www.manaraa.com

3.1 Facts from Thermodynamics of Polymer Chains

Thermodynamics of a polymer chain. The internal energy $\mathcal{U}$ of a polymer chain is usually assumed to be a function of temperature T only:

$$\mathcal{U} = n\,u(T), \tag{3.1}$$

where n is the number of monomers in the chain, and $u(T)$ is the energy per monomer, which depends on the composition of the monomer. It is essential that the internal energy not depend on the distance R between the chain ends. Such a dependence arises in the free energy $\mathcal{F}$,

$$\mathcal{F} = \mathcal{U} - T\mathbb{S}, \tag{3.2}$$

through the dependence of entropy $\mathbb{S}$ of the chain, on R,

$$\mathbb{S} = nS(R), \tag{3.3}$$

where $S(R)$ is the entropy per one monomer. Based on a detailed analysis of the stochastic model with freely rotating Kuhn segments, in what follows, we use for $S(R)$ the quadratic approximation developed from the one-dimensional random walk polymer model

$$S(R) = -\frac{3}{2}\frac{R^2}{\ell^2 n^2}. \tag{3.4}$$

It holds, if one means by n the number of Kuhn segments, i.e. the number of segments that can be viewed as rotating independently. Accordingly, $S(R)$ is the entropy per one Kuhn segment. Total entropy of the chain is thus also a quadratic function of R:

$$\mathbb{S} = -\frac{3}{2}\frac{R^2}{\ell^2 n}. \tag{3.5}$$

The quadratic approximations (3.4) and (3.5) work reasonably well for conditions when the distance between the chain ends R does not exceed about 20 percent of the chain length ℓn.

www.manaraa.com

Force acting on the chain end. Let both ends of the polymer chain be fixed. Then due to thermal motion, there is a force acting on each end. If R_i are components of the vector going from chain end A to chain end B, and the chain is placed in a thermostat with temperature T, then the external force f_i that should be applied at end B to keep the chain in equilibrium is

$$f_i = \frac{\partial \mathcal{F}}{\partial R_i} = -Tn\frac{\partial S}{\partial R_i}. \tag{3.6}$$

Equation (3.6) follows from the energy equation: if end B was not fixed but free to move for dR_i, then

$$d\mathcal{F} = f_i dR_i. \tag{3.7}$$

Here and in what follows, summation over repeated indices is implied. Using the quadratic approximation for entropy (3.4), we get for the force,

$$f_i = \frac{3T}{\ell^2 n} R_i. \tag{3.8}$$

As follows from (3.8), the chain tends to contract to form a "blob" with $R_i = 0$. For very large n, (3.6) and (3.8) hold for adiabatically isolated chains as well. Equation (3.6) can be used for any point of the chain as long as the average velocity of this point is much smaller than the velocity of thermal motion, and the dependence of entropy on the coordinate of this point is known. In particular one can apply (3.6) to the sticking point of the chain, point C in Fig. 3.1.

3.2 Dynamics of the Sticking Point in an External Field

Consider a massless particle moving along a line in a smooth external field with potential $H(x)$, x being the coordinate on the line. Assume a friction force $\mu dx/dt$, and a random excitation force $\zeta(t)$ acting on the particle, μ being the friction coefficient. Then, the particles's equation of motion is

$$\mu\frac{dx}{dt} = -\frac{dH(x)}{dx} + \zeta(t). \tag{3.9}$$

www.manaraa.com

Let $\zeta(t)$ up to a deterministic average value $\bar{\zeta}$, be proportional to white noise $\dot{w}(t)$ ($w(t)$ is a Wiener process)

$$\zeta(t) = \bar{\zeta} + \beta\dot{w}(t). \tag{3.10}$$

The deterministic part of the excitation $\bar{\zeta}$ may depend on x. The solution of the stochastic differential equation (3.9) is conveniently described in terms of the probability density function $f(t,x)$ of the positions of the particle. This function obeys the Fokker-Planck equation

$$\frac{\partial f\,(t,x)}{\partial t} + \frac{\partial}{\partial x}\left(\frac{1}{\mu}\left(-\frac{dH(x)}{dx} + \bar{\zeta}\right) f - D\frac{\partial f}{\partial x}\right) = 0, \tag{3.11}$$

where the diffusion coefficient D depends on the magnitude of the random excitation β, and friction coefficient μ

$$D = \frac{\beta^2}{2\mu^2}. \tag{3.12}$$

To apply this classical theory of particle motion under random excitation to the motion of the polymer chain end, one has to explain the meaning of all variables in (3.11): μ, $H(x)$, $\bar{\zeta}$ and D. We begin with the parameters of the random excitation $\bar{\zeta}$ and D. Let $H(x) = 0$, and the chain end be free. Then from any initial value, the probability density evolves to the equilibrium density, which is given by Einstein's formula

$$f_\infty(x) = const\, e^{\mathbb{S}(x)}, \tag{3.13}$$

$\mathbb{S}(x)$ being the entropy of the polymer chain. The probability flux,

$$\frac{1}{\mu}\bar{\zeta}f - D\frac{df}{dx}, \tag{3.14}$$

from (3.11) must vanish at the equilibrium distribution (3.13). This yields the value of $\bar{\zeta}$

$$\frac{1}{\mu}\bar{\zeta} = D\frac{d\mathbb{S}}{dx}. \tag{3.15}$$

Comparing (3.15) with (3.6) written for one-dimensional motion, we find that the external

www.manaraa.com

force f is equal to the negative of the "internal force" $\bar{\zeta}$. In addition, using (3.3) we get

$$D = \frac{T}{\mu} \quad \text{or} \quad \frac{\beta^2}{2\mu} = T. \tag{3.16}$$

This is an analogy of Einstein's formula for the diffusion coefficient in Brownian motion. In our situation however, the origin of diffusion of particle positions is quite different. Random force, and therefore, diffusion is the result of the conformal motion of the polymer chain.

Relations (3.15) and (3.16) do not depend on the presence of external forces. One can verify this by including an external force in derivation of (3.15) and (3.16). Therefore, for a nonzero external force, (3.11) takes the final form

$$\frac{\partial f(t,x)}{\partial t} + \frac{1}{\mu}\frac{\partial}{\partial x}\left(\left(-\frac{dH(x)}{dx} + T\frac{d\mathbb{S}(x)}{dx}\right) f - T\frac{\partial f}{\partial x}\right) = 0. \tag{3.17}$$

Potential energy $H(x)$ can be interpreted as the interaction energy between the sticking point C in Fig. 3.2, and the neighboring chain cc'. If point C is moving over the neighboring chain, there are places of "good" and "bad" connections. Interaction energy is small at "good" connections and large at "bad" connections. We take the simplest form of $H(x)$, assuming that it is a periodic function of x. The period h is assumed to be much smaller than the scale change of $d\mathbb{S}/dx$: $d\mathbb{S}/dx$ is practically constant on distances of the order h.

3.3 Motion of Particle Under Random Excitation in Periodic Field

As follows from (3.17), the friction coefficient μ affects only the rate of the processes and can be eliminated by choosing a new time $\tau = t/\mu$. The motion of a piece of polymer chain modeled by a single sticking point C interacting with a neighboring polymer chain, is reduced to the solution of the differential equation

$$\frac{\partial f}{\partial \tau} + \frac{\partial}{\partial x}\left(\left(-\frac{dH(x)}{dx} + \Lambda\right) f - T\frac{\partial f}{\partial x}\right) = 0, \tag{3.18}$$

where we introduce the notation,

$$\Lambda = T d\mathbb{S}/dx\ . \tag{3.19}$$

www.manaraa.com

Here Λ may be treated as a constant, because it does not change on the distances of the order of the period h. We are interested in the behavior of the solution at large τ. This is a homogenization problem for a parabolic equation with a fast oscillating coefficient. It was studied by [Jikov et al., 1994] in Chapter 2 in the general multidimensional case. Their approach applied to our one-dimensional case, allows an analytical treatment outlined in Appendix B. Here, we summarize the results of this analysis. Note that motion of a particle in a periodic field under random excitation has been studied previously in [Risken, 1989], but the homogenization approach used here is simpler.

The particle will move with some average velocity v that depends on the external force Λ acting on the chain. The equation that links v and Λ is

$$\frac{hv}{T} = \left[\frac{e^{\Lambda h/T}}{e^{\Lambda h/T} - 1} \left\langle e^{-\int_0^y \frac{\Phi(y')h}{T} dy'} \right\rangle - \left\langle \int_0^y e^{-\int_0^{\tilde{y}} \frac{\Phi(y')h}{T} dy'} d\tilde{y} \right\rangle \right]^{-1}, \tag{3.20}$$

where

$$\Phi = -\frac{1}{h}\frac{dH}{dy} + \Lambda, \quad y \equiv \frac{x}{h}, \tag{3.21}$$

and $\langle \cdot \rangle$ means average over the period, i.e. the integral over y on $[0, 1]$. The dependence of v on Λ is affected by the energy of the weak link $H(y)$, and temperature T. Note that v in (3.20) is the particle velocity in (x, τ) variables. For v to be the velocity in physical (x, t) variables, the factor μ must be included in the left hand side of (3.20).

Dependence of drift velocity v on the force Λ can be studied numerically from (3.20). To this end, we introduce the following dimensionless quantities:

$$\begin{aligned} &\text{external force:} && \hat{\Lambda} = \frac{\Lambda h}{T} \\ &\text{periodic force:} && \hat{\Phi}(y) = \frac{\Phi(y)h}{T} = -\frac{1}{T}\frac{dH}{dy} + \hat{\Lambda} \\ &\text{velocity:} && \hat{v} = \frac{vh\mu}{T} \end{aligned} \tag{3.22}$$

and rewrite (3.20) in dimensionless form

$$\hat{v} = \left[\frac{e^{\hat{\Lambda}}}{e^{\hat{\Lambda}} - 1} \left\langle e^{-\int_0^y \hat{\Phi}(y')dy'} \right\rangle - \left\langle \int_0^y e^{-\int_0^{\tilde{y}} \hat{\Phi}(y')dy'} d\tilde{y} \right\rangle \right]^{-1}. \tag{3.23}$$

www.manaraa.com

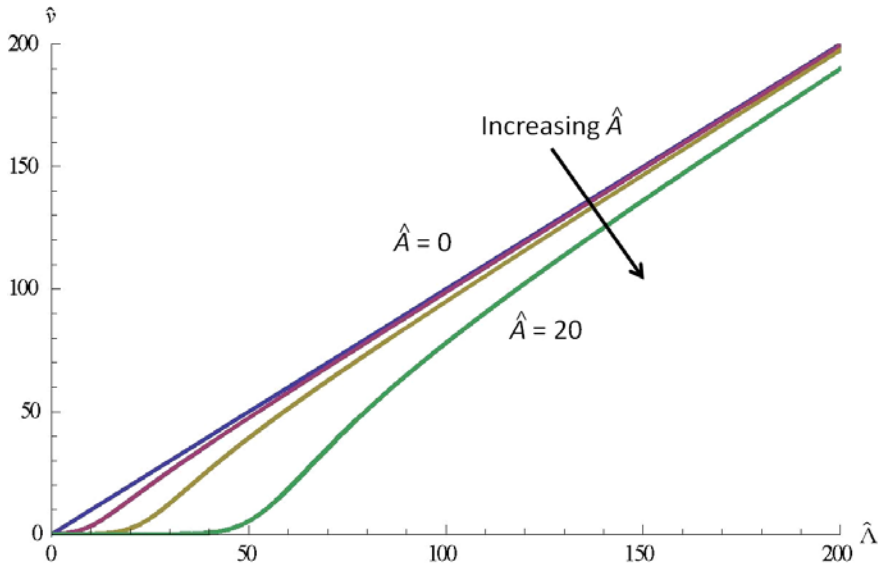

Figure 3.4: Dependence of dimensionless sticking point velocity on the dimensionless external force for different values of the periodic potential amplitude $\hat{A}$.

In Figs. 3.4 and 3.5, the dependence of the particle velocity on the applied external force is shown for a periodic potential field of the form

$$\frac{1}{T}H(y,\hat{A}) = \hat{A}\sin^2(\pi y). \tag{3.24}$$

If $\hat{A} = 0$, i.e. there are no chain interactions, then the sticking point velocity increases linearly with force. The value of velocity is determined by the balance of friction force and the external force. If $\hat{A} \neq 0$, then the sticking point spends some time in energy wells. Accordingly, its velocity becomes smaller. The larger $\hat{A}$, i.e. the larger the chain interaction, the larger the velocity decrease. The velocity decrease is felt much stronger at small external forces. For the external forces being large enough, the sticking point "flies" over the energy barriers and its velocity approaches the limit values for $\hat{A} = 0$, Fig. 3.4.

It is not convenient to employ the dependence of velocity on the external force (3.23), and we replace it by a sufficiently simple analytical relation. As such, we use the formula:

$$\hat{v}(\hat{\Lambda}) = c\hat{\Lambda} + ad\ln\left[\frac{\cosh\left(\frac{b-\hat{\Lambda}}{a}\right)}{\cosh\left(\frac{b+\hat{\Lambda}}{a}\right)}\right] = \Psi(\hat{\Lambda}), \tag{3.25}$$

www.manaraa.com

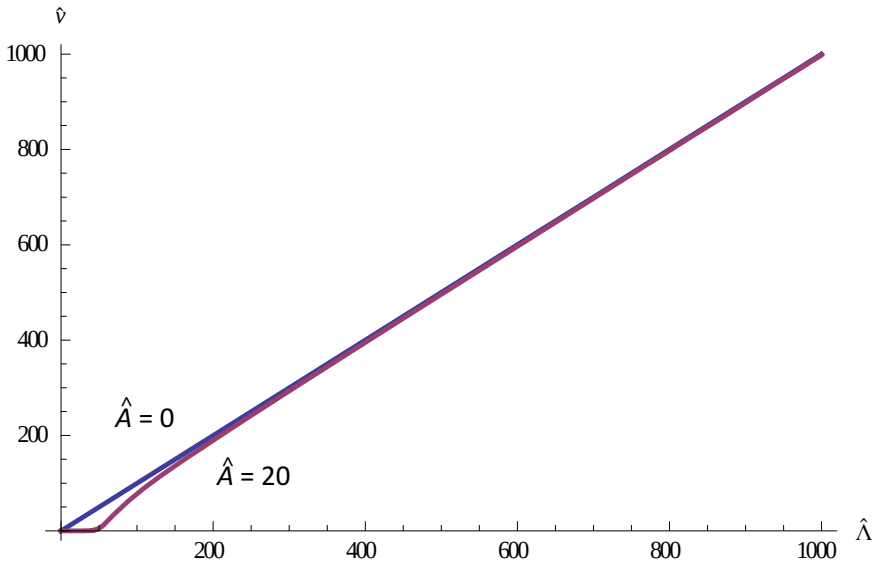

Figure 3.5: Given a large enough external force, the sticking point velocity for large periodic potential amplitudes, e.g. $\hat{A} = 20$, approaches that of no periodic potential, i.e. $\hat{A} = 0$.

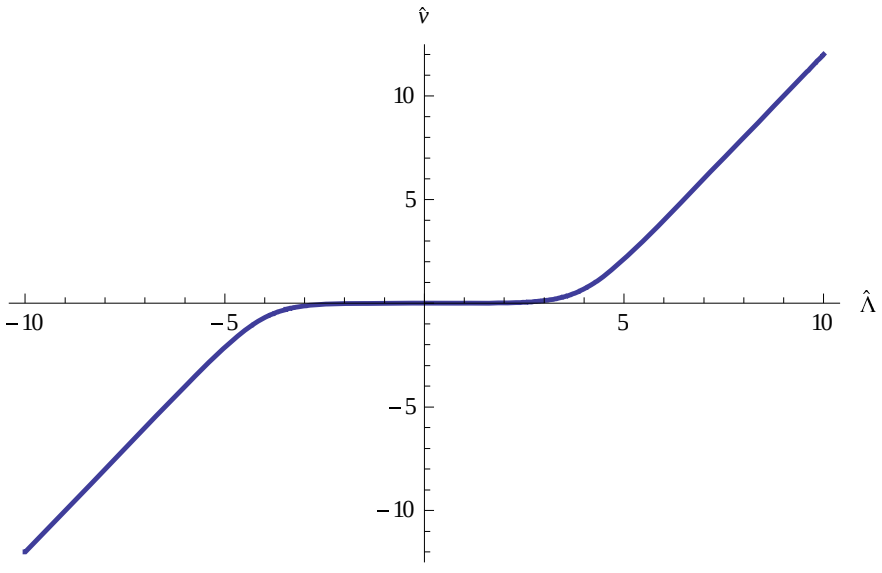

Figure 3.6: Sticking point velocity dependence on the external force (3.25) for $a = 1,\ b = 4,\ c = 2,\ d = 1$.

www.manaraa.com

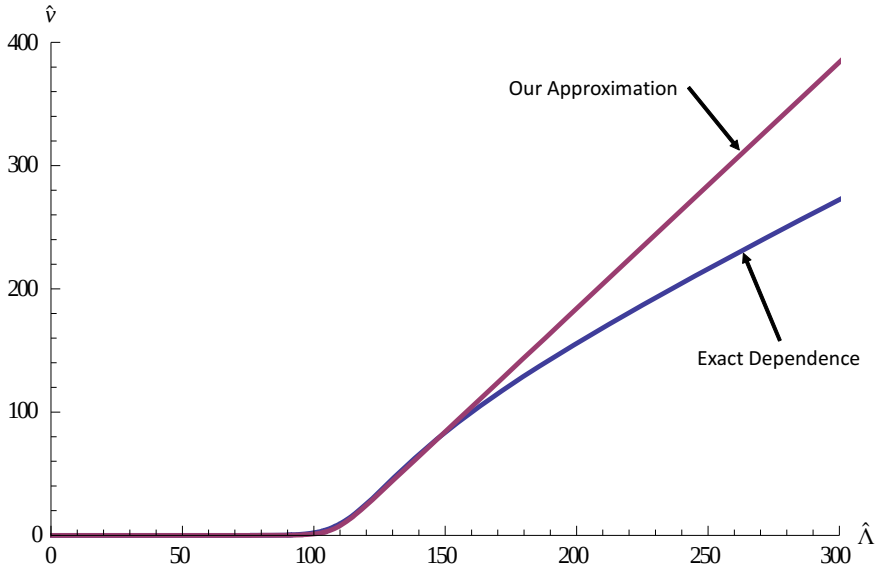

Figure 3.7: We choose to do the best fit of (3.25) to the transistion zone and ignore the differences at large values of force.

where $a,\ b,\ c,\ d$ are the parameters. Function (3.25) is shown in Fig. 3.6 for $a = 1,\ b = 4,\ c = 2,\ d = 1$. The required general shape of the curve of Fig. 3.6 is maintained, if a, b, c, d obey the constraints (see Appendix C for details)

$$a > 0, \quad b \geq 0, \quad d \geq 0, \quad 0 \leq 2d \leq c. \tag{3.26}$$

In further applications of (3.25) we need to capture correctly the behavior of the velocity-force relationship for small velocities. Therefore we choose parameters $a,\ b,\ c,\ d$ in (3.25) to properly approximate the velocity-force dependence in the small velocity range, and do not care of the proper capturing of the large force dependence. This is illustrated by Fig. 3.7 where, at a sufficiently high velocity, the exact dependence and our approximation begin to diverge.

3.4 Dynamics of One Polymer Chain

Consider the polymer chain sketched in Fig. 3.1. Let segments AC and CB of the chain contain n' and n'' Kuhn segments, respectively. Thus $n = n' + n''$ is the total number of segments in the chain. We assume that the line cc' is parallel to AB and denote the distance

www.manaraa.com

between these two lines by η. Let the projection of C on line AB be C_o. Denote the distance AC_o by x. We consider here the quadratic approximation for entropy (3.4). Entropy of the chain ACB is the sum of entropies of sub-chains AC and CB. Thus, in the quadratic approximation, entropy of the chain is

$$\mathbb{S} = -\frac{3}{2}\frac{x^2+\eta^2}{\ell^2 n'} - \frac{3}{2}\frac{(R-x)^2+\eta^2}{\ell^2 n''}. \tag{3.27}$$

In equilibrium, the equilibrium value of x maximizes (3.27).

If we let end A be fixed and end B move, the distance R between A and B changes. Presumably, the weak link at point C is strong enough not to respond immediately to the movement of end B. Then point C is no longer at equilibrium: there is a nonzero force acting on C. Point C then begins its slow motion to a new equilibrium position. As follows from (3.19) and (3.27), the velocity of point C is a function of the force Λ

$$\Lambda = T\frac{d\mathbb{S}}{dx} = -\frac{3T}{\ell^2 n'}x + \frac{3T}{\ell^2 n''}(R-x). \tag{3.28}$$

Approximating the dependence of velocity on the force by (3.25), we obtain the differential equation for x :

$$\frac{dx}{dt} = \Psi\left(p(R-x) - qx\right), \tag{3.29}$$

where p and q are the constants linearly depending on temperature,

$$p = \frac{3T}{\ell^2 n''}, \qquad q = \frac{3T}{\ell^2 n'}. \tag{3.30}$$

At first glance, in the quadratic approximation η falls out from the dynamic equation. One can expect however, that the energy landscape $H(x)$ depends on η: with extension of AB, η decreases and the interaction energy between the chains increases. We return to this issue when developing a model of polymer foams.

One note is in order about energy relations. The original dynamical equation for motion of one particle (3.9) yields the following energy equation

www.manaraa.com

$$\frac{d(H-T\mathbb{S})}{dt}=-\mu\left(\frac{dx}{dt}\right)^2+\beta\dot{w}(t)\frac{dx}{dt}. \tag{3.31}$$

The first term in the right hand side of (3.31) is the negative viscous dissipation, the second term is the work of internal forces related to conformations.

After averaging, the dynamical equation (3.9) transforms to (3.25), which, being resolved with respect to TdS/dt, reads

$$T\frac{d\mathbb{S}}{dx}=\Psi^{-1}\left(\frac{h\mu}{T}\frac{dx}{dt}\right). \tag{3.32}$$

Here Ψ^{-1} is the inversion of the function Ψ. Hence, the averaged energy equation is

$$T\frac{d\mathbb{S}}{dt}=\frac{dx}{dt}\Psi^{-1}\left(\frac{h\mu}{T}\frac{dx}{dt}\right). \tag{3.33}$$

Comparing (3.31) and (3.33), we conclude that the right hand side of (3.33) has the meaning of averaged negative right hand side of (3.31) (average of periodic function H is a constant and does not contribute to (3.33)).

3.5 Thermodynamic Functions of an Ensemble of Cross-linked Polymer Chains: Preliminary Reasoning

In this section, a simplified version of thermodynamic functions is constructed, and will be put in a final form in Section 3.7. For a polymer, the total entropy is the sum of entropies of all chains. Therefore, for each chain we need to include the kinematic variables x, η, R, n', n''. In the spirit of Treloar statistical mechanics of rubbers [Flory, 1969, Flory, 1976, Treloar, 1976, Treloar, 2009], we assume there are average values of $r=x/R$ and η over all chains. First, we set on average $n'=n''=n/2$. Moreover, we take n to be the same for all chains and equal to the average number of Kuhn segments over all chains. Later, we generalize that construct. From (3.27), for a large ensemble of N chains with initial distances between the ends $\mathring{R}_\alpha$, $\alpha=1,...,N$,

$$\mathring{\mathbb{S}}=-\frac{3}{\ell^2 n}\left[\left(r^2+(1-r)^2\right)\sum_{\alpha=1}^{N}\mathring{R}_\alpha^2+2N\eta^2\right]. \tag{3.34}$$

www.manaraa.com

The symbol $\mathring{}$ over variables indicates their values at the initial instant.

If in (3.34) we set $r = 1/2$ and $\eta = 0$, we recover the classic Treloar formula for entropy of an ensemble of polymer chains.

Denote by $\mathring{R}^a_\alpha$ the components of the vector connecting the ends of the α^{th} chain in the undeformed state. Latin indices run through values 1, 2, 3. Let the macropolymer be homogeneously deformed. We assume that each vector $\mathring{R}^a_\alpha$ is subject to an affine deformation with distortion matrix x^i_a. This means that the vector R^i_α connecting the ends of the α^{th} polymer chain in the deformed state is

$$R^i_\alpha = x^i_a \mathring{R}^a_\alpha \tag{3.35}$$

with the same matrix x^i_a for all chains. Distortion x^i_a can be presented as a product of a positive symmetric matrix h_{ab} and an orthogonal matrix O^i_a (so called polar decomposition):

$$x^i_a = h^b_a O^i_b. \tag{3.36}$$

Orthogonality of O^i_b means that

$$O^i_b O^i_c = \mathring{g}_{bc}, \quad O^i_a O^j_b \mathring{g}^{ab} = \delta^{ij}, \tag{3.37}$$

where $\mathring{g}_{ab}$ is the metric tensor in the initial state, and δ^{ij} is Kronecker's delta. We assume that Lagrangian coordinates in the initial state are chosen to be Cartesian, and $\mathring{g}_{ab} = \delta_{ab}$. Due to this fact, we do not distinguish further between upper and lower indices and just do summation over repeated indices. However, we do distinguish between Lagrangian and Eulerian indices; Lagrangian indices can only be summated with Lagrangian indices, and Eulerian indices can only be summated with Eulerian indices (for details see [Berdichevsky, 1989] p.76). For Lagrangian and Eulerian indices, we use the letters a, b, c..., and i, j, k, ..., respectively. Equation (3.36) corresponds to superposition of two deformations: first R^a_α is rotated by orthogonal transformation O^i_a, and then elongations are made along the principle axes of

www.manaraa.com

tensor h_{ab}. The metric tensor of the deformed state g_{ab}, is the squared matrix h_{ab} :

$$g_{ab} = x_a^i x_b^i = h_{ac} h_{cb}. \tag{3.38}$$

Matrix h_{ab} is also called the square root of g_{ab}. After rotation with orthogonal matrix O_a^i, the position of the weak link C on the α^{th} chain is $rO_a^i \mathring{R}_\alpha^a$. The squared distance AC is $r^2 \mathring{R}_\alpha^a \mathring{R}_\alpha^a$, while the squared distance CB becomes

$$\left(R_\alpha^i - rO_a^i \mathring{R}_\alpha^a\right)\left(R_\alpha^i - rO_b^i \mathring{R}_\alpha^b\right). \tag{3.39}$$

Here and in (3.40), no summation is taken over α. Taking into account (3.35) - (3.37), (3.39) can be written as

$$\begin{aligned}
&\left(x_a^i - rO_a^i\right) \mathring{R}_\alpha^a \left(x_b^i - rO_b^i\right) \mathring{R}_\alpha^b = \\
&= \left(h_a^c O_c^i - r\delta_a^c O_c^i\right) \mathring{R}_\alpha^a \left(h_b^d O_d^i - r\delta_b^d O_d^i\right) \mathring{R}_\alpha^b = \\
&= \left(h_a^c - r\delta_a^c\right)\left(h_b^d - r\delta_b^d\right) O_c^i O_d^i \mathring{R}_\alpha^a \mathring{R}_\alpha^b = \\
&= \left(h_a^c - r\delta_a^c\right)\left(h_b^d - r\delta_b^d\right) \mathring{g}_{cd} \mathring{R}_\alpha^a \mathring{R}_\alpha^b = \\
&= \left(h_a^c - r\delta_a^c\right)\left(h_{bc} - r\mathring{g}_{bc}\right) \mathring{R}_\alpha^a \mathring{R}_\alpha^b.
\end{aligned} \tag{3.40}$$

Since entropy of the chain ensemble is the sum of chain entropies, the entropy of the deformed polymer is

$$\mathbb{S} = -\frac{3}{\ell^2 n}\left[r^2 \sum_{\alpha=1}^{N} \mathring{R}_\alpha^a \mathring{R}_\alpha^b + \left(h_a^c - r\delta_a^c\right)\left(h_{cb} - r\mathring{g}_{cb}\right) \sum_{\alpha=1}^{N} \mathring{R}_\alpha^a \mathring{R}_\alpha^b + 2N\eta^2\right]. \tag{3.41}$$

We assume that the material is isotropic. Then the tensor $\sum_{\alpha=1}^{N} \mathring{R}_\alpha^a \mathring{R}_\alpha^b$ must be proportional to the metric tensor in the initial state $\mathring{g}_{ab}$,

$$\sum_{\alpha=1}^{N} \mathring{R}_\alpha^a \mathring{R}_\alpha^b = const\ \mathring{g}_{ab}. \tag{3.42}$$

www.manaraa.com

Thus,

$$\mathbb{S} = -\frac{2G\,|V|}{3T}\left[3r^2 + (h_{ab} - r\mathring{g}_{ab})\,(h_{ab} - r\mathring{g}_{ab})\right] - \tilde{G}\eta^2, \tag{3.43}$$

where G and $\tilde{G}$ are some constants, and $|V|$ the volume of the specimen. The factor $2/3$ is introduced to give the coefficient G the meaning of shear modulus for small deformations. As follows from our derivation, the relation for entropy (3.41) is temperature independent. Therefore, the coefficient G introduced by (3.41) must linearly depend on temperature

$$G = const\,T. \tag{3.44}$$

Parameter η changes in compression/dilatation. It is known for polymers that the bulk Young modulus is much larger than the shear modulus. Therefore in the following approximation, polymers can be assumed incompressible, and we drop η in (3.43). Finally, the total entropy of the polymer is

$$\mathbb{S} = -\frac{2G\,|V|}{3T}\left[3r^2 + (h_{ab} - r\mathring{g}_{ab})\,(h_{ab} - r\mathring{g}_{ab})\right]. \tag{3.45}$$

Denote by S and U the entropy and internal energy per unit volume, respectively. For polymers, U is a function of temperature T only. Free energy per unit volume F, is a function of temperature T , the metric tensor of the deformed state g_{ab}, and the internal parameter r:

$$F\,(T, g_{ab}, r) = U(T) - TS\,(r, g_{ab}) = U(T) + \frac{2}{3}G\left[3r^2 + (h_{ab} - r\mathring{g}_{ab})\,(h_{ab} - r\mathring{g}_{ab})\right]. \tag{3.46}$$

At equilibrium, the internal parameter r maximizes entropy and minimizes free energy.

It is convenient to write free energy in terms of strains ε_{ab}. From the definition of the strain tensor,

$$\varepsilon_{ab} = h_{ab} - \mathring{g}_{ab}, \tag{3.47}$$

then

$$F\,(T, \varepsilon_{ab}, r) = U(T) + \frac{2}{3}G\left[3r^2 + 3\,(1-r)^2 + \varepsilon_{ab}\varepsilon_{ab} + 2\,(1-r)\,\varepsilon_{aa}\right]. \tag{3.48}$$

www.manaraa.com

As follows from (3.48) for small deformations, the equilibrium value of r is $1/2$. At this value

$$F\left(T, \varepsilon_{ab}, 1/2\right) = U(T) + \frac{2}{3} G\left[\varepsilon_{aa} + \varepsilon_{ab}\varepsilon_{ab}\right] + const. \tag{3.49}$$

This is apparently different from the Treloar energy [Treloar, 1976, Treloar, 2009],

$$F\left(T, \varepsilon_{ab}\right) = U(T) + \frac{G}{2} g_{aa} = U(T) + \frac{G}{2} h_{ab} h_{ab} =$$

$$= U(T) + \frac{G}{4}\left(\varepsilon_{aa} + \frac{1}{2}\varepsilon_{ab}\varepsilon_{ab}\right) + const. \tag{3.50}$$

As shown in Appendix A, the differences are only for finite deformations, and in the linear approximation (3.49) and (3.50) are identical. The origin of the difference between energy at equilibrium (3.48) and Treloar energy (3.50) will be explained in Section 3.7, where we modify the derivation of (3.48) to get energy that is equal to Treloar energy at equilibrium.

3.6 Closed System of Equations

The equations of the model introduced in Section 3.5 can be closed in the following manner. If r is fixed, and displacements of the boundary of a polymer specimen are prescribed, then the equilibrium displacements inside the specimen minimize the total free energy

$$\mathbb{F} = \int_V F\left(T, h_{ab}, r\right) dV \tag{3.51}$$

on the set of all displacements obeying the incompressibility condition

$$\det \|h_{ab}\| = const. \tag{3.52}$$

Including the constraint (3.52) in the functional (3.51) with some Lagrange multiplier p, one arrives at the equilibrium equations. These equations are written down in general nonlinear case in [Berdichevsky, 1989] in Section 7.2. Since in further applications we use only linear approximation, we do not reproduce these nonlinear equations here. The linear equation is constructed as follows. The equations for the minimizer of (3.51) must be complemented by

www.manaraa.com

the evolution equation for r. Consider the "force" acting on the internal parameter r. By definition, this is the derivative of free energy with respect to r,

$$T\frac{\partial S}{\partial r} = -\frac{\partial F}{\partial r}. \tag{3.53}$$

We assume that the rate of the internal parameter dr/dt, is linked to the force (3.53) by an equation of the type (3.25). In the nonlinear case we can take into account that $R \simeq const\sqrt{g_{ab}\mathring{g}^{ab}}$. Then the evolution equation has the form.

$$\frac{d}{dt}\left(r\sqrt{g_{ab}\mathring{g}^{ab}}\right) = -\Psi\left(\frac{\partial F}{\partial r}\right). \tag{3.54}$$

Here Ψ is the function (3.25). The minus sign in (3.54) is necessary to satisfy the second law of thermodynamics. This is explained in more detail in Section 3.8 for the similar situation for polymer foams.

3.7 Thermodynamic Functions of an Ensemble of Cross-linked Polymer Chains

Here we weaken an assumption of Section 3.5 that the parameter r is the same for all chains as rendering oversimplified kinematics of deformation. Due to that assumption, the corresponding continuum parameter was a scalar. Instead, we admit that the internal parameter describing the deviation from equilibrium is a tensor. Accordingly, the diagonal tensor $r\mathring{g}_{ab}$ that appears in (3.45), is replaced by a symmetric tensor r_{ab}. Then (3.45) should be replaced by the relation

$$\mathbb{S} = -\frac{G}{T}\left[\beta r_{ab}r_{ab} + (h_{ab} - r_{ab})\,(h_{ab} - r_{ab})\right]|V|\,. \tag{3.55}$$

Here we introduce an additional phenomenological dimensionless constant β which accounts for asymmetry of positions of sticking points. Apparently, $\beta > 0$.

First, let $\beta = 1$. Maximum entropy (3.55) over r_{ab} is achieved at

$$r_{ab} = \frac{1}{2}h_{ab}. \tag{3.56}$$

www.manaraa.com

At this value of r_{ab}, entropy coincides with Treloar entropy:

$$\mathbb{S} = -\frac{G}{2T} h_{ab} h_{ab} \left| V \right| = -\frac{G}{2T} g_{aa} \left| V \right|. \tag{3.57}$$

In the general case $\beta \neq 1$, and the equilibrium value of r_{ab} is

$$r_{ab} = \frac{1}{1+\beta} h_{ab} \tag{3.58}$$

and for the equilibrium value of entropy we have

$$\mathbb{S} = \frac{G_{eq}}{T} g_{aa} \left| V \right|, \tag{3.59}$$

where we denote by G_{eg} the equilibrium value of the shear modulus,

$$G_{eq} = \frac{\beta}{\beta+1} G. \tag{3.60}$$

The constant G has the meaning of the current (nonequilibrium) shear modulus. Because $\beta > 0$, the equilibrium value of the shear modulus is smaller than the current value.

Closing of the system of equations is done in the same way as in Section 3.6 with replacement of free energy (3.51) by the free energy,

$$\mathbb{F} = \int_V G \left(\beta r_{ab} r_{ab} + (h_{ab} - r_{ab})(h_{ab} - r_{ab}) \right) dV. \tag{3.61}$$

The generalization of dynamic equations (3.54) can be done in several ways. For example, one can assume, that the tensors dr_{ab}/dt and $\partial F/\partial r_{ab}$ have the same principle axes and their principle values, dr_a/dt and $\partial F/\partial r_a$, are linked by the equations

$$\frac{dr_a}{dt} = -\Psi \left(\frac{\partial F}{\partial r_a} \right). \tag{3.62}$$

The minus sign in (3.62) is necessary as in (3.54) to satisfy the second law of thermodynamics. This is explained in more detail in Section 3.8 for a similar situation for polymer foams.

www.manaraa.com

3.8 Polymer Foams

The polymer models considered thus far are characterized by only one elastic characteristic, shear modulus G, and a dimensionless parameter β describing the deviation of the current and equilibrium shear moduli. In contrast, polymer foams are compressible and possess an additional characteristic, the bulk modulus K. Compressibility is due to foam microgeometry, and elasticity of the microstructure. Bulk modulus K is some function of G and foam microgeometry.

If the polymer foam was purely elastic and isotropic, then the material's energy density is a quadratic form of deformations,

$$F\left(T,\varepsilon_{ab}\right)=U(T)+\frac{1}{2}K\left(\varepsilon_{aa}\right)^{2}+G\varepsilon'_{ab}\varepsilon'_{ab}, \tag{3.63}$$

with K and G being the elastic constants and $\cdot'$ marks the deviators, in particular $\varepsilon'_{ab}=\varepsilon_{ab}-\frac{1}{3}\varepsilon_{cc}\delta_{ab}$. Further, we consider isothermal processes, and therefore drop $U(T)$. Polymer foams are not purely elastic and exhibit deviations of the current elastic moduli from the equilibrium elastic moduli. Therefore, as in the previous consideration, we introduce internal parameters ξ_{ij} which reach their equilibrium values if strains or stresses are kept constant. These equilibrium values minimize free energy. We take for free energy the expression which is similar to (3.48):

$$F=\frac{1}{2}K\left(\alpha\xi_{kk}^{2}+\left(\varepsilon_{kk}-\xi_{kk}\right)^{2}\right)+G\left(\beta\xi'_{ij}\xi'_{ij}+\left(\varepsilon'_{ij}-\xi'_{ij}\right)^{2}\right). \tag{3.64}$$

The material is characterized by four positive material parameters, K,G,α,β. We consider sufficiently rigid foams which exhibit small deformations usually not exceeding 2 percent strain. In this deformation range, nonlinear effects of the foam cell deformation, like micro-buckling, formation of plastic hinges or micro-fracturing, can be ignored. Therefore, the parameters ξ are associated only with the chain-slippage processes inside the polymer material itself.

www.manaraa.com

From the definition of the stress tensor,

$$\sigma_{ij} = \frac{\partial F}{\partial \varepsilon_{ij}}, \tag{3.65}$$

and thus the constitutive equations are

$$\sigma_{ij} = K\left(\varepsilon_{kk} - \xi_{kk}\right)\delta_{ij} + 2\mu\left(\varepsilon'_{ij} - \xi'_{ij}\right). \tag{3.66}$$

There is a "second stress tensor," which describes the internal stresses caused by deviation of parameters ξ_{ij} from the equilibrium values,

$$p_{ij} = \frac{\partial F}{\partial \xi_{ij}}. \tag{3.67}$$

At equilibrium,

$$p_{ij} = 0. \tag{3.68}$$

From (3.64),

$$p_{ij} = K\left[\left(\alpha + 1\right)\xi_{kk} - \varepsilon_{kk}\right]\delta_{ij} + 2\mu\left[\left(1 + \beta\right)\xi'_{ij} - \varepsilon'_{ij}\right]. \tag{3.69}$$

Equilibrium values of ξ_{ij} are designated by the symbol $\check{}$. They are found from (3.68) and (3.69)

$$\check{\xi}'_{ij} = \frac{1}{1+\beta}\varepsilon'_{ij}, \quad \check{\xi}_{kk} = \frac{1}{1+\alpha}\varepsilon_{kk}. \tag{3.70}$$

For the equilibrium value of energy we get

$$F_{eq} = \frac{1}{2}K_{eq}\varepsilon_{kk}^2 + G_{eq}\varepsilon'_{ij}\varepsilon'_{ij}. \tag{3.71}$$

Here K_{eq} and G_{eq} are the equilibrium elastic moduli. They are linked to the instantaneous moduli K, G by

$$K_{eq} = K\frac{\alpha}{\alpha+1}, \quad G_{eq} = G\frac{\beta}{1+\beta}. \tag{3.72}$$

Equilibrium values of elastic moduli are always smaller than the instantaneous values since $\alpha > 0$, $\beta > 0$.

www.manaraa.com

Sometimes it is convenient to express energy in terms of $\varepsilon_{ij}, \xi_{ij}$ and Lamé parameters. The corresponding formula is

$$F = \frac{1}{2}\lambda\left[\bar{\beta}\xi_{kk}^2 + (\varepsilon_{kk} - \xi_{kk})^2\right] + \mu\left[\beta\xi_{ij}\xi_{ij} + \left(\varepsilon_{ij} - \xi_{ij}\right)\left(\varepsilon_{ij} - \xi_{ij}\right)\right] \tag{3.73}$$

where we introduce the notations

$$\bar{\beta} = \frac{\alpha K - \frac{2\beta\mu}{3}}{\lambda}, \qquad \lambda = K - \frac{2\mu}{3}, \qquad \mu = G. \tag{3.74}$$

The system of equations is closed by inclusion of equilibrium equations,

$$\frac{\partial \sigma_{ij}}{\partial x_j} = 0 \tag{3.75}$$

and the evolution equation for the internal parameters ξ_{ij}

$$\frac{d\xi_i}{dt} = -\Psi\left(\frac{\partial F}{\partial \xi_i}\right), \tag{3.76}$$

where ξ_i and $\partial F/\partial \xi_i$ are the eigenvalues of the tensors ξ_{ij} and $\partial F/\partial \xi_{ij}$ respectively, and principle axes of $d\xi_{ij}/dt$ and $\partial F/\partial \xi_{ij}$ are assumed to coincide.

Here we explain the thermodynamic reasoning for the negative sign in (3.54), (3.62) and (3.76). From the first law of thermodynamics

$$\rho dU = \sigma_{ij} d\varepsilon_{ij} + dQ^{(e)}, \tag{3.77}$$

while the second law of thermodynamics reads

$$\rho T dS = dQ^{(e)} + dQ^{(i)}, \quad dQ^{(i)} \geq 0. \tag{3.78}$$

It follows from (3.77) and (3.78) that free energy

$$F = U - TS, \tag{3.79}$$

www.manaraa.com

obeys the Clausius-Duhem inequality for isothermal processes, i.e. $T = const$,

$$\rho dF - \sigma_{ij} d\varepsilon_{ij} \leq 0. \tag{3.80}$$

According to (3.73), F is a function of ε_{ij} and ξ_{ij},

$$F = F(\varepsilon_{ij}, \xi_{ij}), \tag{3.81}$$

and (3.80) becomes

$$\rho \frac{\partial F}{\partial \varepsilon_{ij}} d\varepsilon_{ij} + \rho \frac{\partial F}{\partial \xi_{ij}} d\xi_{ij} - \sigma_{ij} d\varepsilon_{ij} \leq 0. \tag{3.82}$$

Equation (3.82) holds true for all processes. If σ_{ij} depend on the current values of ε_{ij} and ξ_{ij}, but do not depend on the rates $\dot{\varepsilon}_{ij}$ and $\dot{\xi}_{ij}$, then (3.82) yields the constitutive equations

$$\sigma_{ij} = \rho \frac{\partial F}{\partial \varepsilon_{ij}}. \tag{3.83}$$

Indeed, setting $\xi_{ij} = 0$, we see that

$$\rho \frac{\partial F}{\partial \varepsilon_{ij}} d\varepsilon_{ij} - \sigma_{ij} d\varepsilon_{ij} \leq 0 \tag{3.84}$$

for all $d\varepsilon_{ij}$. The linear function of $d\varepsilon_{ij}$ can be non-positive for all $d\varepsilon_{ij}$ only if (3.83) holds. From (3.82) and (3.83) it follows that the evolution must go in such a way that

$$\frac{\partial F}{\partial \xi_{ij}} d\xi_{ij} \leq 0. \tag{3.85}$$

There are many constitutive relations that obey (3.85). For example, one can assume that the principal axes of $\partial F/\partial \xi_{ij}$ and $d\xi_{ij}/dt$ coincide, and in principal coordinates

$$\begin{aligned} \frac{d\xi_{11}}{dt} &= -\Psi\left(\frac{\partial F}{\partial \xi_{11}}\right), \quad \frac{d\xi_{22}}{dt} = -\Psi\left(\frac{\partial F}{\partial \xi_{22}}\right), \quad \frac{d\xi_{33}}{dt} = -\Psi\left(\frac{\partial F}{\partial \xi_{33}}\right), \\ \frac{d\xi_{ij}}{dt} &= 0 \quad \text{for} \quad i \neq j. \end{aligned} \tag{3.86}$$

In Chapter 4, the model described is applied to the prediction of deformations of poly-

www.manaraa.com

methacrylimide foam for simple tensile creep and stress relaxation tests. Additional model predictions are explored for more complex loadings of polymethacrylimide foam in Chapter 5

www.manaraa.com

CHAPTER 4

Some Experimental Results

Polymer foam used as a structural element in composite structures is typically the weakest component of such structures. Therefore understanding its response to mechanical loads is of significant importance. This chapter reports the results of the experimental study of tensile creep and stress relaxation in a polymethacrylimide (PMI) foam. The experimental results are used to validate the analytical model proposed in Chapter 3. In the results that follow, the model is shown to adequately capture the basic features of the foam material behavior.

Usually, three types of tests are employed to quantify rheologic behavior: creep, stress relaxation, and periodic loading. Due to equipment limitations, only the first two tests are conducted.

The chapter outline is as follows. In Section 4.1, the experimental observations are summarized and issues related to measurements are discussed. Section 4.2 investigates the manifestation of variability in the results due to material variability. Specifically, the effect of material density on the elastic modulus is further investigated. Finally, validation of the model from Chapter 3 as it applies to the axial loading of a foam beam, along with selection of the model parameters to creep and stress relaxation tests is covered in Section 4.3.

4.1 Experimental Observations

PMI foams exhibit quite interesting rheological behavior, while some of its distinguished signatures are characteristic to the behavior of other polymers. In this section, the results of studies previously performed on 31 IG [Berdichevsky and Herman, 2011] are reevaluated for insight into the proposed model. We report further creep and stress relaxation results for Rohacell 31 IG which has a nominal density of 31 kg/m^3, along with an elastic modulus versus density study which includes 51 IG and 71 IG, with densities of 51 kg/m^3 and 71 kg/m^3, respectively.

All results reported herein are in engineering stress (applied force per initial cross-sectional area of the test specimen) and engineering strain (change in gage length referenced to the

www.manaraa.com

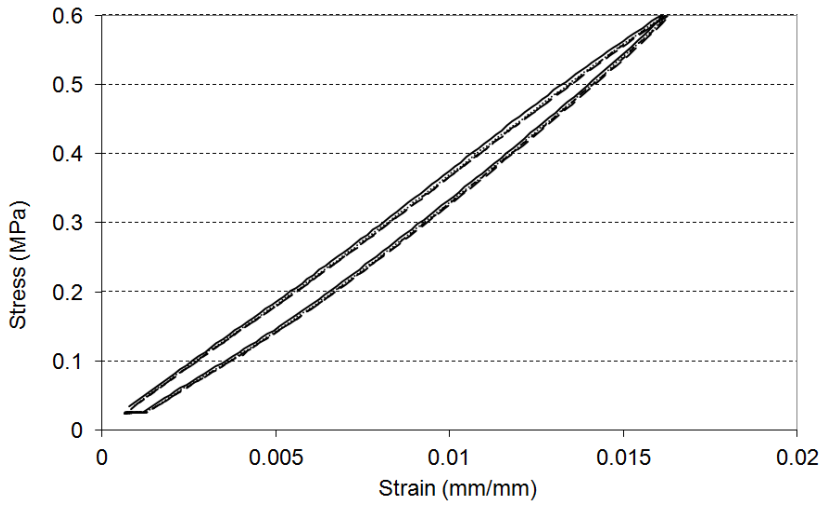

Figure 4.1: Stress-strain plot for load/unload/recovery test cycle at a crosshead speed of 1 mm/minute for four repeats on a single specimen.

original gage length). For all testing a gage length of 50 mm is used on a dog-bone specimen with nominal rectangular cross section of 15 x 12 mm. All loading/unloading is done at a crosshead speed of 1 mm/minute unless indicated otherwise.

Consider first loading and unloading under constant strain rate . Fig. 4.1 shows the stress-strain curves for loading and unloading at a material effective strain rate $\cong 0.00001$ s^{-1}. It is seen that the material is not purely elastic. However, after unloading and holding nearly zero stress, the material contracts to the original length during the recovery period, and the stress-strain curve becomes "closed." For partial unloading, that is, unload at a constant strain rate to some intermediate prescribed strain, and then hold the strain constant, it is observed the stress starts building up. It appears the material intends to close the stress-strain curve in the vertical direction, but instead, stress relaxation begins and the stress starts decaying slowly, Fig. 4.2. The process of the short-term stress increase, followed by the long-term stress relaxation is clearly seen in the time history plot, Fig. 4.3.

As is the case for other polymers, the "thickness" of the stress-strain curve depends on the maximum loading stress or strain. Fig. 4.4 shows the load/unload/recovery curves of a single specimen loaded to various maximum stress levels. Sufficient time was allowed between tests for the material to return to its original macroscopic state. A higher loading stress, and

www.manaraa.com

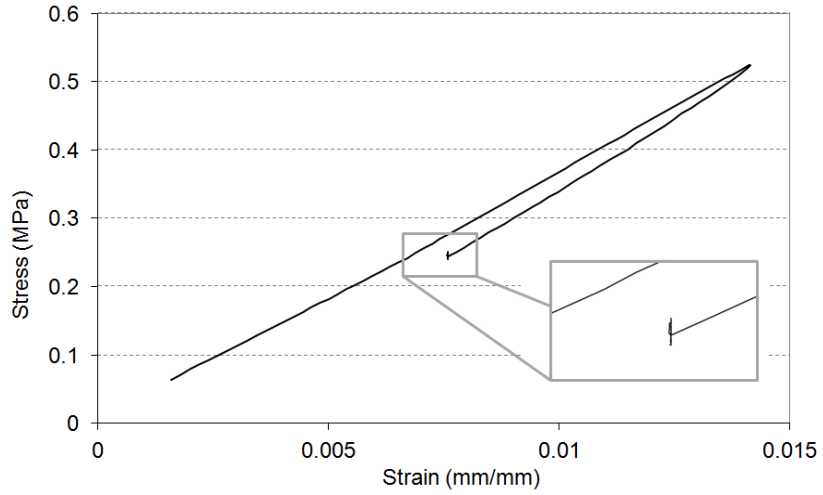

Figure 4.2: Stress-strain behavior for load/partial-unload/hold test to an intermediate strain level. Specimen is held at the intermediate strain for an extended time.

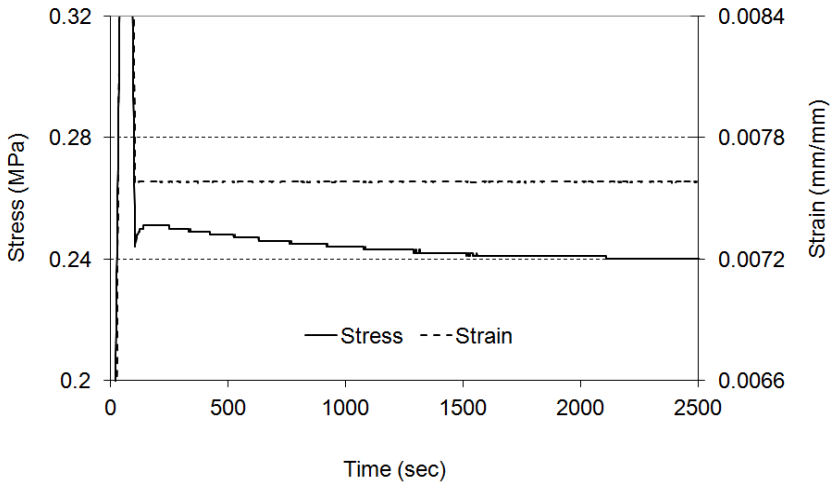

Figure 4.3: Stress time history for load/partial-unload/hold test. At the partial unload point, the strain is held constant at 0.00758. Note the increase, then decrease of stresses after partial unloading, while the strain is held constant.

www.manaraa.com

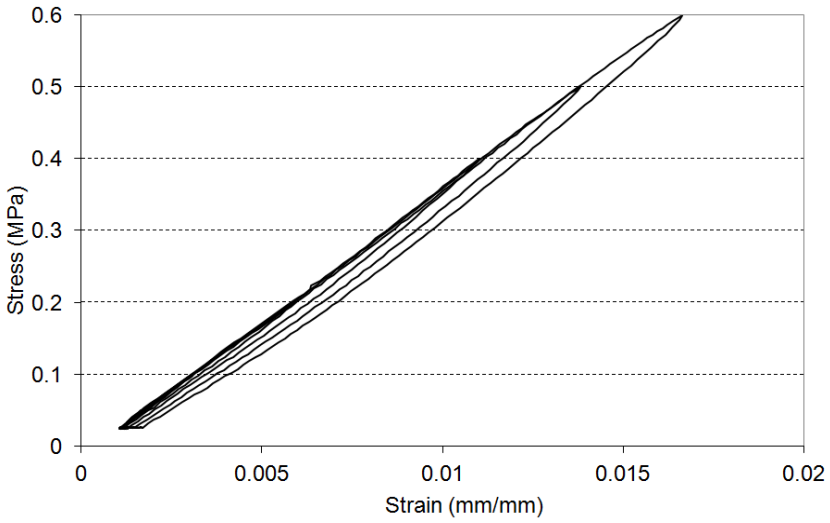

Figure 4.4: Stess-strain behavior for load/unload/recovery test to various strain levels for a single specimen. The "thickness" of the stress-strain curve increases as the maximum loading strain increases.

conversely a higher loading strain, results in an increase in the difference between the loading and unloading curves, i.e. increased hysteresis.

The stress and strain profiles for an instantaneous unloading test are shown in Fig. 4.5. The specimen is loaded at a constant strain rate and when the desired strain is achieved, the load is suddenly released. It is observed that while the stress level vanishes immediately and completely, the strain takes some time to vanish. The slow strain decay causes the loop of the corresponding stress-strain curve to close, Fig. 4.6.

Instantaneous unloading tests were run on different specimens at various maximum strain loadings. From Fig. 4.7, it is observed two regimes occur during the unloaded phase. A "fast" regime which occurs in the first 2-3 minutes, and then a "slow" regime ensues for the remaining time period.

Creep tests were performed at various stress levels on different specimens. In Fig. 4.8, a considerable amount of spread in the creep data is observed. Normalizing the data to the initial loading strain ε_o, a more consistent performance is seen, Fig. 4.9.

Finally, a set of stress relaxation tests was run at various strain levels, Fig. 4.10. It is noteworthy that after normalizing to the maximum stress level σ_o, the curves do not coincide,

www.manaraa.com

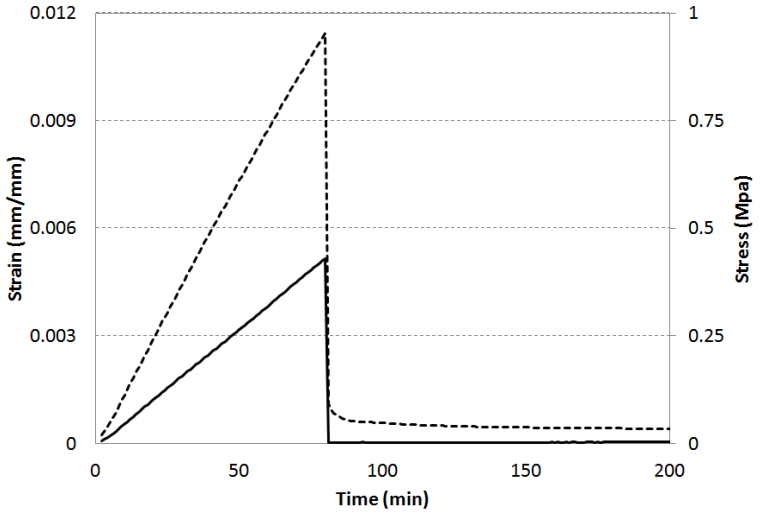

Figure 4.5: Strain (dashed line) and stress (solid line) time history for a load/instantaneous-unload test. Strain does not instantaneously go to zero with the instantaneous release of the load (stress).

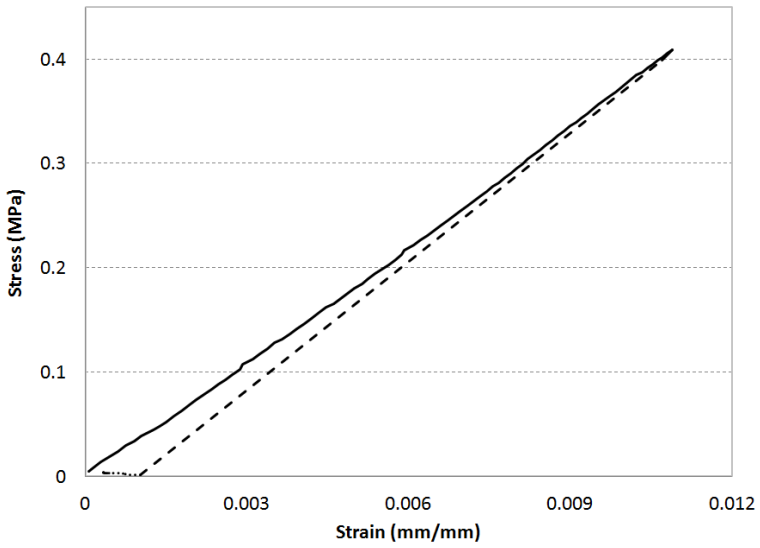

Figure 4.6: Stress-strain curve for load/instantaneous-unload test. The gap along the strain-axis between the loading (solid line) and unloading (long dash) portions of the test, indicates a residual strain remains after the immediate release of the load. As the strain decays (short dash), the stress-strain loop closes.

www.manaraa.com

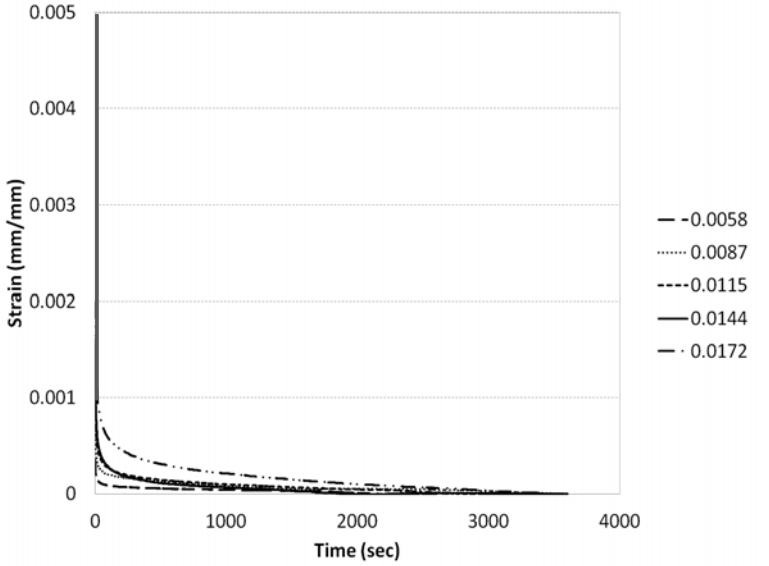

Figure 4.7: Load/instantaneous-unload test showing the decay of strain over time for various levels of maximum loading strain.

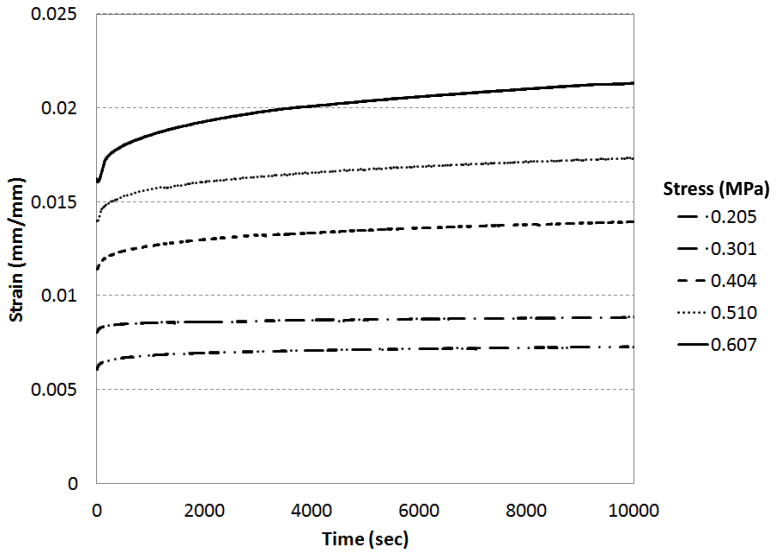

Figure 4.8: Creep tests performed at different levels of initial loading stress.

www.manaraa.com

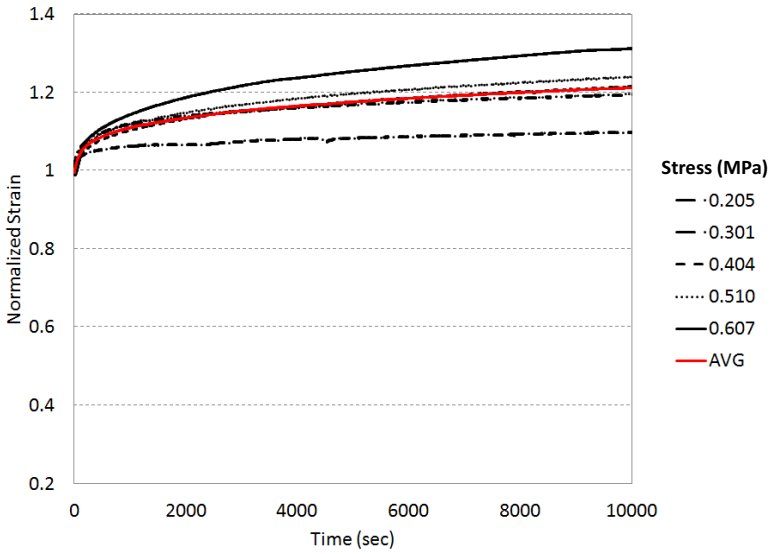

Figure 4.9: Creep data of Fig. 4.8, normalized to the initial loading strain level ε_o. Except for the test $\sigma_o = 0.301$, all tests are in close proximity once normalized.

Fig. 4.11. Two interpretations are possible for the existence of bunches of curves in Figs. 4.9, 4.11: material variability or material nonlinearity. This issue is addressed in Section 4.2.

4.1.1 Technical details of experiments

A MTS 45G electromechanical load frame with a 500 N load cell is used for this work. Pneumatic grips with diamond-tipped serrated faces are used to hold the specimen. Air pressure is adjusted to $4\frac{1}{2}$ psi to maintain sufficient grip forces, while minimizing specimen damage. Pneumatic grips provide a constant clamp force for the test duration as air pressure controls the clamping mechanism. Separate valves for the upper and lower grips allow instantaneous unloading tests to be performed. A knife-edge extensometer with a 50 mm gage length is used.

Clamping of the material is critical to minimize bending of the specimen. Small foam blocks help align the specimen and the grip faces. This allows the grips to contact the specimen squarely, minimizing extraneous forces in the test train.

A knife-edge extensometer can easily damage the surface of the specimen. Excessive attachment forces cause the knife edges to sink into the material. Rubber bands used to

www.manaraa.com

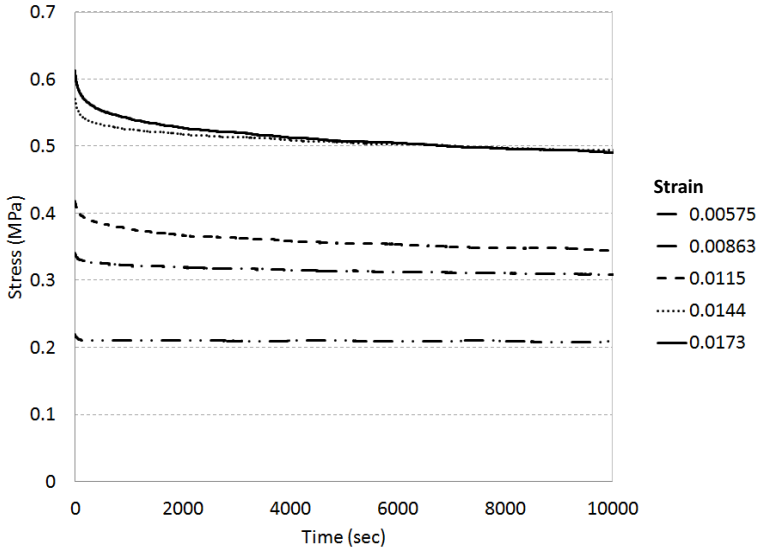

Figure 4.10: Stress relaxation tests performed at different levels of maximum strain.

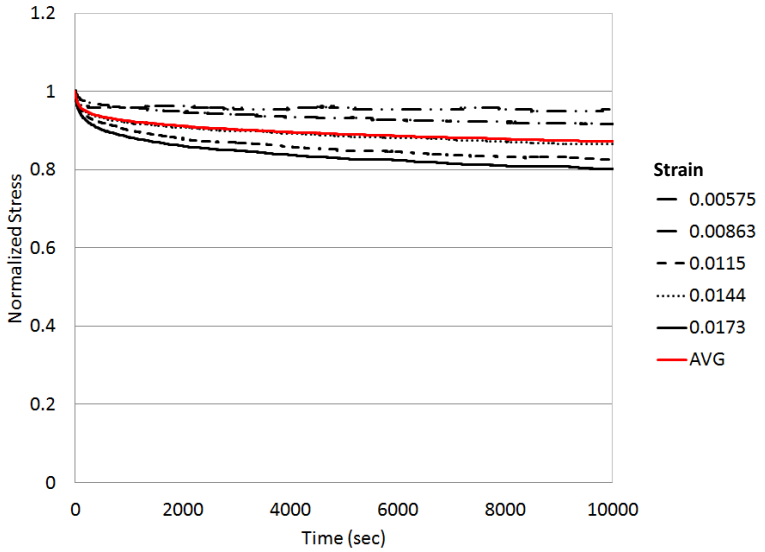

Figure 4.11: Stress relaxation time history of Fig. 4.10, normalized to the initial stress level σ_o. Unlike the normalized creep tests, a considerable spread exists in the normalized stress relaxation data as time increases.

www.manaraa.com

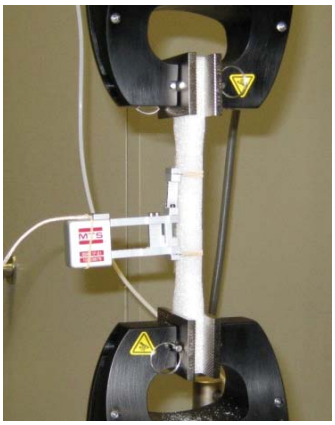

Figure 4.12: Typical test setup of the foam specimen showing the extensometer and clamp arrangments. Not readily visible are plastic protectors and double-sided tape used to prevent stress risers in the specimen.

attach the extensometer easily cause notches to be formed in the specimen edges. Damage of this type contributes to stress risers, which can lead to erroneous test results. Several methods are employed to minimize specimen damage. Two plastic sleeves placed under the rubber band contact area protect the specimen edges. Small pieces of double-sided cellophane tape placed under the knife edges help prevent damage, and provide a secondary method to prevent extensometer slippage. Figure 4.12 shows a typical test setup.

Measurement Variability. A measurement variability study was performed on the micrometers, load cell, and extensometer. Six sigma (i.e. six standard deviations) analysis determined the maximum error in the cross-sectional area measurement to be ± 0.8%. The maximum error of the load cell based on calibration documents is ± 1.0%. Thus, the maximum measurement error for the stress calculation is ± 1.8%. Based on the extensometer calibration, the maximum error for strain is ± 0.5%. To investigate variability induced by equipment drift, tests were performed on the machine crosshead position, load cell, and extensometer over a 24 h period. The results show drift to be insignificant, as our creep and stress relaxation tests are typically less than 8 h total duration. To verify the overall machine repeatability, a linear steel spring with stiffness similar to the elastic modulus of 31 IG was tested. Similar stress levels and hold times as used for material tests were used. As expected, the load/hold/unload profile produces a straight line in the stress-strain plot where no hysteresis is observed.

www.manaraa.com

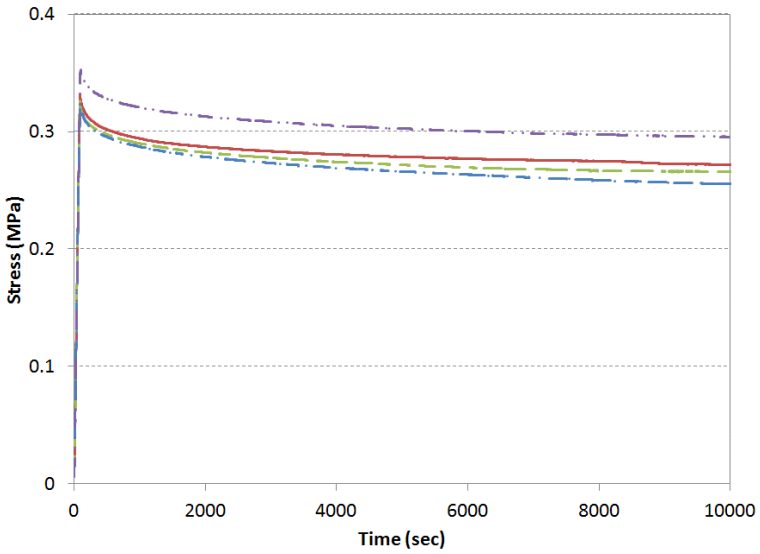

Figure 4.13: Typical stress relaxation data for multiple specimens of Rohacell 31IG.

4.2 Discussion

4.2.1 Material Variability

A set of stress relaxation tests of PMI 31 IG, all cut from the same sheet and all loaded to the same strain level, is shown in Fig. 4.13. The specimen to specimen variation in stress levels at $t = 12,000$ s is $\pm$ 8%. Figure 4.14 is a stress-strain plot of the same data as Fig. 4.13. Variation is also observed in the elastic modulus value between the specimens, Fig. 4.14.

Creep tests were run on new specimens of PMI 31 IG, also cut from the same sheet as the stress relaxation material. Results are shown in Fig. 4.15. The specimen to specimen variation in the strain levels at $t = 12,000$ s is $\pm$ 5%. Figure 4.16 is a stress-strain plot of the same tests as Fig. 4.15.

As a validation of the observed variability, David Ostberg from US Army TARDEC laboratory in Warren, Michigan performed confirmation tests on the same batch of material. Every reasonable attempt was made to duplicate the test procedures and settings of the primary lab. The amount of material variability seen in the second laboratory data was consistent with the testing from the primary laboratory. Because the creep performance and the

www.manaraa.com

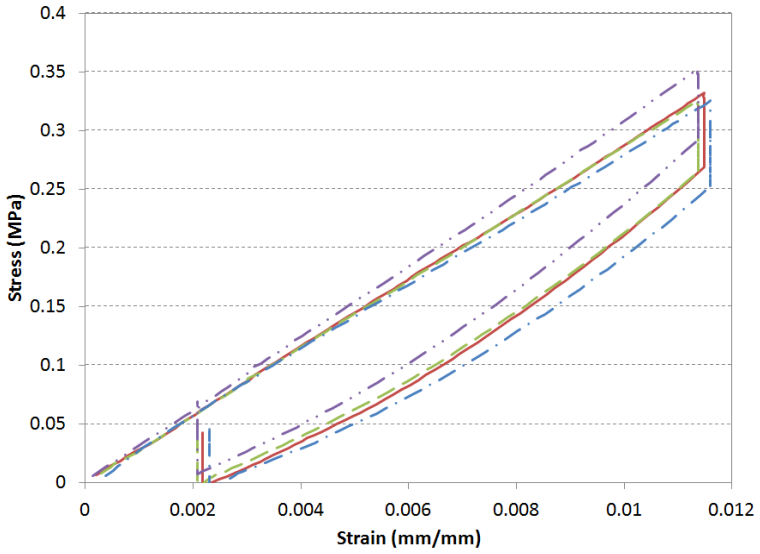

Figure 4.14: Stress-strain plots of the same Rohacell 31 IG specimens of Fig. 4.13.

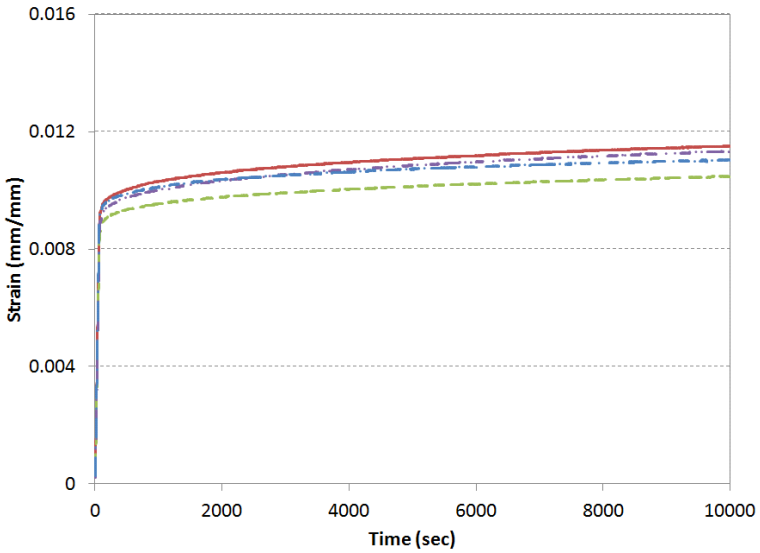

Figure 4.15: Dispersion of strain time history data for creep tests of four specimens of Rohacell 31 IG loaded to identical conditions.

www.manaraa.com

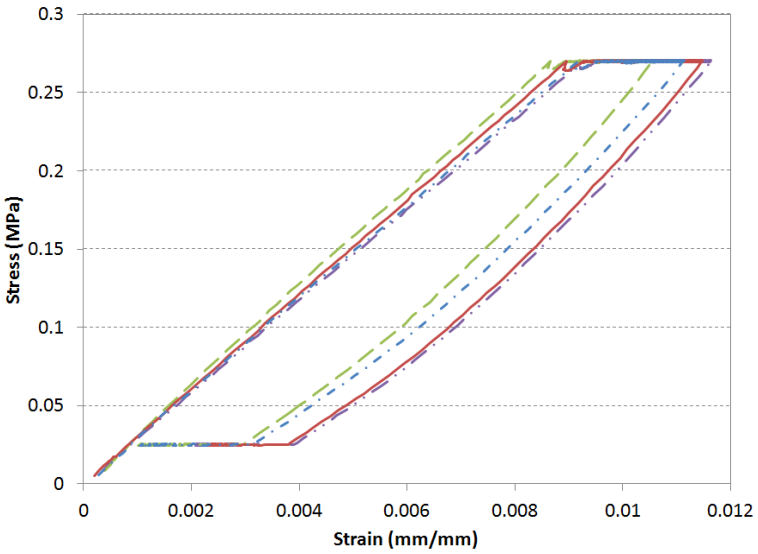

Figure 4.16: Dispersion of stress-strain data for the four specimens of Fig. 4.15.

test results' variability are consistent, the significant variability in the results is likely due to variability in the material properties.

4.2.2 Elastic Modulus

Another manifestation of material variability is the variance of elastic moduli for foams of the same industrial grade, i.e. foams with the same mass density. For this study, foams with nominal densities of 31 kg/m^3, 51 kg/m^3 and 71 kg/m^3 were tested. Results are shown in Fig. 4.17. All specimens with density 31 kg/m^3 were cut from the same sheet, as were the specimens with 51 kg/m^3 , while the specimens with density 71 kg/m^3 were cut from various sheets. As expected, the latter showed the greatest spread in the results.

It is known that the elastic moduli of polymer foams are strongly dependent on the foam density. Most foam properties follow the relationship [Zenkert et al., 2006]:

$$\bar{\zeta} = \alpha \bar{\rho}^n, \tag{4.1}$$

where $\bar{\zeta}$ is a mechanical property of the foam normalized with its value for the fully dense material, and $\bar{\rho}$ is the relative density defined as the ratio of the foam density to the solid

www.manaraa.com

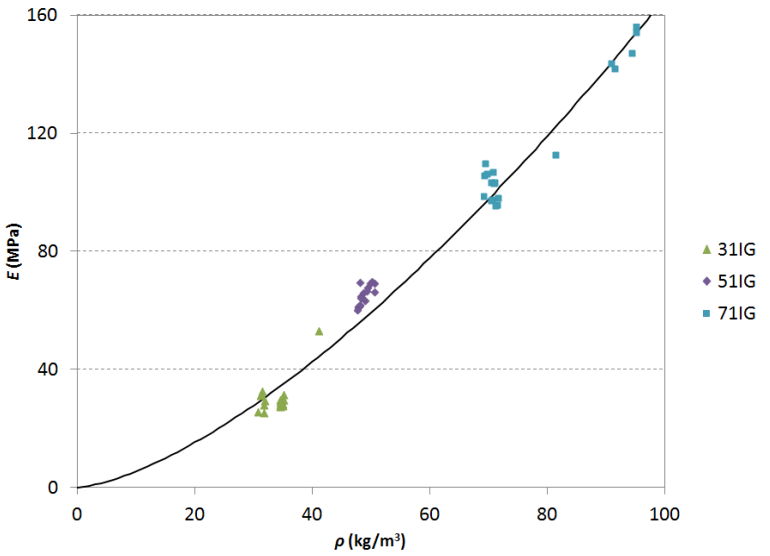

Figure 4.17: Dependence of the elastic modulus of Evonik Rohacell IG on material density ρ. Solid line is the power law $E = 0.18\rho^{1.5}$.

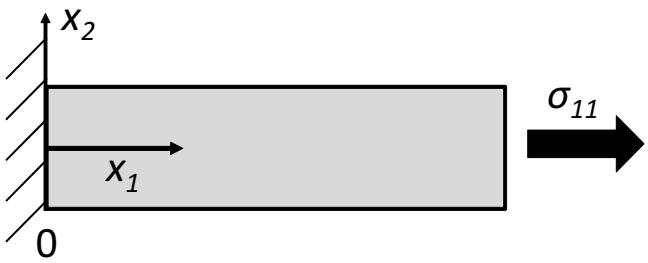

Figure 4.18: Notation used in Section 4.3.

material density. In our case, PMI is not available in the non-foamed state, which results in "messier" units for (4.1). In our non-normalized case, the elastic modulus relates to foam density with $n = 1.5$ and $\alpha = 0.18$ MPa/(kg/m^3)$^{3/2}$.

4.3 Modeling the Extension of a Foam Beam

To employ the model developed in Chapter 3, first the problem of a polymer foam beam extension is solved. The beam is deformed by a force applied at one end, while the other end is clamped, Fig. 4.18.

Denote by x_1 the axial coordinate. Projections of tensors on the other two coordinates are

www.manaraa.com

marked by Greek indices, $\alpha, \beta = 2, 3$; small Latin indices $i,\ j,\ k$ run through values 1, 2, 3, and summation over repeated indices is implied.

The free energy (3.73) is a function of strains $\varepsilon_{11},\ \varepsilon_{1\alpha},\ \varepsilon_{\alpha\beta}$ and internal parameters $\xi_{11},\ \xi_{1\alpha}$, and $\xi_{\alpha\beta}$:

$$F = \frac{1}{2}\lambda\left[\bar{\beta}\xi_{kk}^2 + (\varepsilon_{11} - \xi_{11})^2 + 2(\varepsilon_{11} - \xi_{11})(\varepsilon_{\alpha\alpha} - \xi_{\alpha\alpha}) + (\varepsilon_{\alpha\alpha} - \xi_{\alpha\alpha})^2\right]$$

$$+\mu\beta\xi_{ij}\xi_{ij}$$

$$+\mu\left[(\varepsilon_{\alpha\beta} - \xi_{\alpha\beta})(\varepsilon_{\alpha\beta} - \xi_{\alpha\beta}) + 2(\varepsilon_{1\alpha} - \xi_{1\alpha})(\varepsilon_{1\alpha} - \xi_{1\alpha}) + (\varepsilon_{11} - \xi_{11})^2\right]. \tag{4.2}$$

In this problem, stresses $\sigma_{\alpha\beta}$ and $\sigma_{1\alpha}$ vanish. This is equivalent to minimization of (4.2) over $\varepsilon_{1\alpha}$ and $\varepsilon_{\alpha\beta}$. Minimizing over $\varepsilon_{1\alpha}$ yields $\varepsilon_{1\alpha} = \xi_{1\alpha}$, while minimizing over $\varepsilon_{\alpha\beta}$ results in the equation

$$\varepsilon_{\alpha\beta} - \xi_{\alpha\beta} = -\nu(\varepsilon_{11} - \xi_{11})\delta_{\alpha\beta}\ , \tag{4.3}$$

where

$$\nu \equiv \frac{\lambda\mu}{\lambda + \mu}. \tag{4.4}$$

Substituting (4.3) into (4.2) provides free energy as a function of ε_{11} and ξ_{ij}:

$$F = \frac{E}{2}(\varepsilon_{11} - \xi_{11})^2 + \frac{1}{2}\bar{\lambda}\xi_{kk}^2 + \mu\beta\xi_{ij}\xi_{ij}, \tag{4.5}$$

where

$$\bar{\lambda} \equiv \lambda\alpha + \frac{2\mu}{3}(\alpha - \beta). \tag{4.6}$$

A solution is sought with $\xi_{22} = \xi_{33}$, and $\xi_{12} = \xi_{23} = \xi_{31} = 0$. Under such a setting, free energy (4.5) is a function of ε_{11}, ξ_{11} and ξ_{22} only:

$$F = \frac{E}{2}(\varepsilon_1 - \xi_1)^2 + \frac{1}{2}\left(\bar{\lambda} + 2\mu\beta\right)\xi_1^2 + 2\bar{\lambda}\xi_1\xi_2 + 2\left(\bar{\lambda} + \mu\beta\right)\xi_2^2, \tag{4.7}$$

where the notation $\varepsilon_{11} = \varepsilon_1,\ \varepsilon_{22} = \varepsilon_2,\ \xi_{11} = \xi_1,\ \xi_{22} = \xi_2$ is employed.

www.manaraa.com

The "second" stress tensor components associated with the polymer chain slippage are:

$$p_1 = \frac{\partial F}{\partial \xi_1} = E\left(\xi_1 - \varepsilon_1\right) + (\bar{\lambda} + 2\mu\beta)\xi_1 + 2\bar{\lambda}\xi_2 \tag{4.8}$$

$$p_2 = \frac{\partial F}{\partial \xi_2} = 2\bar{\lambda}\xi_1 + 4(\bar{\lambda} + \mu\beta)\xi_2. \tag{4.9}$$

Both parameters ξ_1 and ξ_2 evolve during deformation. It is useful to know their equilibrium values. Minimization of (4.7) with respect to ξ_2 determines the equilibrium value of ξ_2:

$$\check{\xi}_2 = -\frac{\bar{\lambda}}{2\left(\bar{\lambda} + \mu\beta\right)}\xi_1. \tag{4.10}$$

F then depends on the current value of ξ_1 only. We have

$$\min_{\xi_2} F = \frac{E}{2}\left(\varepsilon_1 - \xi_1\right)^2 + \frac{\gamma}{2}\xi_1^2 \tag{4.11}$$

where we introduce the notation

$$\gamma = \mu\beta\frac{3\bar{\lambda} + 2\mu\beta}{\bar{\lambda} + \mu\beta}. \tag{4.12}$$

Further minimization of (4.11) over ξ_1 yields:

$$\check{\xi}_1 = \frac{E}{E + \gamma}\varepsilon_1, \tag{4.13}$$

so at equilibrium we have

$$\min_{\xi_1,\, \xi_2} F = \frac{1}{2}\left(\frac{E\gamma}{E + \gamma}\right)\varepsilon_1^2. \tag{4.14}$$

At equilibrium, elastic energy is a quadratic function of ε_1:

$$F = \frac{1}{2}E_{eq}\varepsilon_1^2. \tag{4.15}$$

The coefficient in (4.15) has the meaning of the equilibrium Young's modulus. Therefore, we get

www.manaraa.com

$$E_{eq} = \frac{E\gamma}{E+\gamma}. \tag{4.16}$$

Apparently, the equilibrium Young's modulus E_{eq} is smaller than the current Young's modulus E.

To close the system of equations, we define the evolution to equilibrium by the equations:

$$\frac{d\xi_1}{dt} = -\Psi(p_1), \quad \frac{d\xi_2}{dt} = -\Psi(p_2), \tag{4.17}$$

where the function $\Psi(\Lambda)$ was introduced in Chapter 3, specifically (3.25):

$$\Psi(\Lambda) = c\Lambda + ad \ln\left[\frac{\cosh\left(\frac{b-\Lambda}{a}\right)}{\cosh\left(\frac{b+\Lambda}{a}\right)}\right]. \tag{4.18}$$

Equations (4.17), (4.18) determine the time-dependent behavior of the material. They contain the material parameters $E,\ \mu,\ \alpha,\ \beta$.

4.3.1 Minimizing Material Variability

In order to negate as much material variability as possible, only those specimens whose elastic moduli were "nearly" the same are used for the creep and stress relaxation fittings, Figs. 4.19, 4.21. The stress-strain curves in Figs. 4.20, 4.22 indicate that the elastic moduli are nearly the same for the four specimens. Exact values are 36.1, 35.7, 37.0, 37.4 MPa.

Of note, the dip in the stress-strain plot of Fig. 4.22 is not solely the result of the material's response. Rather, the root cause of the dip is the MTS controller's inability to transition quickly enough between the loading and hold portion of the test cycle, compared to the rapidly changing material response during the same period.

Stress Relaxation. For a stress relaxation test, the specimen is elongated a prescribed amount, then held at constant strain for a specified time period. The strain application occurs over a relatively short period of time compared to the entire test duration. The material's stress response is measured during the entire test.

Creep. For a creep test, the specimen is loaded (i.e. stressed) a prescribed amount, then held at the constant stress for a specified time period. The stress loading application occurs

www.manaraa.com

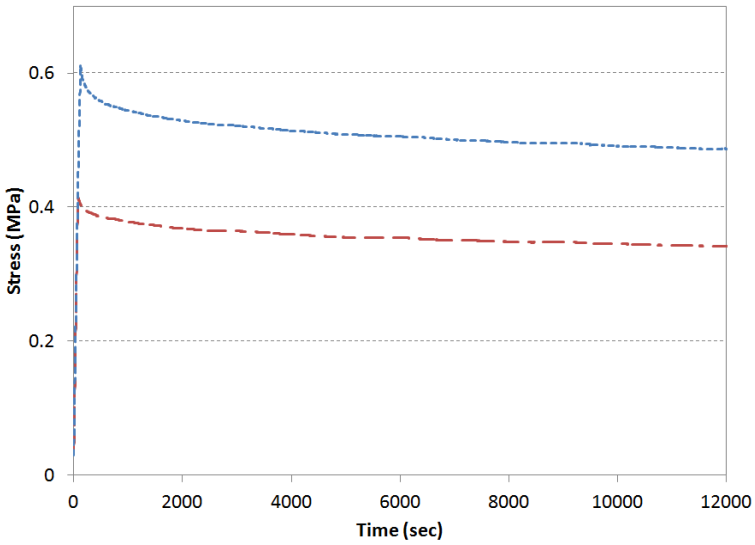

Figure 4.19: Stress relaxation of two specimens of 31 IG which have nearly the same elastic moduli.

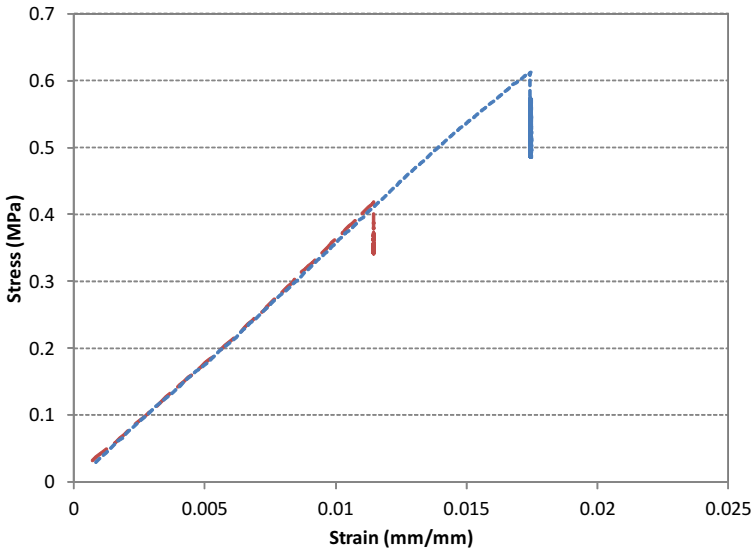

Figure 4.20: Stress-strain plot of the data from Fig. 4.19. The elastic moduli of the two specimens are 35.7 and 36.1 MPa.

www.manaraa.com

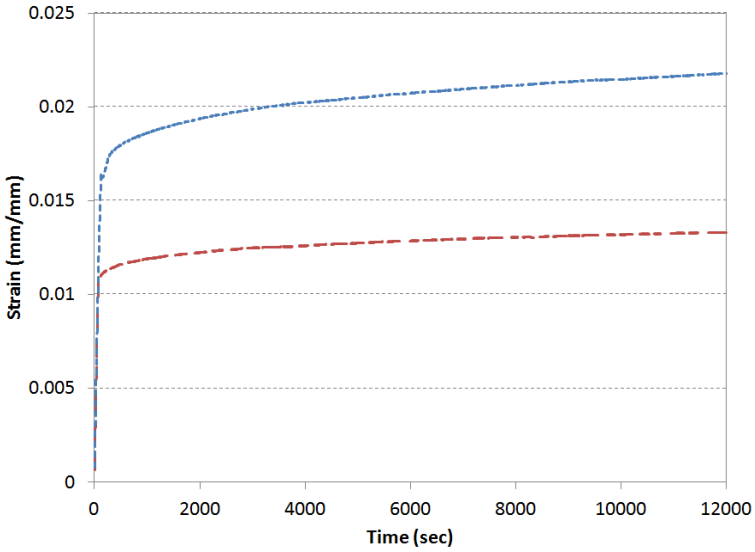

Figure 4.21: Creep tests of two specimens of 31 IG foam. These specimens have nearly the same elastic moduli as those in Fig. 4.19.

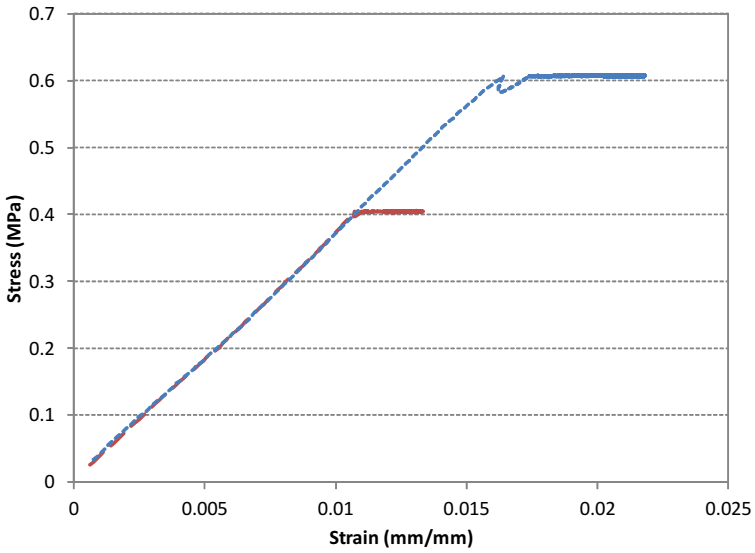

Figure 4.22: Stress-strain plot of the creep data from Fig. 4.21. The elastic moduli of the two specimens are 37.0 and 37.4 MPa.

www.manaraa.com

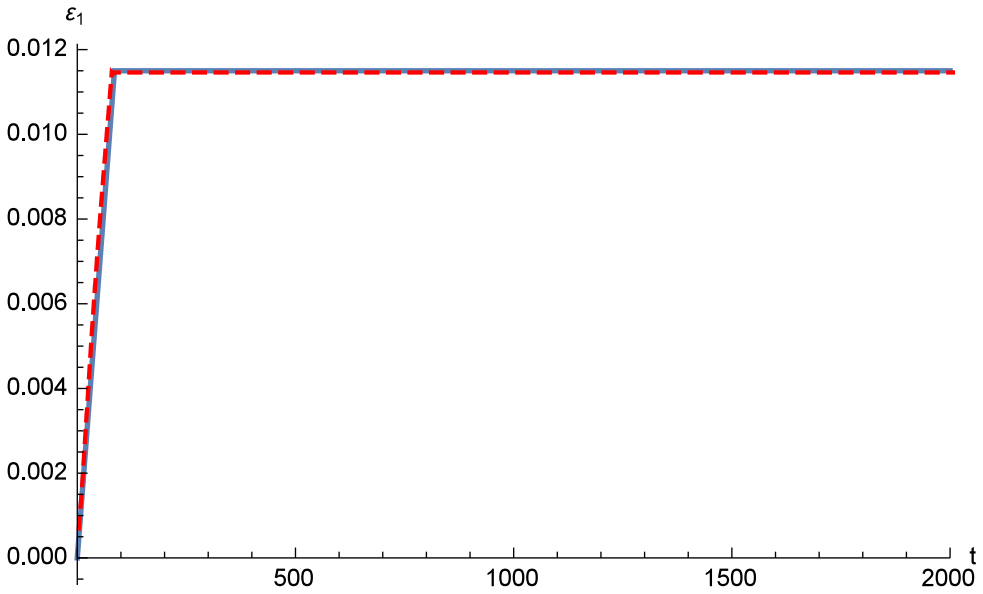

Figure 4.23: Typical strain loading profile for a stress relaxation test. The model uses an idealized strain profile which closely approximates the machine test profile. The dashed (red) line is the experiment creep data. The solid (blue) line is the model prescribed loading. A creep test prescribes a similarly shaped stress profile.

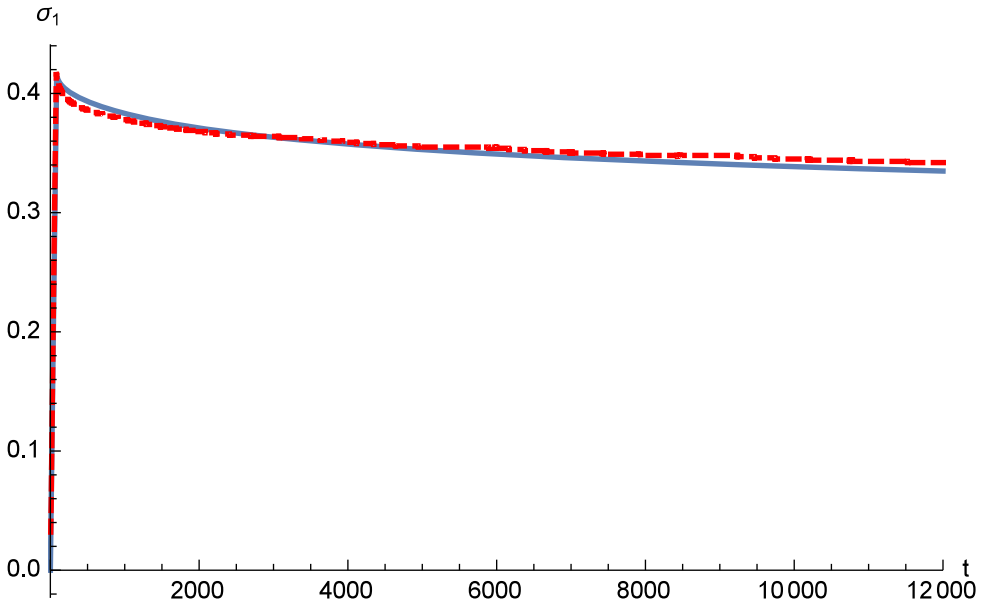

Figure 4.24: Model prediction (solid blue line) comparison to experiment data (dashed red line) for a stress relaxation test performed at a strain of 0.0115.

www.manaraa.com

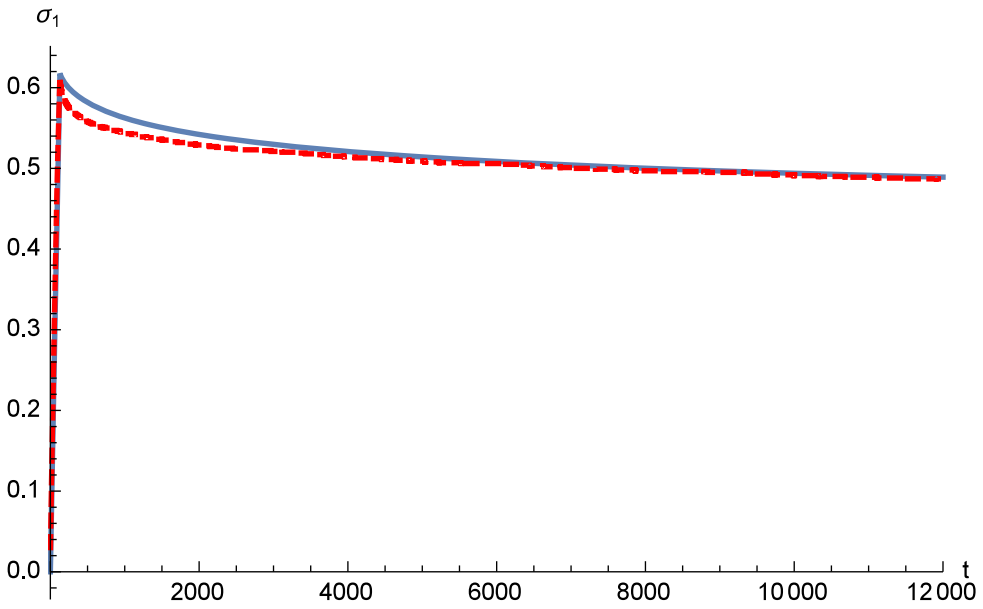

Figure 4.25: Model prediction (solid blue line) comparison to experiment data (dashed red line) for a stress relaxation test performed at a strain of 0.0174.

over a short, finite time interval. The material's strain response is measured during the entire test.

4.3.2 Material Parameters

Material Parameters $E,\ \mu,\ \alpha,\ \beta$. Based on testing and the results of Figs. 4.20, 4.22, the values of material parameters $E,\ \lambda,\ \mu$ for Rohacell 31 IG are

$$E = 36.6 \text{ MPa}, \quad \lambda = 43.3 \text{ MPa}, \quad \mu = 13 \text{ MPa}. \tag{4.19}$$

The material parameters E_{eq}, α, β are determined/estimated based on long-term creep and stress relaxation tests. Based on these tests, $E_{eq} \approx 27.0$ MPa. Equation (4.16) establishes the link between E and E_{eq} with the parameter γ. In this case, $\gamma = 103$ MPa. From (4.6) and (4.12), there is a link between α, β. We estimate the value $\alpha = 5$, which yields $\beta = 2.76$.

Material Parameters $a,\ b,\ c,\ d$. Using iterative fittings, the following dynamic parameters

www.manaraa.com

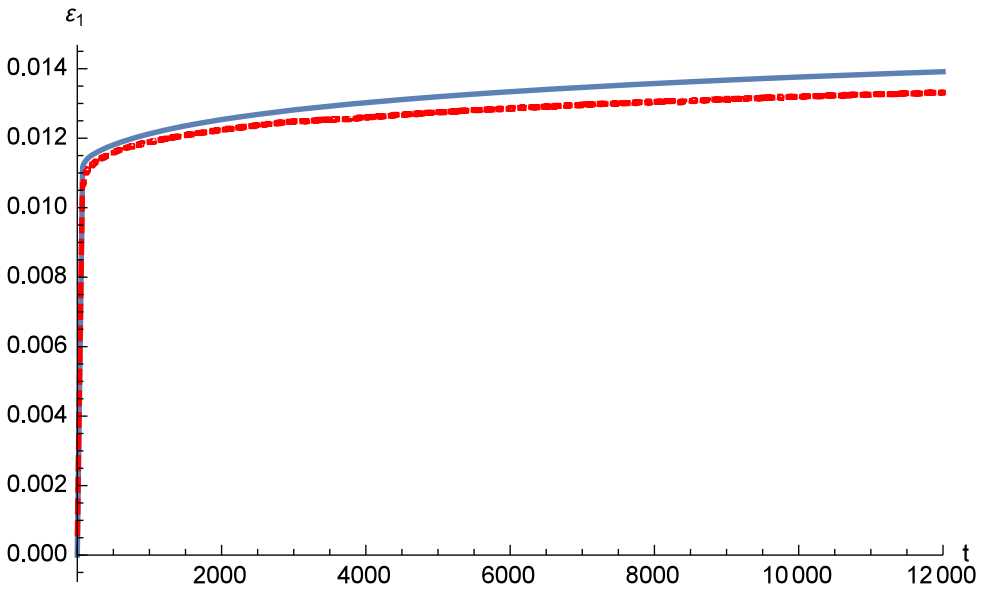

Figure 4.26: Model prediction (solid blue line) comparison to the experiment data (dashed red line) for a creep test performed at a stress of 0.404 MPa.

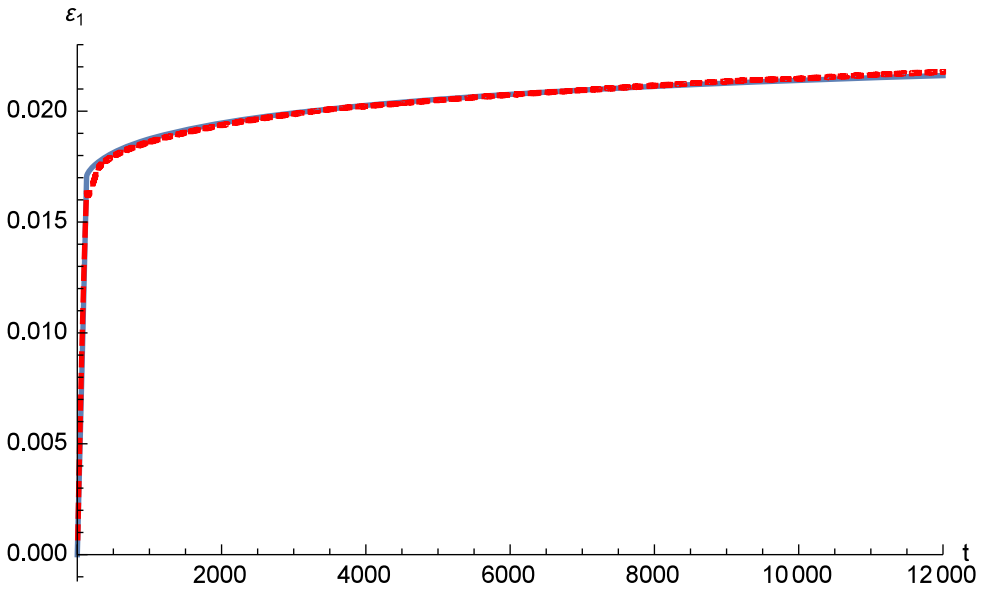

Figure 4.27: Model prediction (solid blue line) comparison to the experiment data (dashed red line) for a creep test performed at a stress of 0.607 MPa.

www.manaraa.com

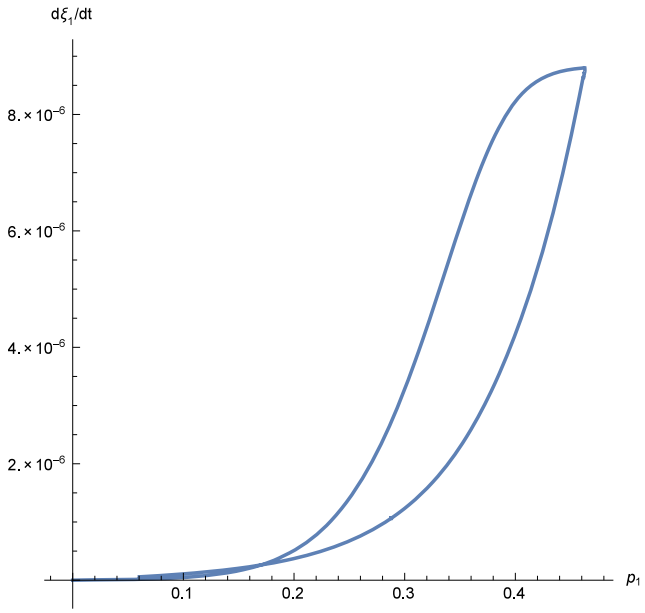

Figure 4.28: Dependence of sticking point velocity $d\xi_1/dt$ on the corresponding thermodynamic force in stress relaxation. This differs from the appearance of Fig. 3.6 because parameters a, b are not constant values, but rather are functions of the lateral strain ε_2, (4.20).

are determined for (4.15);

$$a = 0.078 + 2150\varepsilon_2^2, \quad b = 1.02 + 25,000\varepsilon_2^2, \quad c = 2d, \quad d = 10,000. \tag{4.20}$$

In order to satisfactorily fit all four tests, the parameters a, b are found to be functions of the transverse strain ε_2. Intuitively this seems reasonable. As the beam is extended, the specimen contracts in x_2 placing the polymer chains in closer proximity to each other. Thus, the chain interactions becoming stronger the more closely packed they become. This is observed as a change in the velocity profile at the higher loading/unloading levels and results in the creation of the loop in Fig. 4.28.

4.4 Summary

It has been shown that the model proposed in Chapter 3 is capable of capturing the creep and stress relaxation behavior of a polymethacrylimide foam. It is essential that the values of the material parameters found from creep experiments allow us to properly

www.manaraa.com

predict stress relaxations and vice versa. This appears to be true for the case here. The success in accomplishing this task indicates that the micro-mechanical reasoning used in the construction of the model appears sound and may prove meaningful in gathering further insight into polymer behavior. The model behavior under more complex loading cycles is further explored in Chapter 5.

www.manaraa.com

CHAPTER 5

Closing the Stress-Strain Loop

In Section 4.3, the model does a good job of predicting the material behavior for typical stress relaxation and creep tests. However, a valid model should comprehend many material behaviors, some of which are shown in Sections 4.1 and 4.2. A test in which other models fall short is the complex load/hold/unload/recovery cycle, which is covered for the classic models in Section 2.5. In this chapter, a review of the model behavior for both a load/hold/unload/recovery cycle for a stress relaxation test and a creep test are covered. A load/partial-unload/hold test setup in the form of a stress relaxation test, and a load/unload/recovery test setup in the form of a creep test, are qualitatively analyzed against the experiment data. Finally, a load/instantaneous-unload test is qualitatively evaluated against the experiments.

5.1 Modeling

5.1.1 Load/Hold/Unload/Recovery

Typical stress relaxation and creep tests involve loading the material to either a prescribed strain or stress, then holding the load for a period of time. In such a test, the sticking point parameter ξ_1, spends its time in the first quadrant of the velocity-force plot, Fig. 4.28. An important piece of polymer chain behavior can be observed with the addition of an unload, and recovery phase (i.e. a second hold phase) to the tests. For materials with memory, this addition causes the secondary internal force parameter p_1 to change signs, and the sticking point to change direction. This has the effect of moving the sticking point behavior into the third quadrant of the velocity-force plot as the secondary internal force parameter and sticking point velocity become negative. Typical stress-strain plots for stress relaxation and creep of 31 IG material for a complete load/hold/unload/recovery cycle are observed in Figs. 4.14 and 4.16. Upon removal of the strain or stress as appropriate, given a sufficient recovery time the material will return essentially to its starting position on the stress-strain plot, Figs. 4.14, 4.16. We refer to this as "closing the (stress-strain) loop." Due to test capabilities and

www.manaraa.com

variability, the statement, "closing the loop" is a qualitative statement as opposed to an exact statement. A significant validation of the model then is, it must be able to close the loop of this entire complex loading cycle. To this end, the green dash specimen from Fig. 4.14 and blue dash specimen from Fig. 4.16 are selected for further analysis. These specimens have nearly the same elastic moduli, 28.7 MPa and 29.5 MPa respectively. Since these values differ significantly from those used in the analysis of Section 4.3, a complete refitting of the data is warranted. As in previous tests/analyses, the material is loaded to the final strain or stress (i.e. for stress relaxation or creep test), held for 12,000 s, unloaded at the same rate, and allowed to recover under a minimal load of 5 N. The 5 N load maintained during the recovery eliminates slack in the test train, improving test repeatability.

Material Parameters $E,\ \mu,\ \alpha,\ \beta$. Based on results of Figs. 4.14, 4.16, and engineering judgement, the values of material parameters $E,\ \lambda,\ \mu$ for this modeling of Rohacell 31 IG are

$$E = 28.9 \text{ MPa}, \quad \lambda = 36.6 \text{ MPa}, \quad \mu = 10.4 \text{ MPa}. \tag{5.1}$$

From other testing, $E_{eq} \approx 23.6$ MPa, and the values of the material parameters α, β, γ are estimated to be

$$\alpha = 5, \quad \beta = 4.41, \quad \gamma = 129 \text{ MPa}. \tag{5.2}$$

Material Parameters $a,\ b,\ c,\ d$. Using trial and error, the following dynamic parameters for the new specimens are;

$$a = 0.082, \quad b = 0.99, \quad c = 2d, \quad d = 10,000. \tag{5.3}$$

Of significance, parameters $a,\ b$ need only be constants in order to adequately fit the data, and not functions of the transverse strain ε_2 as in (4.20). This is likely due to the small range of loading used for these specimens, along with fitting to a limited number of specimens. Figs. 5.1 and 5.2 show the complete experiment (red dash line) time history for the stress relaxation and creep test respectively, along with model predictions (solid blue line). For a given specimen, closer correlation of the model to experiment is possible, but here we reinforce

www.manaraa.com

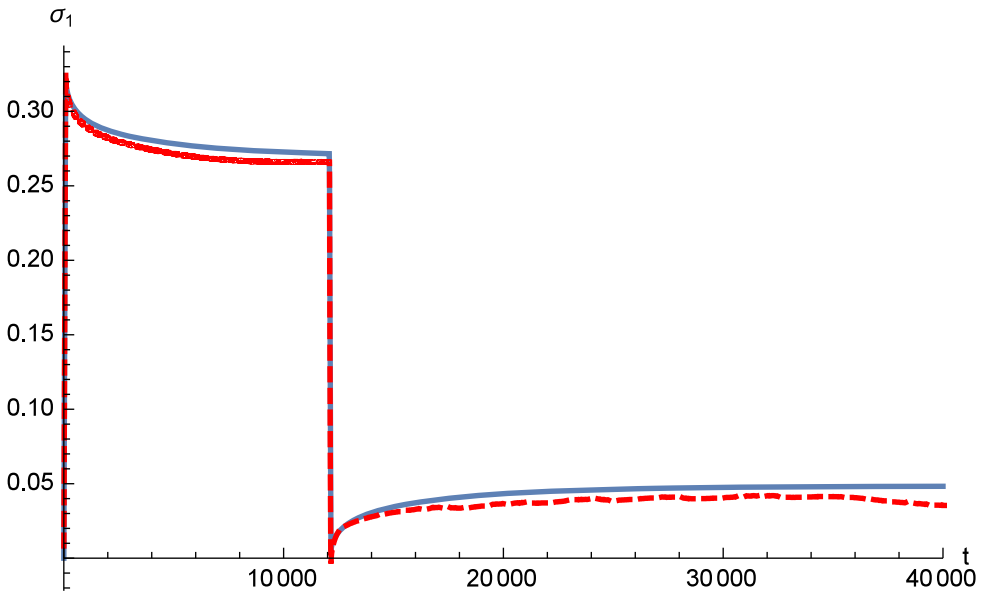

Figure 5.1: Stress time history where the final strain at loading is 0.0114 and held for 12,000 s. Final strain at unloading is 0.0021 and held for 40,000 s. Dashed red line is the experiment data, solid blue line is the model prediction.

that only one set of parameters is needed to adequately predict both material stress relaxation and creep.

5.1.2 Load/Partial-Unload/Hold

The load/partial-unload/hold test, Figs. 4.2, 4.3, is evaluated against the model predictions. We investigate the choice of parameters (5.3) on their ability to display similar behavior to the experiments. Only a qualitative comparison is made instead of another model fitting based solely on the experimental data of Figs. 4.2, 4.3. In Fig. 5.6, the model is loaded to a strain of 0.0175, then immediately unloaded to 50 percent of that value, 0.00875. During the hold time, the change in stress response is not readily apparent in Fig. 5.6; Fig. 5.7 magnifies this range. Fig. 5.7 differs somewhat from Fig. 4.3, in that once the hold period is reached, the model predicts an immediate stress relaxation while for the experiment, the stress increases briefly before starting to decrease. As variability has been a constant distraction with the 31 IG material, the exact differences between the model and experiments may very well be explained by the model parameters being fitted to different specimens which behave differently. Further investigations are performed to determine if the

www.manaraa.com

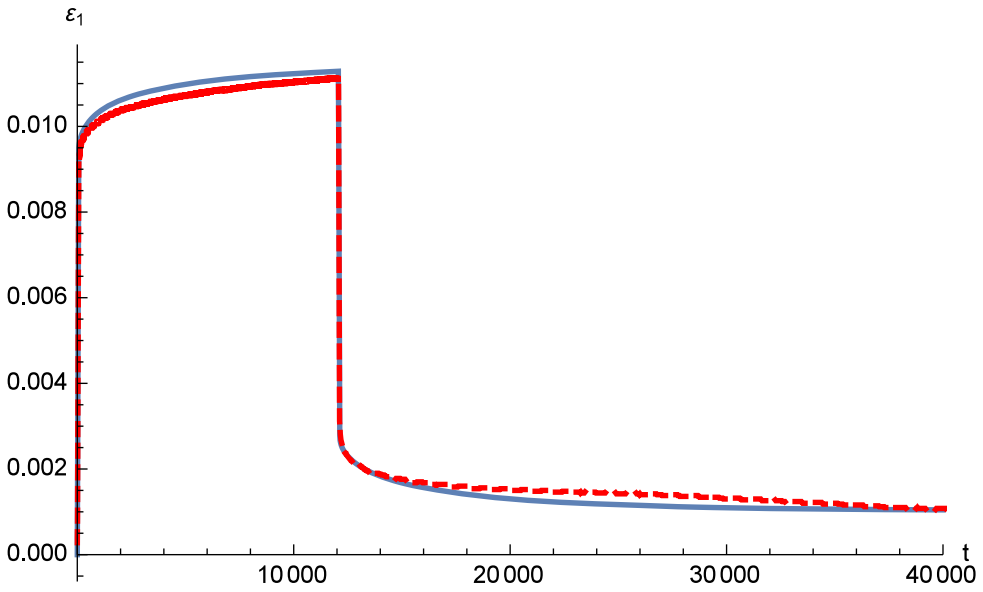

Figure 5.2: Strain time history where the final stress at loading is 0.27 MPa and held for 12,000 s. Final stress at unloading is 0.025 MPa and held for 40,000 s. Dashed red line is the experiment data, solid blue line is the model prediction.

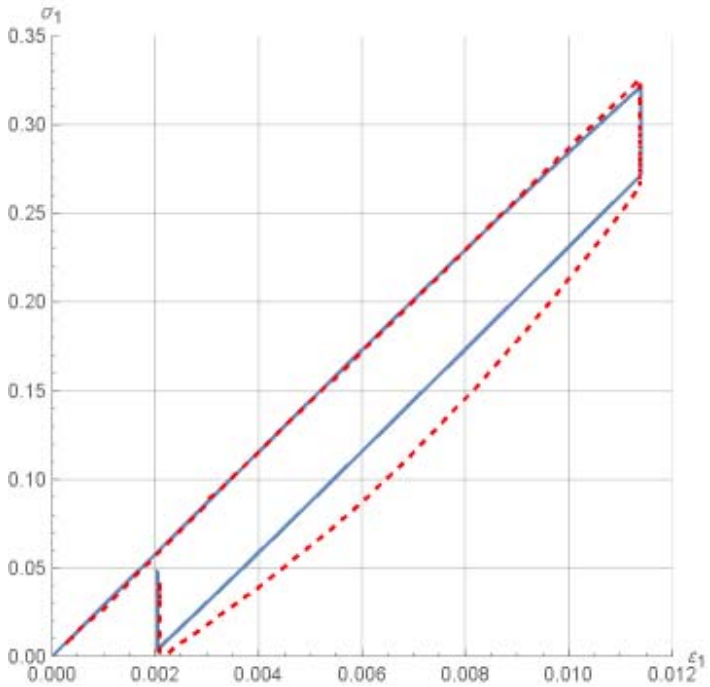

Figure 5.3: Stress-strain plot of the data from Fig. 5.1, comparing the model (solid blue line) to the experiment (dashed red line). During the recovery phase, the strain is held constant, and the material moves to close the loop vertically.

www.manaraa.com

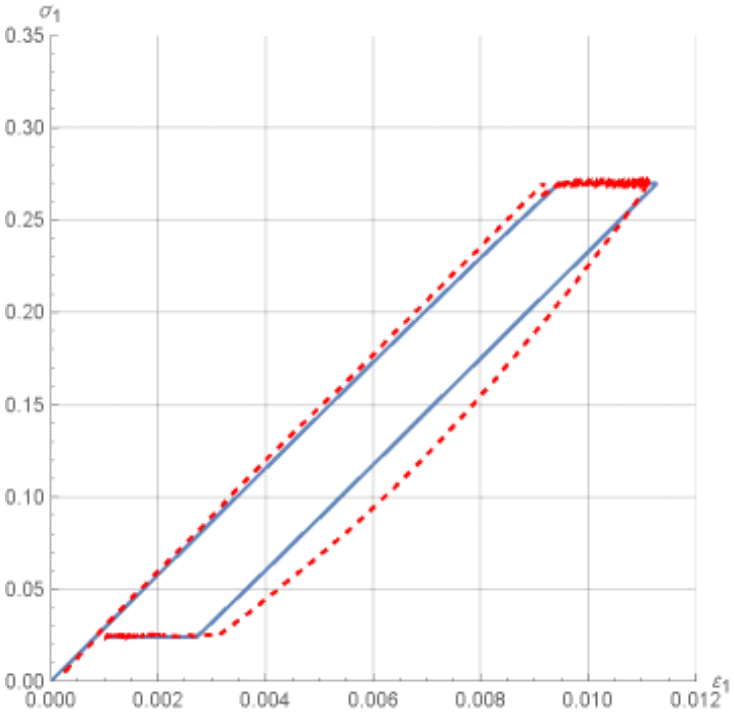

Figure 5.4: Stress-strain plot of the data of Fig. 5.2 comparing the model (solid blue line) to the experiment (dashed red line). During the recovery phase, the stress is held constant, and the material moves to close the loop horizontally.

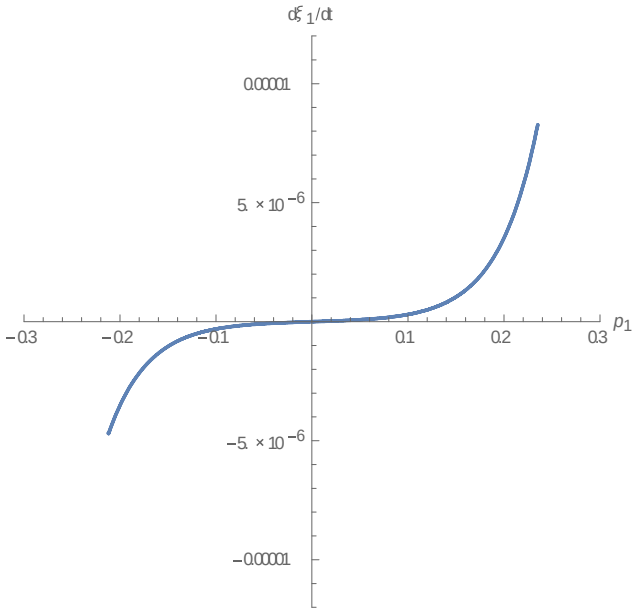

Figure 5.5: Velocity-force relationship for the loading cycle of Fig. 5.4. The plot is anti-symmetric, with the sticking point spending time in the first and third quadrants due to the addition of unload and recovery phases to the standard creep test.

www.manaraa.com

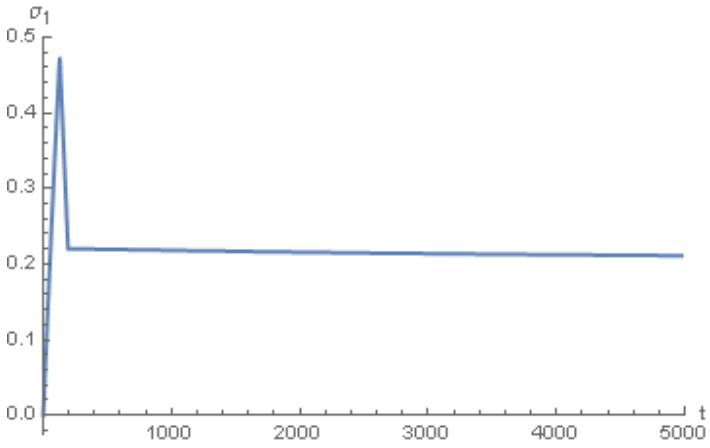

Figure 5.6: Stress time history for load/partial-unload/hold test where the strain at unload is approximately 50 percent of the maximum strain loading. This is the same load cycle as used for Fig. 4.2.

increase/decrease phenomenon is captured by the model at some partial-unloading point.

Indeed, the model captures the observed material behavior when approximately 80 percent unloaded, Figs. 5.9, 5.10, 5.11. Though model changes during the hold time are not as apparent as the experiment, the increase then decrease in the stress response is clearly observed.

5.1.3 Load/Unload/Recovery

Though simple in its execution, the load/unload/recovery test poses unique modeling challenges. This cycle results in small amounts of polymer chain slippage compared to tests of Sections 4.3 and 5.1. As such, the subtleties of the model predictions, or lack thereof, become more apparent. Because of variability in the elastic moduli, only qualitative comparisons of the experimental data of Fig. 4.4 with the fitted model parameters of Section 5.1 are made. For clarity, the 0.6, 0.4 and 0.2 MPa test cycles are isolated and shown on LHS of Fig. 5.12 . The closing of the stress-strain loops is clearly observed in the experiment data. With the stress returned to (nearly) zero, it takes approximately 3000 s for the strain to return to zero. The model also closes the loop, RHS of Fig. 5.12, though it requires approximately 10,000 s to do so. Some general shape differences are observed between the experiments and model predictions, the most noticeable being the barrel shape of the experimental data during the

www.manaraa.com

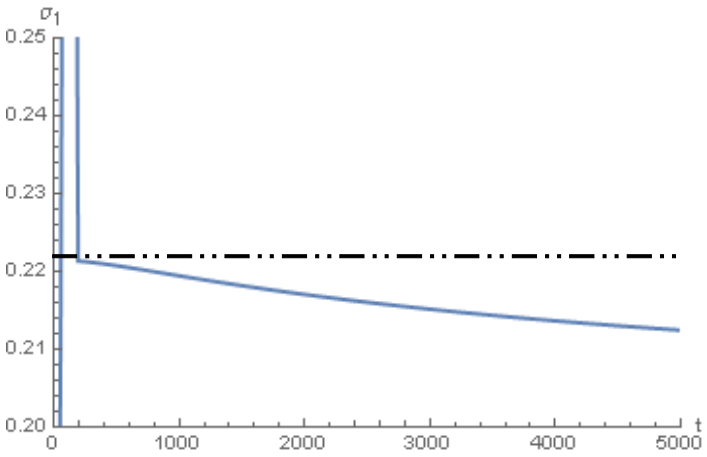

Figure 5.7: Magnification of the hold period of Fig. 5.6 showing immediate stress relaxation of the model once the hold period is started. The dashed horizontal line is used as a reference to accentuate the material behavior. Contrast this with Fig. 4.3, where there is an increase then decrease in the stress.

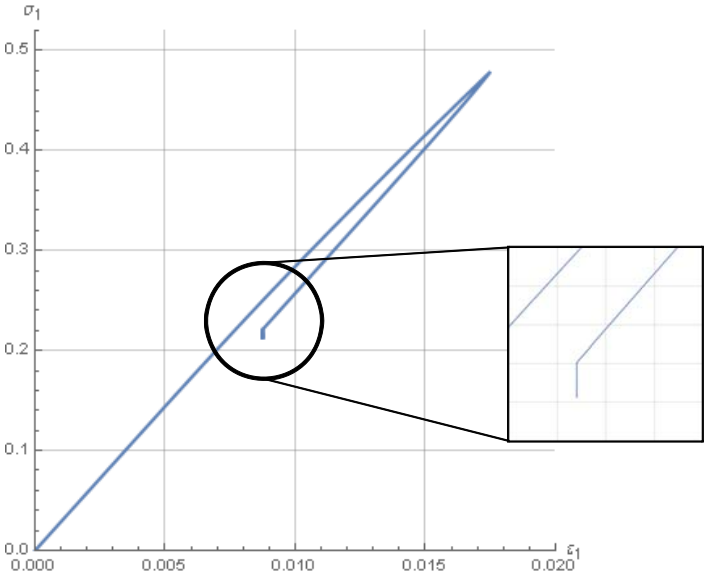

Figure 5.8: Unlike Fig. 4.2, here no increase is noted on the stress-strain plot during the hold period.

www.manaraa.com

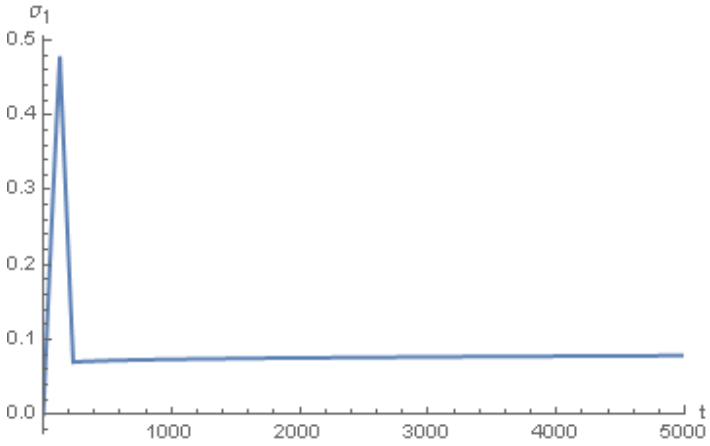

Figure 5.9: Stress time history for load/partial-unload/hold test where the strain at unload is approximately 20 percent of the maximum loading strain.

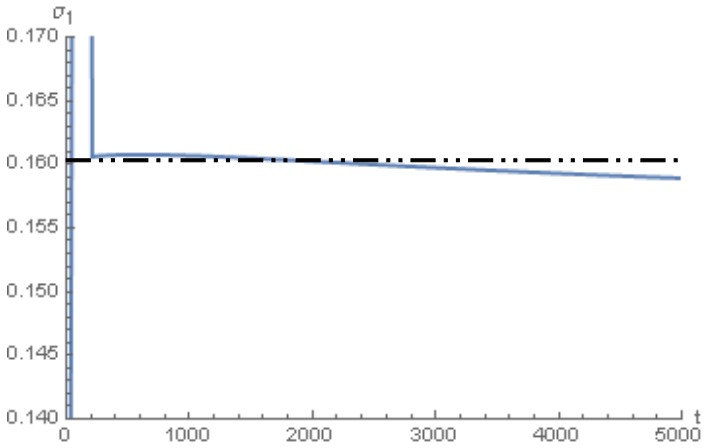

Figure 5.10: Magnification of the hold period of Fig. 5.9 showing the immediate stress increase and then decrease. The dashed horizontal line is used as a reference to accentuate the material behavior. At the greater unloading percentage, the model shows similar behavior as Fig. 4.3.

www.manaraa.com

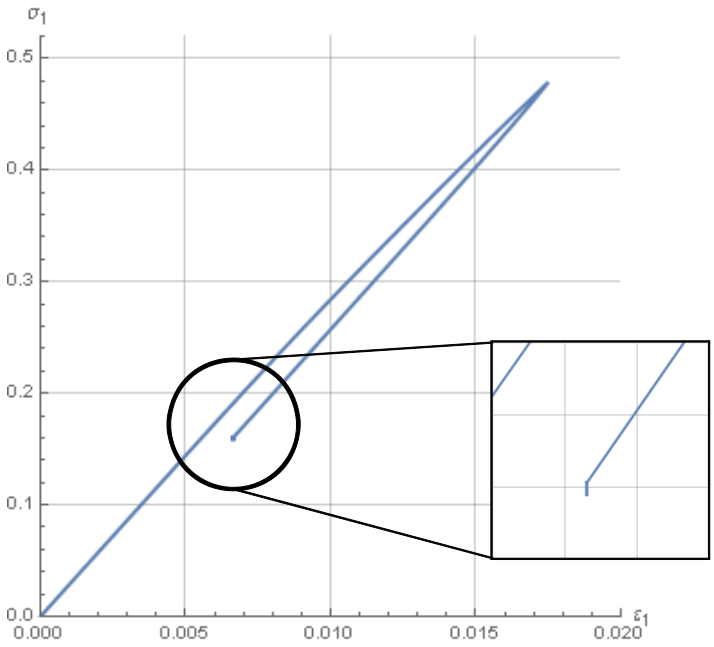

Figure 5.11: Unlike Fig. 5.8, the subtle increase then decrease in stress is noted on the stress-strain plot during the strain hold period. Qualitatively, this behavior is similar to Fig. 4.2.

unload phase versus the more linear response of the model. This results in a wider loop for the model at the unloaded portion, potentially requiring more time to "close." Regardless, the model qualitatively responds in a manner consistent with the experiments.

Insight into the material internal response during the 0.6 MPa load/unload/recovery cycle of Fig. 5.12 is further investigated in Fig. 5.13. Being stress controlled, that is the loading stress is prescribed, the stress profile (thick blue line) is straight and consistent during the various phases of load/unload/recovery. In this test, the sticking point position (long green dash) has its effect on the strain response. Past the time of stress reversal at $t = 150$ s, the sticking point continues in the same direction as it was during loading. In fact, the secondary internal force (short yellow dash) which affects the movement of the sticking point, does not reverse until $t \approx 225$ s. At $t \approx 225$ s, the stress is approximately 50 percent unloaded. Further insight into the behavior of the sticking point during the unloading is gained by observing the sticking point velocity (thin orange line). The sticking point velocity changes signs at $t \approx 225$ s. After $t \approx 225$ s, the sticking point starts operating in the third quadrant of the velocity-force plot. From this point on, the velocity and force remain negative until the

www.manaraa.com

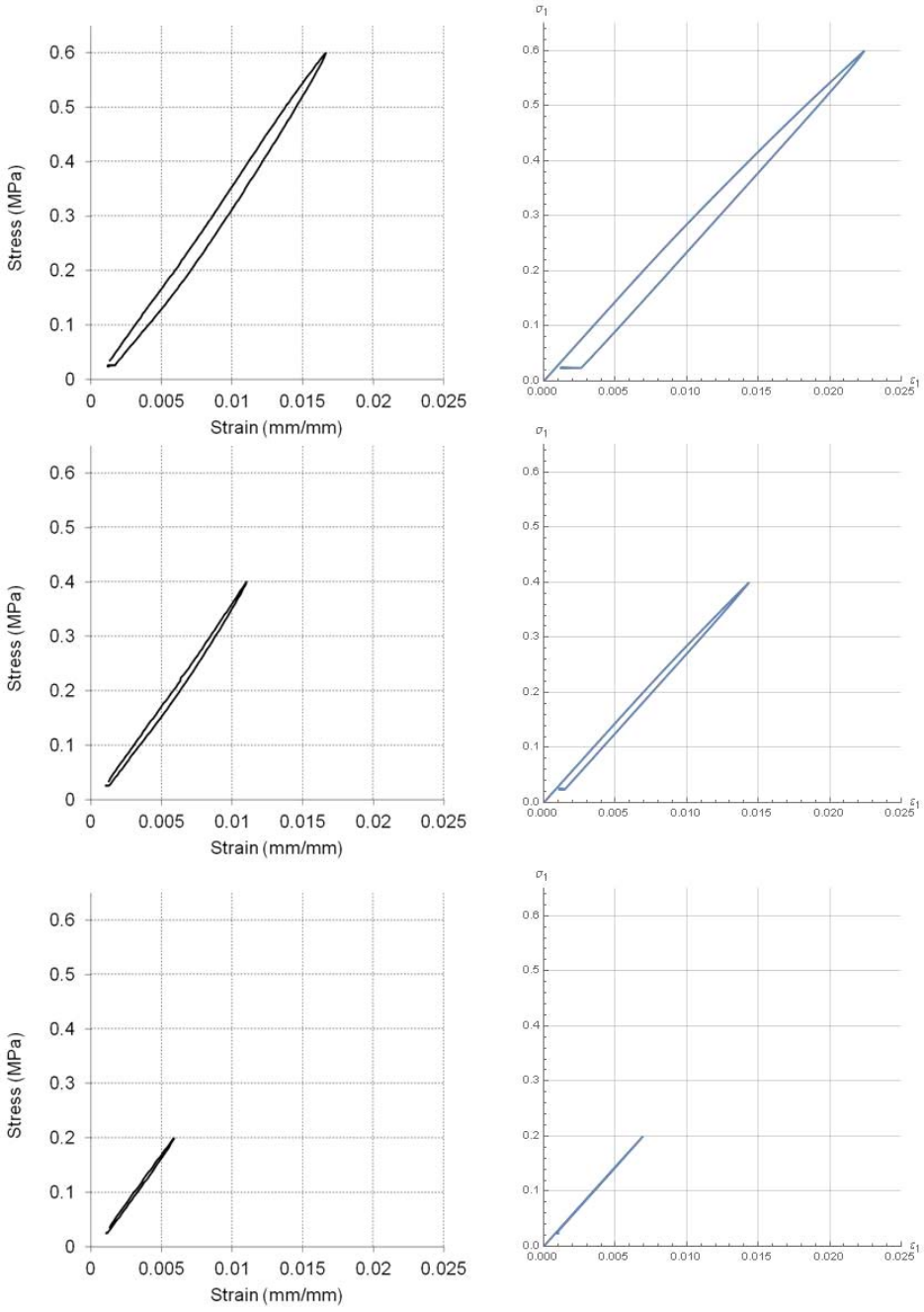

Figure 5.12: Load cycles of 0.6, 0.4, 0.2 MPa (LHS) isolated from Fig. 4.4, which more clearly showes each load/unload/recovery cycle of a single specimen of 31 IG. Closing of the stress-strain loop is observed in all experiment data. Qualitatively the model (RHS) predicts similar performance.

www.manaraa.com

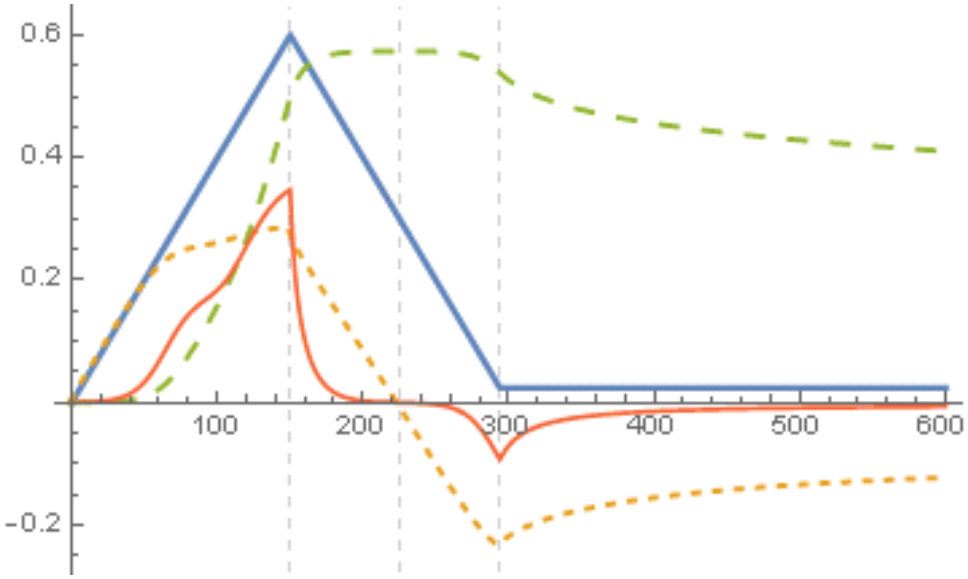

Figure 5.13: Model load/unload/recovery time history of the 0.6 MPa load, Fig. 5.12, for prescribed loading stress (thick blue line), secondary internal force (short yellow dash), sticking point velocity (thin orange), and sticking point position (long green dash). Values are scaled to fit the same y-axis.

sticking point parameter reaches its equilibrium position and the stress-strain loop is closed, Fig. 5.14.

5.1.4 Load/Instantaneous-Unload

An unconventional test performed as part of this work is the load/instantaneous-unload test, Figs. 4.5, 4.6, 4.7. It is here that the premise of a fast and slow regimes of polymer chain motion was theorized. It is fitting then to close this chapter with an analysis of the model predictions against the load/instantaneous-unload experiment data. Because of the "violent" nature of this test, i.e. the instantaneous releasing of the load energy, a significant amount of variability is observed in the unloading results. This is likely due to the use of a mechanical extensometer and the amount of energy released when the lower specimen clamp is opened. However, general trends and material performance can still be drawn As in all analyses in this chapter, the parameters of (5.3) are used for a qualitative evaluation of the model against experiments as opposed to an individual fitting of the model to each experiment run.

Fig. 5.15 shows the first 500 s of the test. Total model run time is 10,000 s. The material

www.manaraa.com

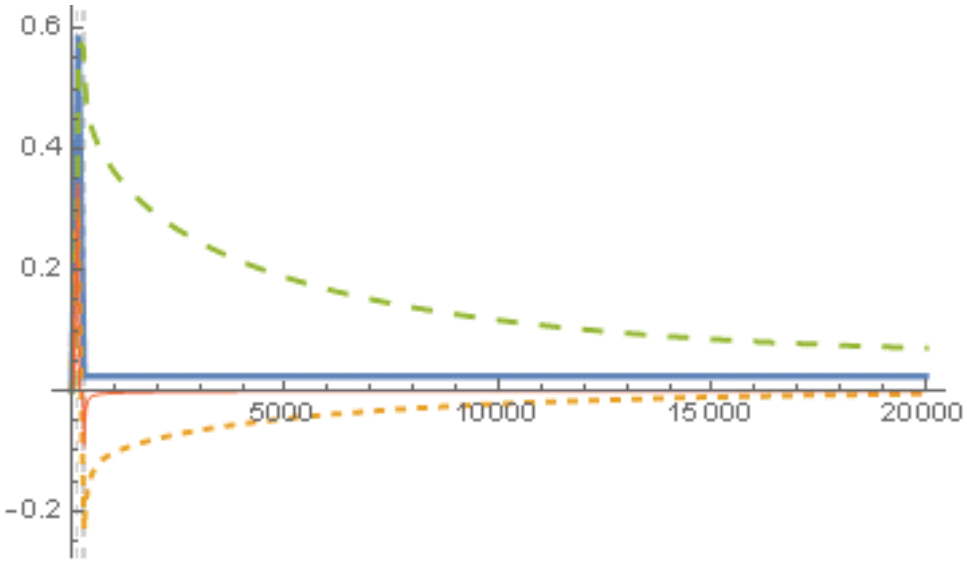

Figure 5.14: Fig. 5.13 time histories for $t = 20,000$ s. All responses are scaled exactly as Fig. 5.13. By $t = 10,000$ s, qualitatively the material closes the loop as observed in Fig. 5.12, though here the material has not quite yet reached its "no-load" equilibrium postition.

is loaded to $\sigma = 0.6$ MPa. At $t = 150$ s, the stress is returned to zero in one second, which is consistent with the experiment result. From $t = 151$ s, $\sigma = 0$ and the material is allowed to recover. The strain time history, Fig. 5.16, demonstrates the results of the microscopic reasoning used in the development of the model. The two regimes of polymer chain motion are clearly observed and are consistent with the experiments of Fig. 4.7. In the fast regime, i.e. the nearly vertical line of Fig. 5.16, the secondary internal force is high enough such that polymer chains move freely past each other. In the slow regime, i.e. the nearly horizontal line, the polymer chains are strongly interacting with their neighbors, slowing the material's return to its macroscopic pretest state. For the load/instantaneous-unload cycle, the stress-strain plot of Fig. 5.17 performs in a manner similar to the experiment results of Fig. 4.6.

Though the stress-strain plot of Fig. 5.17 appears similar to the 0.6 MPa load/unload stress-strain plot of Fig. 3.31, a significant difference exists in the velocity-force plot of the two tests, Fig. 5.18. Quadrant one is identical, as the test loading parameters are identical for both tests. The instantaneous unloading however causes the velocity of the sticking point parameter to become quite high, progressing well into the third quadrant compared to the 1 mm/minute unloading of the "traditional" load/unload profile.

www.manaraa.com

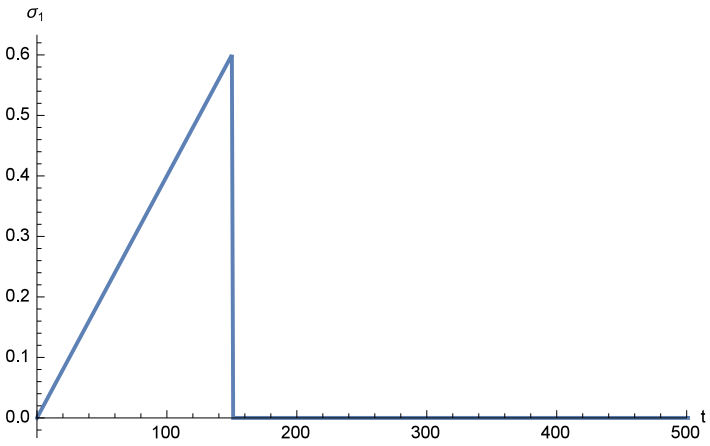

Figure 5.15: Model stress time history for the load/instantaneous-unload test, similar to Fig. 4.5. Removal of the load in one second creates a vertical drop in the loading profile, similar to the experiments.

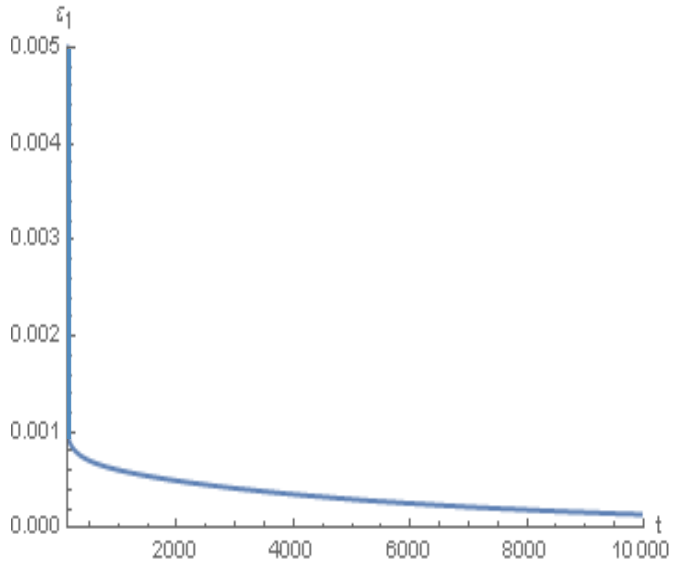

Figure 5.16: Strain time history of the loading profile of Fig. 5.15. Here the fast regime and slow regime of chain motion are observed, similar to Fig. 4.7.

www.manaraa.com

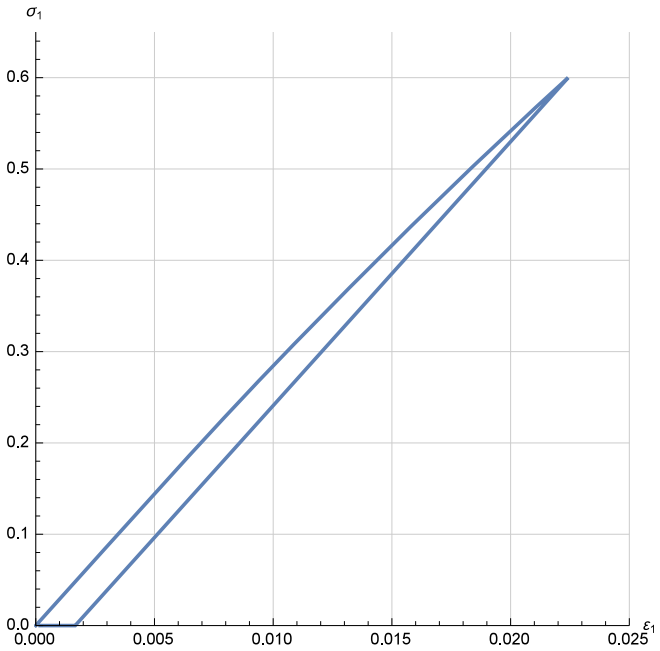

Figure 5.17: Model prediction for the stress-strain plot for the load/instantaneoous-unload test. Qualitatively the model reacts in a similar fashion as the experiment data, Fig. 4.6.

The instantaneous-unload test adds additional information about the material performance. Further work will be needed to improve physical test repeatability in order to provide better correlation of the model and tests, and make the results more meaningful.

5.2 Summary

Not only is the model proposed in Chapter 3 capable of predicting the stress relaxation and creep performance of the foam material, it is also capable of capturing nuances of material behavior during various loading, unloading, and recovery cycles. Though in some cases only qualitative comparisons are made, the model behavior is consistent with the behaviors observed in the experiments. Successful prediction of the material behavior helps to further validate the micro-mechanical reasoning used in the model construction. The primary differences between model predictions and experiments exist in the unload portion of the test cycles. Additional investigations into exact causes of these differences may allow further insight into polymer chain motion and interactions. Areas of future exploration will be touched

www.manaraa.com

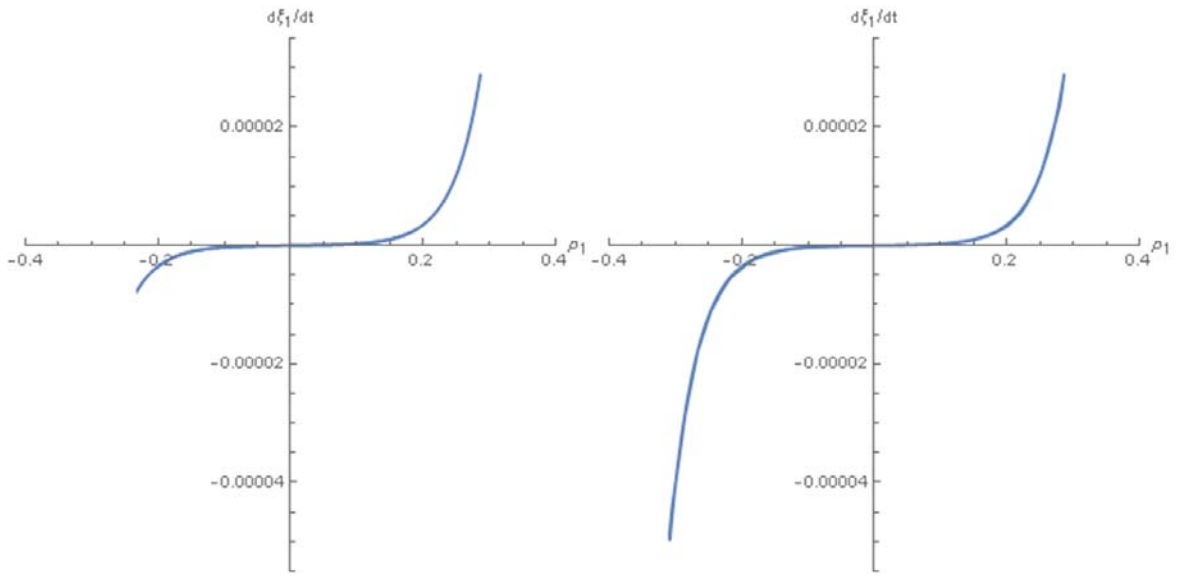

Figure 5.18: Velocity-force plot comparison for load/unload (LHS) and load/instantaneous-unload (RHS) test cycles.

on in Section 6.1.

www.manaraa.com

CHAPTER 6

Conclusions

A model has been proposed to predict the behavior of cross-linked polymers based on the theorized micromechanics of polymer chain interactions under loading. It predicts all the salient features of 31 IG foam when subjected to typical stress relaxation and creep tests. Additionally, it captures the material response during subsequent periods of recovery after stress relaxation and creep, as well as more subtle responses during load/partial-unload/hold, simple load/unload/recovery, and load/instantaneous-unload tests.

In the stationary state, weak van der Waals bonds form between the polymer chains. Under the application of a sufficiently large load, these weak inter-chain forces are easily broken and chain sliding begins. As the chains move past each other, these bonds are continually broken and reformed. Given tensile forces are not too high, the stronger covalent cross-link bonds remain intact and provide the material with memory. This is the impetus for the material's return to its macroscopic preloaded condition. The model described in this work simulates the chain behavior and interaction as a "sticking point" on the chain moving through a periodic energy potential. At "favorable" positions, the sticking point rests in an energy well, resisting further motion. As the force on the chain is increased, the sticking point slowly moves from one well, only to be captured by another. This is the slow regime of chain motion. With a sufficiently large force, the sticking point moves through or "skips" through the wells unencumbered. This is the fast regime of chain motion. The complete behavior is approximated by the solution of the Fokker-Planck equation for a particle moving through a periodic potential. The movement of the particle approximates the evolution of the polymer chain to its equilibrium position.

The complete model is based on thermodynamic reasoning. The free energy of the polymer chain is developed as a function of the external applied strain and an internal sticking-point parameter. The material model has two key features. First is the migration of the polymer to a long-term equilibrium condition as described by two material parameters α and β. Second, the driving force behind this migration is due to the change in entropy of the

www.manaraa.com

polymer chains. The migration rate of the polymer to the equilibrium condition is based on the solution to the Fokker-Planck equation of a particle moving through a periodic potential. The periodic potential approximates chain-to-chain interactions. For ease of use, the exact solution of the Fokker-Planck equation is approximated by a simple analytical function which introduces four material parameters a, b, c, d which tune the model's dynamic response. The choice of parameters α, β, a, b, c, d is based on a combination of testing and iterative fittings.

The research contained herein, validates the model through the use of tensile stress relaxation and creep tests on specimens of Rohacell 31 IG thermoset foam. For such tests, the specimen is strained/stressed a prescribed amount using a MTS tensile machine. The material response is measured using a mechanical extensometer and load cell. Additional insight into the material behavior is realized with the addition of an unload and recovery phases to the traditional stress relaxation and creep tests. It is during the recovery phase where the material's memory is apparent, as it returns to its original macroscopic state. Load/partial-unload/hold, load/unload/recovery, and load/instantaneous-unload tests help to further validate the nuances of the model.

The successful completion of this phase of research lends validity to the theorized interaction of polymer chains undergoing tensile loading. Initial validation of the model offers the beginnings to potential new areas of understanding into the physics of polymer chain behavior and the resulting polymer macroscopic material response.

6.1 Areas for Further Exploration

As this research unfolded, side-branches of information presented themselves for potential future exploration. Following are "thought starters" for areas which may merit further investigation for additional model insights and enhancements.

A significant challenge in this research has been due to the choice of 31 IG foam material. Considerable emphasis was needed to minimize variability in the testing, both equipment and material. However, material variability remained a significant issue throughout this research. It made fitting a wide-reaching, consistent model challenging. To further refine the microscopic reasoning behind polymer chain motion, using a more homogeneous polymer

www.manaraa.com

material appears to be a next logical step. Such a material may make it easier to consistently observe and subsequently model the nuances of polymer chain motion.

Due to creep and relaxation, polymer properties such as elastic modulus can be sensitive to test speed. All testing reported in this research was performed at load/unload speeds of 1 mm/minute (except instantaneous unload). Other speeds tested, but not reported herein, appear to indicate an influence on the elastic modulus. However, due to the amount of variability observed at 1 mm/minute loading rates, further test speed tests were not undertaken. Loading speed effects on stress relaxation and creep were not evaluated, but some influence is expected.

Adding the unload and recovery portions to the test cycles provided extremely useful information in model fitting. It is suggested future testing include this modification, regardless of the initial test profile. Performing more load/partial-unload/hold tests may help to more precisely determine the sticking point reversal during unloading. This may lend insight into the barrel shape of the unload portion of the stress-strain plots. Because of this shape, it has been theorized that the assumed antisymmetry of the velocity-force profile may not be 100 percent valid.

A potential model modification being considered is a nonsymmetrical velocity-force profile, Fig. 6.1. This plot is not antisymmetric as the velocity-force relationship of Fig. 3.6. Rather, there is a bias towards the positive x-axis. If necessary, this modification would allow further tailoring of the model when the secondary internal force $p_1 < 0$. Biased parameters would facilitate the model's return to the zero-zero state on the stress-strain plot once the stress is completely removed. Such a change implies polymer chains interact differently with their neighbors, dependent on the direction of movement of the chains. Initial modeling in this area shows nonsymmetric parameters have some effect on the curvature of the unloading portion of the stress-strain plot, though not to the extent observed experimentally.

Finally, the analytical function used to approximate the velocity-force relationship was chosen to provide a close approximation to the exact solution of the Fokker-Planck equation in the small velocity range, while providing sufficient flexibility for fitting. During model fittings, some interactions of parameters a, b, c, d, seemed to exist. A potential exists then to describe some of the parameters as a function of the others, thus simplifying the

www.manaraa.com

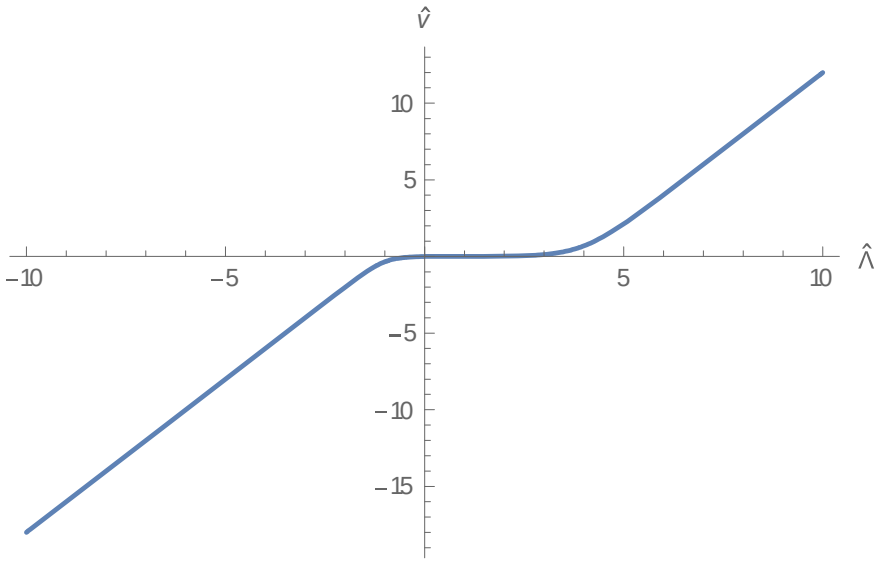

Figure 6.1: Example of a nonsymmetric velocity-force plot in which the values of parameters a, b change depending on the sign of the "second" internal force.

model. While the analytical function used provides a significant flexibility to tailor the model performance, other relationships could be chosen, such as a power law, to provide an acceptable approximation for the solution of the Fokker-Planck equation for a particle in a periodic potential.

6.2 Final Comments

In closing, the quote from E. E. Cummings, "Always the beautiful answer who asks a more beautiful question." seems apropos. While this research begins to address some key questions concerning the micromechanic behavior of polymer chains, it also opens up a host of other questions to be pursued.

www.manaraa.com

APPENDIX A

Linearization of Free Energy

Let us find the linearized version of free energy (3.49) for the case of small deformation of the order ε. Due to the incompressibility condition, the linear term ε_{aa} in (3.49) is actually of the order ε^2. To see that, we write the incompressibility condition in the principle axes of the strain tensor,

$$(1+\varepsilon_1)(1+\varepsilon_2)(1+\varepsilon_3) = 1. \tag{A.1}$$

Keeping the terms up to the second order, we find

$$\varepsilon_1 + \varepsilon_2 + \varepsilon_3 = -(\varepsilon_1\varepsilon_2 + \varepsilon_2\varepsilon_3 + \varepsilon_3\varepsilon_1). \tag{A.2}$$

The RHS of (A.2) can be written in invariant form using the identity

$$\varepsilon_1\varepsilon_2 + \varepsilon_2\varepsilon_3 + \varepsilon_3\varepsilon_1 = \frac{1}{2}\left((\varepsilon_{aa})^2 - \varepsilon_{ab}\varepsilon_{ab}\right), \tag{A.3}$$

On the other hand, there is a relation between any three numbers $\varepsilon_1,\ \varepsilon_2,\ \varepsilon_3$

$$2(\varepsilon_1\varepsilon_2 + \varepsilon_2\varepsilon_3 + \varepsilon_3\varepsilon_1) + \varepsilon_1^2 + \varepsilon_2^2 + \varepsilon_3^2 = (\varepsilon_1 + \varepsilon_2 + \varepsilon_3)^2. \tag{A.4}$$

Therefore using (A.3) and (A.4) in (A.2) and retaining the terms up to ε^2, we obtain

$$\varepsilon_{aa} = \frac{1}{2}\varepsilon_{ab}\varepsilon_{ab}. \tag{A.5}$$

Note that up to terms of the order ε^3

$$\varepsilon_{ab}\varepsilon_{ab} = \varepsilon'_{ab}\varepsilon'_{ab}. \tag{A.6}$$

Substituting (A.5) into (3.49) and using (A.6), we obtain

$$F\left(T, \varepsilon_{ab}, \frac{1}{2}\right) = U(T) + G\varepsilon'_{ab}\varepsilon'_{ab}, \tag{A.7}$$

www.manaraa.com

i.e. G indeed has the meaning of shear modulus for small deformations. Substitution of (A.5) and (A.6) into (3.50) results in (A.7). That is, at $r = 1/2$, (3.48) coincides with Treloar energy.

www.manaraa.com

APPENDIX B

Particle Under Action of Random Force in Periodic Potential

A solution of (3.18) is sought as a function of fast variable $y = x/h$, and slow variables x and τ. First we try to "kill" the oscillations of the coefficient of the first derivative of f. To this end, we make a change of the required function, $f \to u$,

$$f = p(y)u(x, y, \tau), \tag{B.1}$$

where $p(y)$ is a periodic function such that,

$$p(0) = p(1). \tag{B.2}$$

To avoid uncertainty of the multiplicative presentation (B.1) we need to choose a "magnitude" of $p(y)$. We do this by setting

$$\langle p \rangle \equiv \int_0^1 p(y)dy = 1. \tag{B.3}$$

Substituting (B.1) into (3.18), we get

$$p\frac{\partial u}{\partial \tau} + \frac{\partial}{\partial x}\left[\left(-\frac{dH(y)}{dy}\frac{1}{h} + \Lambda\right)pu - T\frac{dp}{dy}\frac{1}{h}u - Tp\frac{\partial u}{\partial x}\right] = 0. \tag{B.4}$$

We choose $p(y)$ as a solution of the differential equation

$$\left(-\frac{dH}{dy}\frac{1}{h} + \Lambda\right)p - T\frac{dp}{dy}\frac{1}{h} = v, \tag{B.5}$$

where v is a yet unknown constant.

For a given v, the boundary value problem (B.5) and (B.2) has a unique solution. The additional constraint (B.3) determines a unique value of the constant v. Indeed, we denote by $\Phi(y)$ the function

$$\Phi(y) = -\frac{1}{h}\frac{dH}{dy} + \Lambda. \tag{B.6}$$

Substituting (B.6) into (B.5) results in the ODE

www.manaraa.com

$$\Phi(y)p - T\frac{dp}{dy}\frac{1}{h} = v. \tag{B.7}$$

The homogeneous equation,

$$\Phi(y)p = \frac{T}{h}\frac{dp}{dy} \tag{B.8}$$

has the solution

$$p = const\, exp\left[\int_0^y \frac{\Phi\left(y'\right)h}{T}dy'\right]. \tag{B.9}$$

Therefore, the solution of the inhomogeneous equation (B.7) has the form

$$p = \tilde{p}(y)exp\left[\int_0^y \frac{\Phi\left(y'\right)h}{T}dy'\right], \quad \tilde{p}(0) = \tilde{p}(1)exp\left[\langle\Phi\rangle\, h/T\right]. \tag{B.10}$$

Further, note that due to periodicity of H,

$$\langle\Phi\rangle = \Lambda. \tag{B.11}$$

The boundary condition for $\tilde{p}(y)$ can be written in terms of the dimensionless external force $\hat{\Lambda} = \Lambda h/T$ as

$$\tilde{p}(0) = \tilde{p}(1)e^{\hat{\Lambda}}. \tag{B.12}$$

Substituting (B.10) into (B.5), we get the equation for $\tilde{p}(y)$,

$$-\frac{T}{h}e^{\int_0^y \frac{\Phi(y')h}{T}dy'}\frac{d\tilde{p}}{dy} = v \tag{B.13}$$

from which

$$\tilde{p}(y) = \tilde{p}(0) - \hat{v}\int_0^y e^{-\int_0^{y'}\frac{\Phi(\tilde{y})h}{T}d\tilde{y}}dy', \quad \hat{v} \equiv \frac{vh}{T}. \tag{B.14}$$

The boundary condition (B.12) determines $\tilde{p}(0)$:

$$\tilde{p}(0) = \left(\tilde{p}(0) - \hat{v}\left\langle e^{-\int_0^y \frac{\Phi(y')h}{T}dy'}\right\rangle\right)e^{\hat{\Lambda}}$$

www.manaraa.com

or

$$\tilde{p}(0) = \frac{\hat{v}e^{\hat{\Lambda}} \left\langle e^{-\int_0^y \frac{\Phi(y')h}{T}dy'} \right\rangle}{e^{\hat{\Lambda}} - 1}. \tag{B.15}$$

So, for a given constant v, $p(y)$ is indeed determined uniquely. The constraint (B.3) selects the value of v. To write this constraint in a convenient form we first transform the relation (B.10) using (B.14) and (B.15) :

$$p(y) = \hat{v}\frac{e^{\hat{\Lambda}}}{e^{\hat{\Lambda}} - 1} e^{\int_0^y \frac{\Phi(\tilde{y})h}{T}d\tilde{y}} \int_0^1 e^{-\int_0^{y'} \frac{\Phi(\tilde{y})h}{T}d\tilde{y}} dy' - \hat{v}\, e^{\int_0^y \frac{\Phi(\tilde{y})h}{T}d\tilde{y}} \int_0^y e^{-\int_0^{y'} \frac{\Phi(\tilde{y})h}{T}d\tilde{y}} dy'$$

$$= \hat{v}\frac{e^{\hat{\Lambda}}}{e^{\hat{\Lambda}} - 1} \int_0^1 e^{\int_0^y \frac{\Phi(\tilde{y})h}{T}d\tilde{y} - \int_0^{y'} \frac{\Phi(\tilde{y})h}{T}d\tilde{y}} dy' - \hat{v} \int_0^y e^{\int_0^y \frac{\Phi(\tilde{y})h}{T}d\tilde{y} - \int_0^{y'} \frac{\Phi(\tilde{y})h}{T}d\tilde{y}} dy'. \tag{B.16}$$

Note that

$$\int_0^y \frac{\Phi(\tilde{y})\, h}{T}d\tilde{y} - \int_0^{y'} \frac{\Phi(\tilde{y})\, h}{T}d\tilde{y} = \int_{y'}^y \frac{\Phi(\tilde{y})\, h}{T}d\tilde{y} =$$

$$= -\frac{1}{T}\left(H(y) - H(y')\right) + \hat{\Lambda}\left(y - y'\right). \tag{B.17}$$

Finally,

$$p(y) = \hat{v}\frac{e^{\hat{\Lambda}}}{e^{\hat{\Lambda}} - 1} \int_0^1 e^{-(H(y)-H(y'))/T + \hat{\Lambda}(y-y')} dy'$$

$$-\hat{v} \int_0^y e^{-(H(y)-H(y'))/T + \hat{\Lambda}(y-y')} dy'. \tag{B.18}$$

Utilizing (B.18), we put (B.3) into the form

$$\frac{e^{\hat{\Lambda}}}{e^{\hat{\Lambda}} - 1} \int_0^1 \int_0^1 e^{-(H(y)-H(y'))/T + \hat{\Lambda}(y-y')} dy dy'$$
$$- \int_0^1 \int_0^y e^{-(H(y)-H(y'))/T + \hat{\Lambda}(y-y')} dy dy' = \frac{1}{\hat{v}}. \tag{B.19}$$

For a given energy landscape $H(y)$, formula (B.19) establishes the correspondence between constants $\hat{\Lambda}$ and $\hat{v}$.

Asymptotics of this correspondence are: If $\hat{\Lambda} \to \infty$, then we can neglect $H(y)$ in (B.19), the leading term $e^{\hat{\Lambda}}/\left(e^{\hat{\Lambda}} - 1\right) \simeq 1$, and the left hand side becomes

$$\int_0^1 \int_0^1 e^{\hat{\Lambda}(y-y')} dy dy' - \int_0^1 \int_0^y e^{\hat{\Lambda}(y-y')} dy' dy =$$

www.manaraa.com

$$= \frac{e^{\hat{\Lambda}}+e^{-\hat{\Lambda}}-2}{\hat{\Lambda}^2} - \left(\frac{e^{\hat{\Lambda}}-1}{\hat{\Lambda}^2} - \frac{1}{\hat{\Lambda}}\right) \simeq \frac{1}{\hat{\Lambda}}. \tag{B.20}$$

Hence, the asymptotics is

$$\hat{v} = \hat{\Lambda}, \tag{B.21}$$

or, in dimension form,

$$v = \Lambda. \tag{B.22}$$

If $\hat{\Lambda} \to 0$, then the leading term $e^{\hat{\Lambda}}/\left(e^{\hat{\Lambda}}-1\right) \simeq 1/\hat{\Lambda}$, and the first integral on the LHS dominates, so we get

$$\hat{v} = \hat{\Lambda} \Big/ \int_0^1 \int_0^1 e^{-(H(y)-H(y'))/T} dy dy' \,. \tag{B.23}$$

According to Cauchy inequality $\left(\left(\int fg\right)^2 \leqslant \int f^2 \int g^2\right)$

$$1 = \left(\int_0^1 e^{-H(y)/2T+H(y)/2T} dy\right)^2 \leqslant \int_0^1 e^{-H(y)/T} dy \int_0^1 e^{H(y')/T} dy' =$$

$$= \int_0^1 \int_0^1 e^{-(H(y)-H(y'))/T} dy dy'. \tag{B.24}$$

Therefore, the denominator in (B.23) is always greater than 1, and velocity for small $\hat{\Lambda}$ is less than velocity at large $\hat{\Lambda}$.

Another important asymptotics are for $T \to 0$, and $T \to \infty$. If $T \to 0$, then

$$\int_0^1 e^{-H(y)/T} dy \sim \frac{e^{-H_{\min}/T}}{\sqrt{2\pi H''_{\min}/T}}, \tag{B.25}$$

$$\int_0^1 e^{H(y)/T} dy \sim \frac{e^{H_{\max}/T}}{\sqrt{2\pi H''_{\max}/T}}, \tag{B.26}$$

where $H_{\min}$, $H_{\max}$ are minimum and maximum values of $H(y)$, $H''_{\min}$ and $H''_{\max}$ are the values of the second derivative of $H(y)$ at the points of minimum and maximum, respectively. If $T \to \infty$, then

$$\int_0^1 e^{-H(y)/T} dy \sim 1 - \frac{\langle H(y)\rangle}{T}, \tag{B.27}$$

$$\int_0^1 e^{H(y)/T} dy \sim 1 + \frac{\langle H(y)\rangle}{T}. \tag{B.28}$$

www.manaraa.com

Hence, for $\hat{\Lambda} \to 0$ and $T \to 0$

$$\hat{v} \simeq 2\pi \sqrt{H''_{\min} H''_{\max}} \frac{\hat{\Lambda}}{T} e^{-(H_{\max} - H_{\min})/T}, \tag{B.29}$$

for $\hat{\Lambda} \to 0$ and $T \to \infty$

$$v = \Lambda. \tag{B.30}$$

After the change of required function (B.1), the equation for u takes the form

$$p(y) \frac{\partial u}{\partial \tau} + \frac{\partial}{\partial x} \left(vu - Tp(y) \frac{\partial u}{\partial x} \right) = 0. \tag{B.31}$$

Here $\langle p \rangle = 1$, $p > 0$, and v is a constant.

If initially u is localized, then this equation describes translational transport with velocity v, and slow diffusion with diffusion coefficient $Tp^2(y)$. To justify this statement, one can first transform (B.31) by introducing an auxiliary coordinate x',

$$dx' = p\left(\frac{x}{h}\right) dx. \tag{B.32}$$

Then (B.31) becomes a parabolic equation with fast oscillating periodic coefficient $Tp^2(y)$

$$\frac{\partial u}{\partial \tau} + \frac{\partial}{\partial x'} \left(vu - Tp^2(y) \frac{\partial u}{\partial x'} \right) = 0. \tag{B.33}$$

This equation has been studied by [Bakhvalov and Panasenko, 1989]. Its solution admits an asymptotic expansion

$$u = \bar{u}\left(\tau, x'\right) + hu_1\left(\tau, y, x'\right) + ...$$

where the leading term $\bar{u}$ is a solution of the parabolic equation with constant coefficients

$$\frac{\partial \bar{u}}{\partial \tau} + v \frac{\partial \bar{u}}{\partial x'} = D_{\text{eff}} \frac{\partial^2 \bar{u}}{\partial x'^2}. \tag{B.34}$$

D_{eff} being the effective diffusion coefficient,

$$D_{\text{eff}} = T \left\langle p^{-2}(y) \right\rangle^{-1}. \tag{B.35}$$

www.manaraa.com

According to (B.34), the particle moves with velocity v in (τ, x')-variables, and its position "diffuses" at the rate $D_{\text{eff}}\tau$. Since D_{eff} is proportional to T, D_{eff} is small.

www.manaraa.com

APPENDIX C

Constraints on Parameters *a, b, c, d*

Values of a, b, c, d must be such that (3.25) yields a qualitative agreement with Fig 3.6. That is, the particle velocity v must remain positive with the application of a positive force Λ, and the initial slope must remain smaller than the slope after the transition period.

If Λ is very large, then (3.25) is asymptotically linear

$$v = c\Lambda \tag{C.1}$$

and since v is positive for positive Λ,

$$c \geq 0. \tag{C.2}$$

If $\Lambda \to 0$, then

$$v \cong \left[c - 2d \tanh\left(\frac{b}{a}\right)\right] \Lambda. \tag{C.3}$$

To maintain the condition $v > 0$ when $\Lambda > 0$, the term $\left[c - 2d \tanh\left(\frac{b}{a}\right)\right]$ must be greater than zero. This results in the constraint

$$c \geq 2d \tanh\left(\frac{b}{a}\right). \tag{C.4}$$

For $b/a \gtrsim 1$, (C.4) reduces to

$$c \geq 2d. \tag{C.5}$$

There is one more constraint caused by the behavior at the transition point between the slow and fast velocity regimes. Let us find the derivative of particle velocity

$$\frac{dv}{d\Lambda} = c - d \tanh\left(\frac{b-\Lambda}{a}\right) - d \tanh\left(\frac{b+\Lambda}{a}\right). \tag{C.6}$$

We see that transitions occur at the points at which hyperbolic tangents vanish, $\Lambda = b$ and

www.manaraa.com

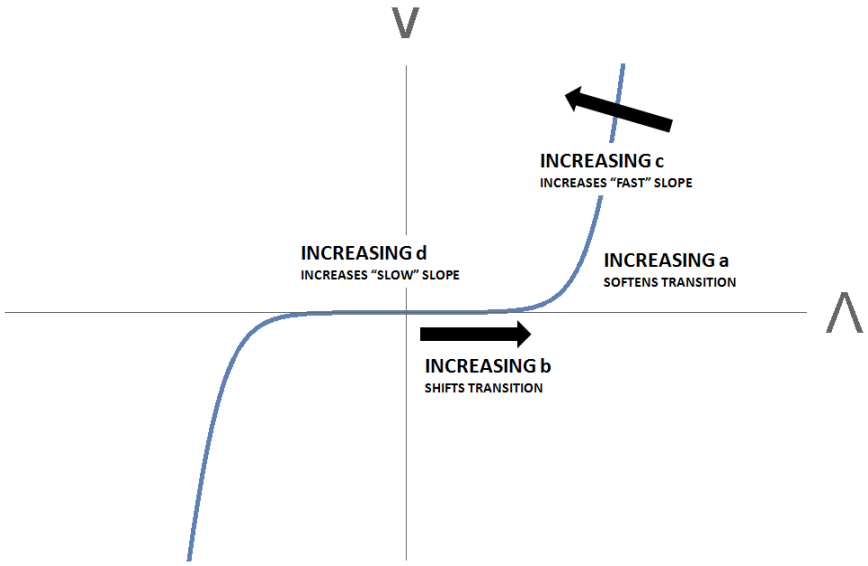

Figure C.1: Qualitative representation of the effect on the sticking point velocity profile by increasing/decreasing the various parameters of (3.26).

$\Lambda = -b$. The global minimum of velocity is to occur when $\Lambda = 0$ while the global maxima is to be seen for $\Lambda < -b$ or $\Lambda > b$. Since from (C.6) $dv/d\Lambda = c$ for $|\Lambda| >> b$, and

$$\frac{dv}{d\Lambda} = c - 2d \tanh\left(\frac{b}{a}\right), \tag{C.7}$$

for $\Lambda = 0$, a and b must have the same sign in order for $v(\Lambda)$ to be smaller at $\Lambda = 0$, compared to $\Lambda < -b$ or $\Lambda > b$. For convention, we choose a and b to be positive

$$a > 0, \quad b \geq 0. \tag{C.8}$$

Parameter Effects. To aid in fitting (3.25) to the experimental data, it is helpful to understand how the parameters a, b, c, d qualitatively affect the plots of $v[F]$ versus F, and $v'[F]$ versus F. Figures C.1, C.2 provide a summary of the effects. The parameter a controls the sharpness of the transition between the slow velocity and fast velocity regimes. The parameter b controls the point when the transition occurs between the slow and fast velocity regimes. Parameter c controls the velocity profile in the fast regime, while d controls the velocity profile in the slow regime.

www.manaraa.com

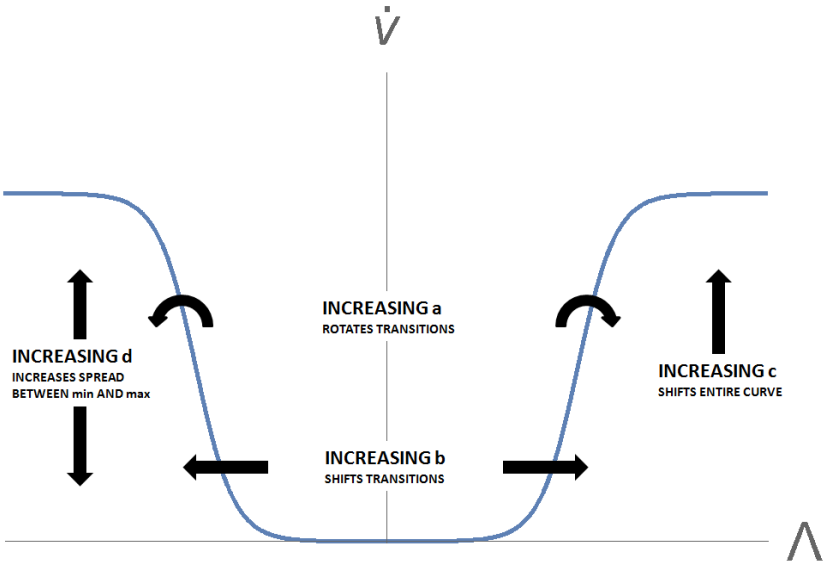

Figure C.2: Qualitative representation of the effect on the sticking point acceleration by increasing/decreasing the various parameters of (3.26).

www.manaraa.com

BIBLIOGRAPHY

Bakhvalov, N. and Panasenko, G. (1989). *Homogenization: Averaging processes in periodic media*. Kluwer.

Berdichevsky, V. L. (1989). *Variational Principles of Continuum Mechanics: 1. Fundamentals*. Springer.

Berdichevsky, V. L. and Herman, J. N. (2011). Modeling the constitutive behavior of polymer foams. In *11th International Conference on Fast Sea Transportation*. Hawaii.

Berdichevsky, V. L. and Herman, J. N. (2015). On rheology of polymers: 1. Slippage of polymer chains and its macroscopic modeling. *International Journal of Engineering Science*. (Accepted).

Bergstrom, J. S. (1999). *Large Strain Time-Dependent Behavior of Elastomeric Materials*. PhD thesis, Massachusetts Institute of Technology.

Black, S. (2014). http://www.compositesworld.com/articles/getting-to-the-core-of-composite-laminates.

Courtney, T. H. (2005). *Mechanical Behavior of Materials*. Waveland Press Inc.

Evonik Industries (2014). http://www.rohacell.com/product/rohacell/en/about/product-stories/pages/default.aspx.

Findley, W. N., Lai, J. S., and Onaran, K. (1989). *Creep and Relaxation of Nonlinear Viscoelastic Materials*. Dover Publications Inc.

Flory, P. J. (1969). *Statistical mechanics of chain molecules*. Interscience Publishers.

Flory, P. J. (1976). Statistical thermodynamics of random networks. *Proc. R. Soc. Lond. A*, 351:351–380.

Flory, P. J. (1990). *Principles of Polymer Chemistry*. Cornell University Press.

Gibson, L. J. and Ashby, M. F. (1997). *Cellular Solids-Structure and Properties*. Cambridge University Press.

Herman, J. N. and Berdichevsky, V. L. (2015). On rheology of polymers: 2. Some experiments on creep and stress relaxation. *International Journal of Engineering Science*. (Accepted).

Jikov, V. V., Kozlov, S. M., and Oleinik, O. A. (1994). *Homogenization of Differential Operators and Integral Functionals*. Springer.

www.manaraa.com

Risken, H. (1989). *The Fokker-Planck Equation*. Springer.

Treloar, L. R. G. (1976). The mechanics of rubber elasticity. *Proc. R. Soc. Lond. A.*, 351:301–330.

Treloar, L. R. G. (2009). *The Physics of Rubber Elasticity*. Oxford University Press, third edition edition.

United States Patent 5928459 (1999).

Zenkert, D., Shipsha, A., and Burman, M. (2006). Fatigue of closed cell foams. *Journal of Sandwich Structures and Materials*, 8:517–538.

www.manaraa.com

ABSTRACT

RHEOLOGY OF CROSS-LINKED POLYMERS AND POLYMER FOAMS: THEORY AND EXPERIMENTAL RESULTS

by

JOHN N. HERMAN

May 2015

Advisor: Dr. Victor Berdichevsky

Major: Mechanical Engineering

Degree: Doctor of Philosophy

Typical polymers have a time-dependent response to loading which results in stress relaxation or creep. Models using springs/dashpots or Volterra integrals are capable of predicting the material response, but place little or no emphasis on the reasoning behind the response. This research proposes a microscopic reasoning behind polymer chain movement, while developing a model to predict the creep and stress relaxation of a polymer foam. Based on the theorized slip/stick of polymer chains as they slide past each other, this model successfully predicts the behavior of a PMI polymer foam under tensile loads. This model lends insights into polymer microscopic behavior, which may be used for the development of future polymer materials.

When possible, industry standard test methods are used to obtain tensile creep and stress relaxation results from rectangular specimens of Rohacell 31 IG foam. A common set of material parameters is fitted to the data, validating the micromechanic reasoning to polymer chain movement. To gain insight into observed test result variability, an investigation of the elastic modulus and material density relationship is performed using nominal foam densities of 31 kg/m^3, 51 kg/m^3, 71 kg/m^3.

Additional testing and modeling is performed to validate the model under load/partial-unload/hold, load/unload/recovery, and load/instantaneous-unload test cycles. The model successfully captures the observed material nuances during these more complex loading cycles.

www.manaraa.com

AUTOBIOGRAPHICAL STATEMENT

John Herman is the Acoustic, Endurance, and Testing Manager for Bosal's North American Operations. Bosal is a leading supplier of original equipment exhaust systems to automobile manufacturers world-wide. In 1996, John left a 10 year engineering career at General Motors to join the Bosal organization where he was the third person hired in their North American technical center. Now in his 19th year with Bosal, he has been responsible for the development of over 30 exhaust systems ranging from General Motor's minivan and cross-over vehicles, mid-size and small car platforms, to Chrysler's Jeep Wrangler and the Fisker Karma hybrid vehicle. In this same time frame, he has helped to grow the engineering organization to over 30 individuals, while the exhaust developments have required Bosal to add three manufacturing facilities to their North American operations.

John received his BSME from Michigan Technological University in 1986. Though he swore off any desire to continue a path into higher education, in 2006 he was asked by Karel Bos, Bosal's owner and founder, to pursue a doctorate degree in mechanical engineering. He received his MSME from Wayne State University in 2008, at which time he was accepted into Wayne State's mechanical engineering doctorate program. Since 2009 he has been working with Dr. Victor Berdichevsky to develop a novel model for the rheologic behavior of polymers based on the micromechanics of polymer chain motion and interaction.

www.manaraa.com